LOCALIZATION OF METAL IONS IN DNA

A Thesis Submitted to the College of Graduate Studies and Research
in Partial Fulfillment of the Requirements for the
Degree of Doctor of Philosophy
in the Department of Biochemistry
University of Saskatchewan, Saskatoon

By

Michael John Dinsmore

PERMISSION TO USE

In presenting this thesis in partial fulfillment of the requirements for a postgraduate degree from the University of Saskatchewan, I agree that the Libraries of this University may make it freely available for inspection. I further agree that permission for copying of this thesis in any manner, in whole or in part, for scholarly purposes may be granted by the professors who supervised my thesis work, or in their absence, by the Head of the Department or the Dean of the College in which my thesis work was done. It is understood that any copying or publication or use of this thesis or parts thereof for financial gain shall not be allowed without my written permission. It is also understood that due recognition shall be given to me and to the University of Saskatchewan in any scholarly use which may be made of any materials in my thesis.

Requests for permission to copy or make other use of material in this thesis in whole or in part should be addressed to:

Head of the Department of Biochemistry
University of Saskatchewan
Saskatoon, Saskatchewan S7N 0W0

ABSTRACT

M-DNA is a novel complex formed between DNA and transition metal ions under alkaline conditions. The unique properties of M-DNA were manipulated in order to rationally place metal ions at specific regions within a double-stranded DNA helix. Investigations using thermal denaturation profiles and the ethidium fluorescence assay illustrate that the pH at which M-DNA formation occurs is influenced heavily by the DNA sequence and base composition. For instance, DNA with a sequence consisting of poly[d(TG)•d(CA)] is completely converted to M-DNA at pH 7.9 while DNA consisting entirely of poly[d(AT)] remains in the B-DNA conformation until a pH of 8.6 is reached. The pH at which M-DNA formation occurs is further decreased by the incorporation of 4-thiothymine (s^4T). DNA oligomers with a mixed sequence composed of half d(AT) and the other half d(TG)•d(CA) showed that only 50% of the DNA is able to incorporate Zn^{2+} ions at pH 7.9. This suggests that only regions corresponding to the tracts of d(TG)•d(CA) are being transformed.

Duplex DNA monolayers were self-assembled on gold through a Au-S linkage and both B- and M-DNA conformations were studied using X-ray photoelectron spectroscopy (XPS) in order to better elucidate the location of the metal ions. The film thickness, density, elemental composition and ratios for samples were analyzed and compared. The DNA surface coverage, calculated from both XPS and electrochemical measurements, was approximately 1.2×10^{13} molecules/cm^2 for B-DNA. All samples showed distinct peaks for C 1s, O 1s, N 1s, P 2p and S 2p as expected for a thiol-linked DNA. On addition of Zn^{2+} to form M-DNA the C 1s, P 2p and S 2p showed only small changes while both the N 1s and O 1s spectra changed considerably. This result is consistent with Zn^{2+} interacting with oxygen on the phosphate backbone as well as replacing the imino protons of thymine (T) and guanine (G) in M-DNA. Analysis of the Zn 2p spectra also demonstrated that the concentration of Zn^{2+} present under M-DNA conditions is consistent with Zn^{2+} binding to both the phosphate backbone as well as replacing the imino protons of T or G in each base pair. After the M-DNA monolayer is washed with a buffer containing only Na^+ the Zn^{2+} bound to the phosphate backbone is removed while the Zn^{2+} bound internally still remains. Variable angle x-ray photoelectron

spectroscopy (VAXPS) was also used to examine monolayers consisting of mixed sequence oligomers. Preliminary results suggest that under M-DNA conditions, the zinc to phosphate ratio changes relative to the position of the d(TG)•d(CA) tract being at the top or bottom of the monolayer.

Electrochemistry was also used to investigate the properties of M-DNA monolayers on gold and examine how the localization of metal ions affects the resistance through the DNA monolayer. The effectiveness of using the $IrCl_6^{2-/3-}$ redox couple to investigate DNA monolayers and the potential advantages of this system over the standard $Fe(CN)_6^{3-/4-}$ redox couple are demonstrated. B-DNA monolayers were converted to M-DNA by incubation in buffer containing 0.4 mM Zn^{2+} at pH 8.6 and studied by cyclic voltammetry (CV), electrochemical impedance spectroscopy (EIS) and chronoamperometry (CA) with $IrCl_6^{2-/3-}$. Compared to B-DNA, M-DNA showed significant changes in CV, EIS and CA spectra. However, only small changes were observed when the monolayers were incubated in Mg^{2+} at pH 8.6 or in Zn^{2+} at pH 6.0. The heterogeneous electron-transfer rate (k_{ET}) between the redox probe and the surface of a bare gold electrode was determined to be 5.7 x 10^{-3} cm/s. For a B-DNA modified electrode, the k_{ET} through the monolayer was too slow to be measured. However, under M-DNA conditions, a k_{ET} of 1.5 x 10^{-3} cm/s was reached. As well, the percent change in resistance to charge transfer (R_{CT}), measured by EIS, was used to illustrate the dependence of M-DNA formation on pH. This result is consistent with Zn^{2+} ions replacing the imino protons on thymine and guanine residues. Also, at low pH values, the percent change in R_{CT} seems to be greater for $d(TG)_{15}$•$d(CA)_{15}$ compared to oligomers with mixed d(AT) and d(TG)•d(CA) tracts. The $IrCl_6^{2-/3-}$ redox couple was also effective in differentiating between single-stranded and double-stranded DNA during dehybridization and rehybridization experiments.

PUBLISHED WORKS

Dinsmore, M.J., Lee, J.S. (2008). Characteristic Differences in the X-ray Photoelectron Spectrum between B-DNA and M-DNA Monolayers on Gold. J Inorg Bioch (Accepted)

Dinsmore, M.J., Lee, J.S. (2008). Hexachloroiridate (IV) as a Redox Probe for the Electrochemical Discrimination of B-DNA and M-DNA Monolayers on Gold. J Electroanal Chem (Accepted)

Sutherland, T. C., Dinsmore, M.J., Kraatz, HB., Lee, J.S. (2004). An analysis of mismatched duplex DNA unzipping through a bacterial nanopore. Biochem Cell Biol *82*, 407-412.

Kindrachuk, J., Parent, J., Davies, G. F., Dinsmore, M.J., Attah-Poku, S., Napper, S. (2003). Overexpression of L-isoaspartate O-methyltransferase in Escherichia coli increases heat shock survival by a mechanism independent of methyltransferase activity. J Biol Chem *278*, 50880-50886.

Wood, D. O., Dinsmore, M. J., Bare, G. A. & Lee, J. S. (2002). M-DNA is stabilised in G*C tracts or by incorporation of 5-fluorouracil. Nucleic Acids Res *30*, 2244-2250.

ACKNOWLEDGEMENTS

I would sincerely like to thank my supervisor Dr. Jeremy Lee for giving me the opportunity to work on such a novel and exciting project. Your knowledge and expertise, creative ideas, easy going personality and passion for science and business have all made this experience “jolly good”. I also appreciate the freedom I was given to indulge my curiosity and take the project down different paths. My appreciation also extends to the members of my advisory and examining committee for their advice, criticism, support and patience.

Special thanks to Dr. Todd Sutherland who was an excellent teacher, motivator and thinker. His knowledge and help in electrochemistry were immeasurable. I would also like to thank Dr. Yitao Long, Dr. Sergiy Nohkrin and Dr. David Wood for their illuminating discussions and helpful suggestions. I am also indebted to the Biochemistry student lab for allowing me unlimited access to all their supplies and equipment, providing me the opportunity to work as a teaching assistant for Biochemistry 212 and 310 labs and, of course, for the birthday cake. As well, graduate studies has been a rewarding and enriching experience because of the friends I have made along the way. I would like to thank you all for introducing me to new cultures, traditions, ideas, books, and music, and for sharing many laughs over lunch.

Finally, I owe immeasurable thanks and gratitude to my family. Thanks to my brother Andrew for being a great older brother and an even better friend. Thanks to my older sister for being a caring, thoughtful and sincere person. To my parents, I cannot begin to thank you enough for all of your love, support and constant encouragement to do my best in life. Last, but certainly not least, I want to thank my wife Sarah. You have added so much to my life, thank you for being such an integral part of this exciting and challenging experience.

Financial support from the Department of Biochemistry, the College of Medicine, the College of Graduate Studies and Research, the Natural Science and Engineering Research Council of Canada (NSERC) and personal research grants of Dr. Jeremy Lee were all greatly appreciated.

DEDICATION

To my wife Sarah
Thank you for making every part of my life better.
I love you.

To my parents Bev and Garry Dinsmore
I am truly blessed and grateful to have parents like you.

TABLE OF CONTENTS

LIST OF TABLES

LIST OF FIGURES

LIST OF ABBREVIATIONS

Symbol	Meaning
Γ_{DNA}	DNA surface density
Ω	Ohms
α	Transfer coefficient
Φ	Work function
λ	Inelastic mean free path
λ-496	A 496 bp fragment from Lambda DNA
σ	Scofield coefficient
Abbreviations	**Meaning**
A_{260}	Absorbance at 260 nm
A_{345}	Absorbance at 345 nm
A	Adenine
A	Electrode area
BE	Binding energy
bp	Base-pair
C	Cytosine
C	Concentration
CA	Cyclic Amperometry
Cdl	Double-layer capacitance
CE	Counter electrode
CHA	Concentric hemispherical analyzer
CHES	2-[*N*-cyclohexylamino]ethanesulfonic acid
CPE	Constant phase element
CT	Calf Thymus
CV	Cyclic Voltommetry
D	Diffusion coefficient
d	deoxyribo prefix

dd	Double-distilled
d	Thickness of monolayer
DNA	deoxyribonucleic acid
ds	Double-stranded prefix
DTT	Dithiothreitol
E_0	Formal potential
E_{pa}	Anodic peak potential
E_{pc}	Cathodic peak potential
EAL	Effective attenuation length
E. coli	*Escherichia coli*
EDTA	Ethylenediaminetetraacetic acid
EIS	Electrochemical Impedance Spectroscopy
EtBr	Ethidium bromide
F	Faraday constant
FRET	Fluorescence resonance electron transfer
FWHM	Full width at half maximum
G	Guanine
I	Photoelectron intensity
I_{pa}	Anodic peak current
I_{pc}	Cathodic peak current
IMPF	Inelastic mean free path
k_{ET}	Electron transfer rate
KE	Kinetic energy
L_x	EAL for x electrons in the film
m^6A	6-methyladenine
n	Number of electrons
N_A	Avogadro's number
NIST	National Institute of Standards and Technology
PCR	Polymerase chain reaction

PEAL	Average practical EAL
Pu	Purine
Py	Pyrimidine
Qdl	Capacitive charge
QEAL	EAL for quantitative analysis
R_{CT}	Charge transfer resistance
RE	Reference electrode
R_S	Solution resistance
s^2T	2-thiothymidine
s^4T	4-thiothymidine
SNP	Single nucleotide polymorphism
SAM	Self-assembled monolayer
T	Thymidine
T	Analyzer transmission function
T_m	Melting Temperature
TOA	Take-off angle
TRIS	Tris(hydroxymethyl)aminomethane
UPS	Ultraviolet photoelectron spectroscopy
UV	Ultraviolet
v	Scan rate
VAXPS	Variable angle x-ray photoelectron spectroscopy
W	Warburg impedance
WC	Watson-Crick
WE	Working electrode
XPS	X-ray photoelectron spectroscopy
z^6A	7-deazaadenine

1.0 INTRODUCTION

On February 28, 1953, Francis Crick entered the Eagle pub in Cambridge, England and proclaimed that he and James Watson had found the secret to life (Watson, 1968). Together, they had solved the structure of deoxyribonucleic acid, or DNA, and suggested its fundamental role in the storage and transfer of life's genetic material. Since their discovery, the vast majority of DNA research has been focused around its biological properties, in particular its role in genetic inheritance, disease and aging. However, regardless of its central importance in biology, the applications of DNA are no longer restricted to just the biological sciences.

The idea of building machines and mechanical devices out of individual atoms was originally proposed in a speech by the Nobel Laureate Richard Feynman in 1959. Inspired by that speech, Eric Drexler not only pursued this area, but has been credited with increasing public interest and spawning the beginning of the nanotechnology revolution. Naturally, due to its ability to self-assemble through complementary base pairs, participate in molecular recognition and be easily manipulated by a vast array of enzymes, DNA has become one of the most promising biomolecules for future applications in nanotechnology. It has already been manipulated in order to design intricate geometric shapes (Chen and Seeman, 1991; Zhang and Seeman, 1994; Shih *et al.*, 2004; Rothemund, 2006), construct various nanoscale mechanical devices (Mao *et al.*, 1999; Yurke *et al.*, 2000; Sherman and Seeman, 2004; Shin and Pierce, 2004; Ye and Mao, 2004) and has recently attracted considerable interest in molecular electronics (Murphy *et al.*, 1993; Aich *et al.*, 1999; Fink and Schonenberger, 1999). The interactions of metal ions with DNA have been shown to profoundly effect not only the conformation of DNA, but properties such as the electrical conductivity. Therefore, the introduction of this thesis will focus on the structural features and properties of DNA,

how these are affected in the presence of various metal ions and the techniques used to study them.

1.1 Structure of DNA

1.1.1 DNA Subunits

The fundamental components of DNA are monomeric units called nucleotides. Each nucleotide consists of a sugar, a nucleobase and a phosphate group (Figure 1.1). The sugar in DNA is the cyclic β-D-furanose form of ribose and is referred to as β-D-2′-deoxyribose as the hydroxyl group on the 2′ carbon of the ribose ring is replaced with hydrogen. Also depicted in figure 1.1 are the four major nucleobases found in DNA which are derived from the two parent compounds purine and pyrimidine. The two major purine bases are adenine (A) and guanine (G) whereas the two major pyrimidine bases are cytosine (C) and thymine (T). The carbon numbers in the furan sugar are designated with a prime symbol in order to distinguish them from the numbered atoms in the nucleobase. Each nucleobase is attached to the sugar through a β-glycosyl C1′—N linkage (N1 of pyrimidines and the N9 of purines) whereas the phosphate is attached to the sugar through an ester bond at the 5′ carbon. In the absence of the phosphate group, the molecule is referred to as a nucleoside.

A strand of DNA is simply formed from successive nucleotides covalently linked to each other through a phosphodiester bond in which the 5′-phosphate group of one nucleotide is attached to the 3′-hydroxyl group of the next nucleotide creating a polynucleotide chain that can be described and written in a specific direction. For instance, in figure 1.2, a four base DNA oligonucleotide with the sequence 5′-CTAG- 3′ is shown.

When the nucleotides are linked as described in the above section, the resulting polynucleotide chain is highly flexible due to the large number of conformations around the rotatable bonds in the phosphoribose backbone, the sugar and around the N-glycosidic bond (Figure 1.3).

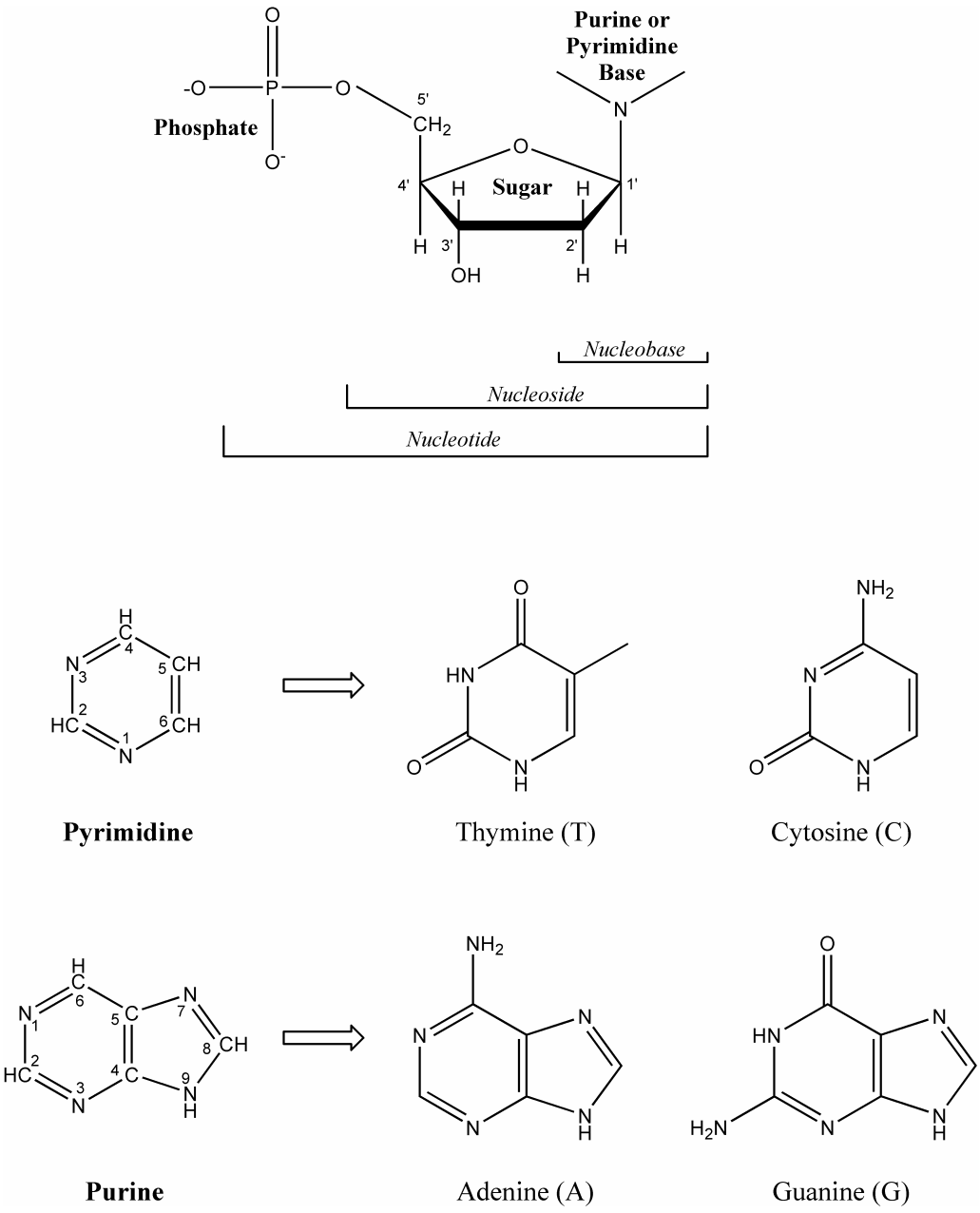

Figure 1.1 The general structure of a nucleotide along with the four major purine and pyrimidine nucleobases found in DNA. Also shown are the numbering conventions for the furan sugar and the parent pyrimidine and purine bases which apply to all four bases as well as their analogues.

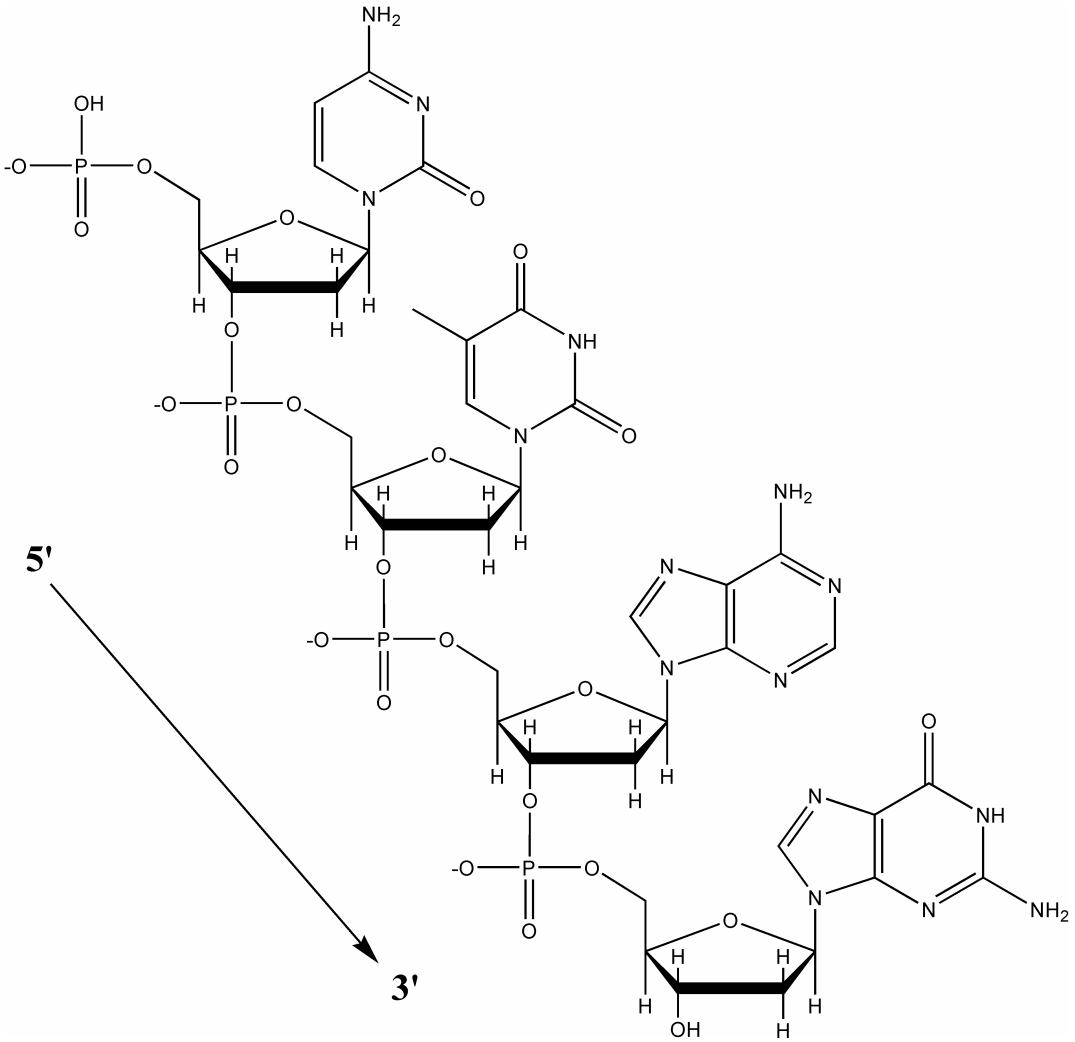

Figure 1.2 The deoxytetranucleotide dCTAG in a chain that extends from the 5′-terminus to the 3′ terminus.

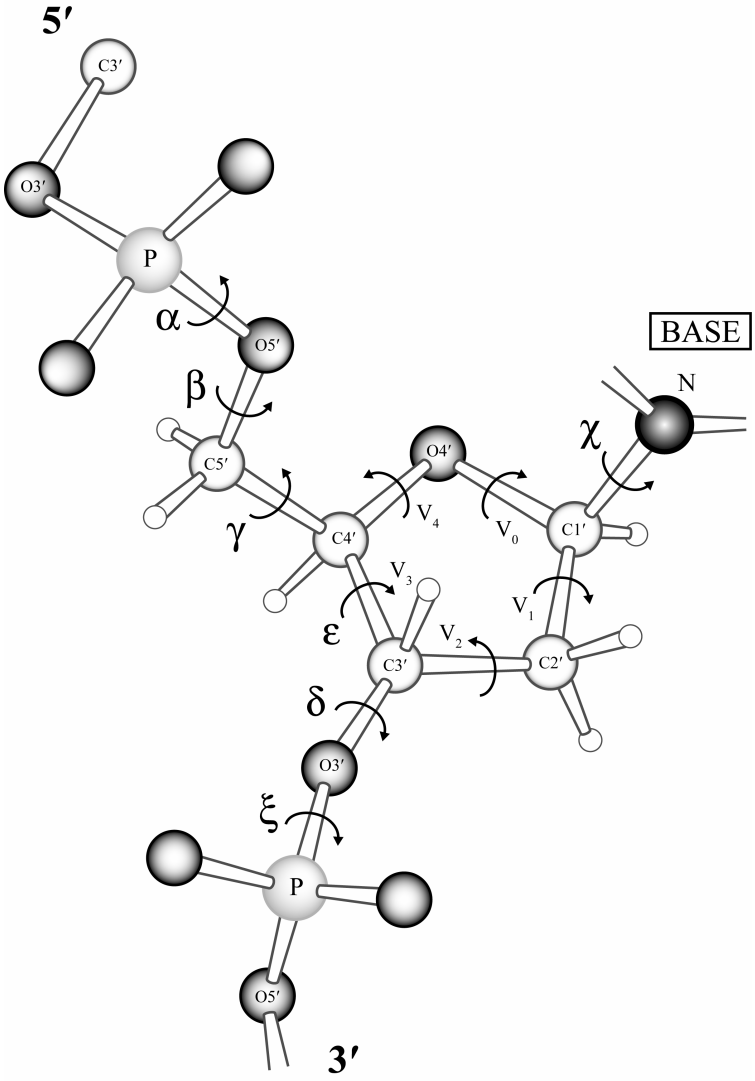

Figure 1.3 The rotatable angles in a nucleotide unit are defined by torsion angles along the phosphoribose backbone (α to ξ), within the sugar ring (v_0 to v_4) as well as the rotation of the nucleobase relative to the sugar (χ). Adapted from (Sriram, 1996).

Of particular importance to DNA structure, are the rotations about the bonds in the sugar ring. In order to relieve steric strain between atoms, the deoxyribose sugar becomes slightly nonplanar with only four out of five atoms remaining in the same plane. The different conformations, termed "sugar puckers", are therefore defined by the direction in which the one atom in the ring deviates from this plane. As illustrated in figure 1.4, a plane is formed by the C1′-O-C4′ atoms. The sugar pucker, then, is defined by the positions of the C2′ or C3′ atoms relative to this plane. When the atoms are displaced from this plane on the same side as the C5′ and the nucleobase, then they are referred to as *endo* atoms, while those on the opposite side are referred to as *exo* atoms. The sugar pucker is conformationally important in DNA because it determines the orientation of the phosphate groups relative to the sugar residue.

The other torsion angle that strongly affects the structure of DNA is the χ-angle around the glycosidic bond (Figure 1.5). The base can be orientated in either the *anti* conformation, where it extends away from the ribose ring, or in the *syn* conformation, in which case the base lies over top or toward the sugar. The *anti* conformation is most often observed since there is less steric hindrance in that position. However, the *syn* conformation may occur when purine bases are present but is rarely observed with pyrimidine bases since the sugar residue sterically interferes with its C2′ substituent.

1.1.2 Structure of Double-Stranded DNA

The interaction of two DNA strands is referred to as hybridization and is mediated through specific base-pairing. First proposed by Watson and Crick, A only pairs with T (AT) and G only pairs with C (GC) (Watson and Crick, 1953). This proposal confirmed earlier observations made by Chargaff that DNA samples always contained equivalent amounts of A to T as well as G to C (Chargaff *et al.*, 1951). The specificity of Watson Crick (WC) base-pairing is achieved through the formation of intermolecular hydrogen bonds between the two DNA strands (Figure 1.6).

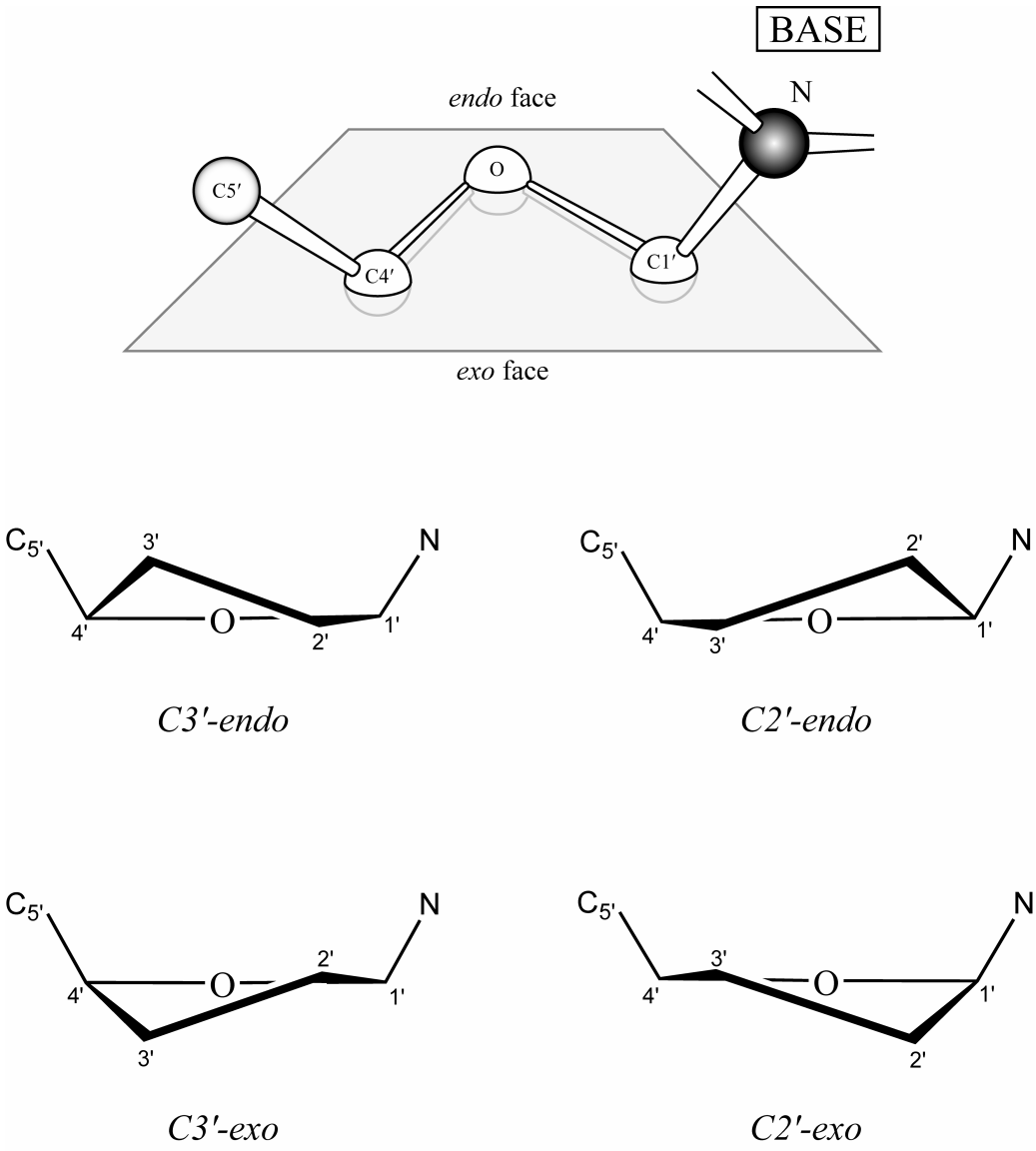

Figure 1.4 The pucker of the sugar in DNA is described as the displacement of the C2′ and C3′ atoms relative to the plane formed by the C1′-O-C4′ plane. The *endo* face lies above the plane, toward the C5′ and the glycosidic bond, while the *exo* face lies below the plane. Adapted from (van Holde, 2006).

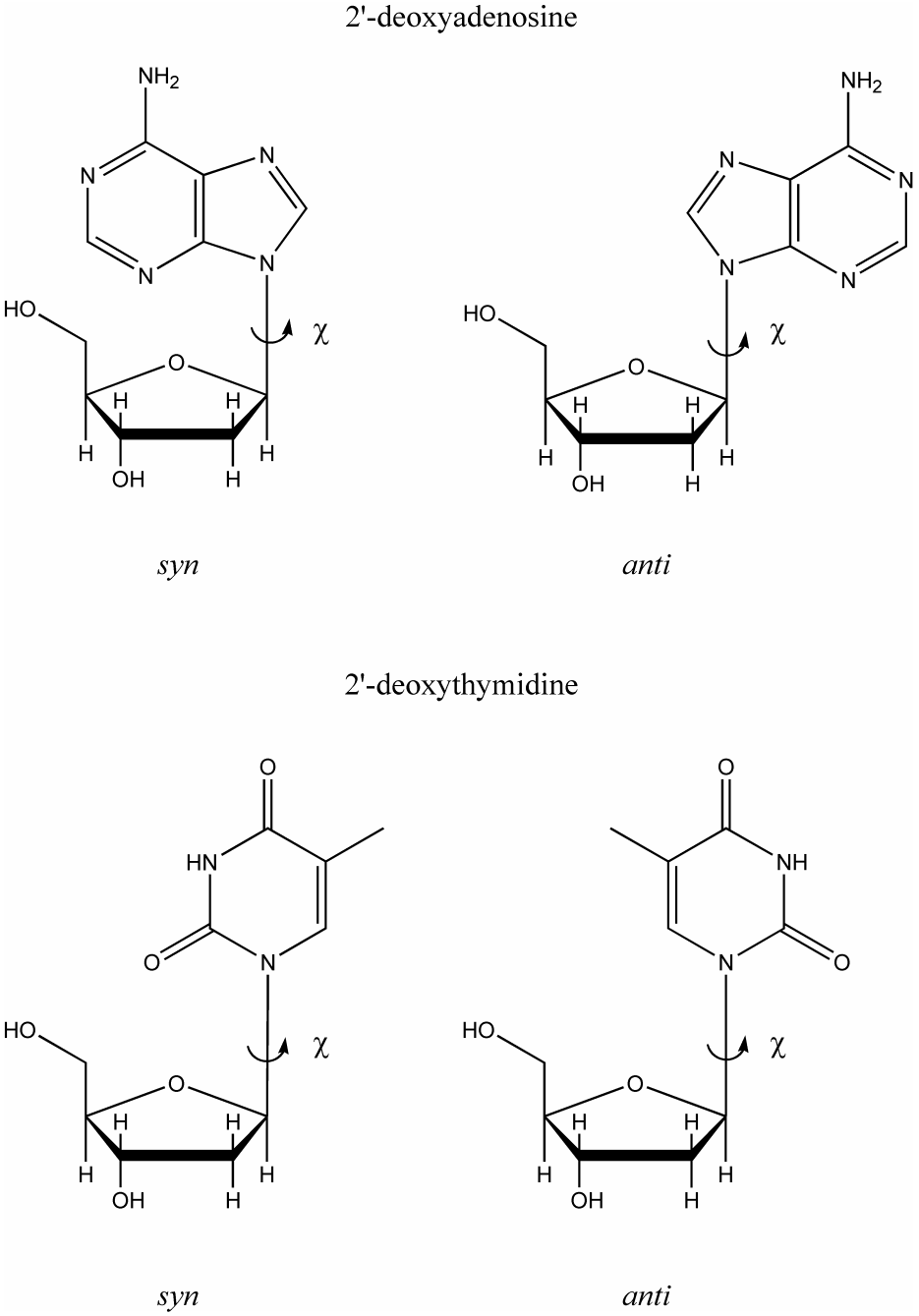

Figure 1.5 The rotations of the nucleotides 2′-deoxyadenosine and 2′-deoxythymine relative to the sugar moiety. The bases are either extended away from the sugar (*anti*-conformation) or situated above the ring (*syn*-conformation).

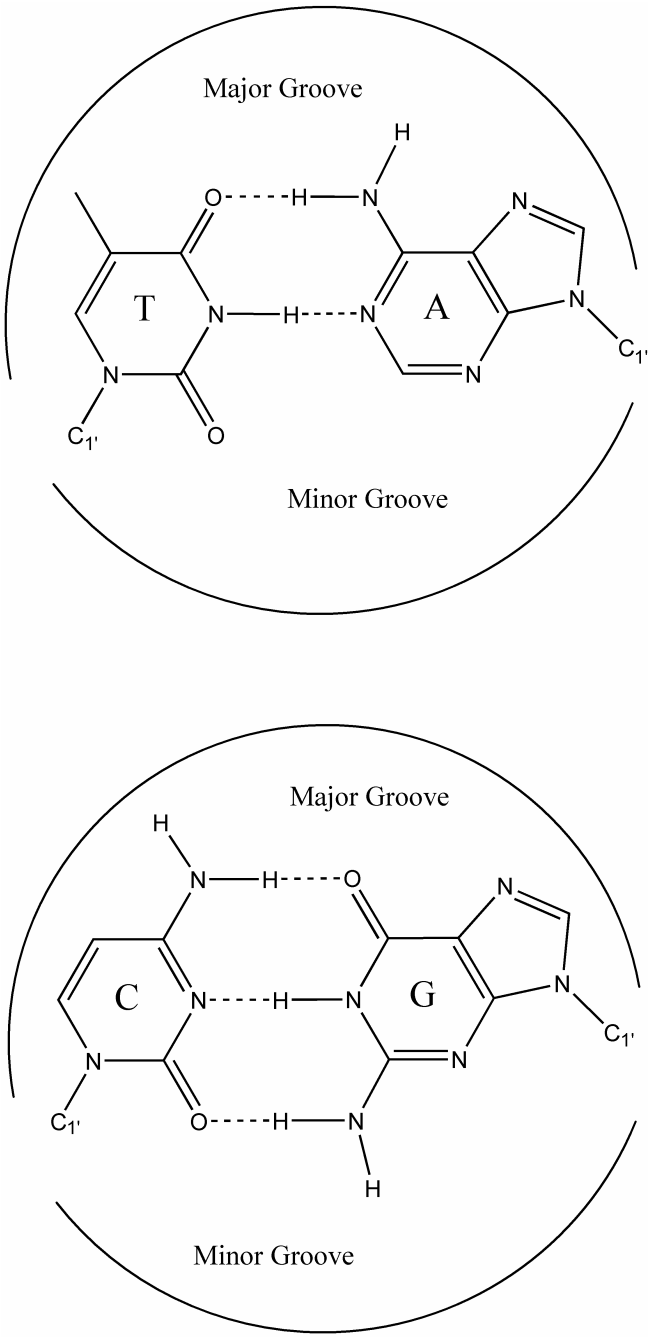

Figure 1.6 The standard WC base-pairing schematic for AT and GC base pairs with the major and minor grooves indicated.

Hydrogen bonds are noncovalent, dipole interactions caused as a result of the attractive force between hydrogen atoms containing a partial positive charge interacting with the electronegative keto oxygens or nitrogens on the complementary base. There are three hydrogen bonds in GC base-pairs and only two in AT base-pairs. However, the classic WC base-pairing is only one of several hydrogen bonding patterns observed. Ten years after Watson and Crick's discovery, Karst Hoogsteen showed that adenine and thymine were able to form hydrogen bonds involving the N7 atom of the purine ring compared to the N1 atom normally found in the WC base-pairing (Hoogsteen, 1963). Although this alternative Hoogsteen geometry is the most favorable one for AT base-pairs in solutions, it is not the cases for double-stranded helices. On the other hand, GC base-pairs are only able to form this geometry in acidic pH where protonation of the C is essential for pairing. However, the four bases can be arranged in 28 different ways where there is still at least two hydrogen bonds maintained. Shown in figure 1.7 are some commonly found conformations including reverse WC, Hoogsteen and Wobble base pairs (Donohue, 1956; Donohue and Trueblood, 1960). The bases can also exist in different chemical isomeric forms. For example, the C6 keto position of guanine can undergo a tautomerization to an enol form with an –OH group at the C6 position.

Although the hydrogen bonding between base-pairs provides specificity, it provides little stability to the duplex as there would be just as many hydrogen bonds between denatured DNA and the solvent. Therefore, it is the base stacking interactions which are principally responsible for the stabilization of the duplex (Bugg *et al.*, 1971). The parallel stacking of the bases effectively excludes water from the interior of the duplex. Therefore the hydrogen-bonding groups are largely sequestered from the competing interactions with water and thus hydrogen bonding becomes more favorable. This parallel stacking of the base pairs also maximizes the van der Waals interactions between bases. Most duplex DNA has the bases separated by 0.34 to 0.37 nm, the average sum of van der Waals radii of the base atoms. Therefore the electrostatic dipole, and dipole-induced dipole interactions associated with the van der Waals interactions allow stable base stacking through the charge distributions within their π-electron systems (Devoe and Tinoco, 1962; Hanlon, 1966).

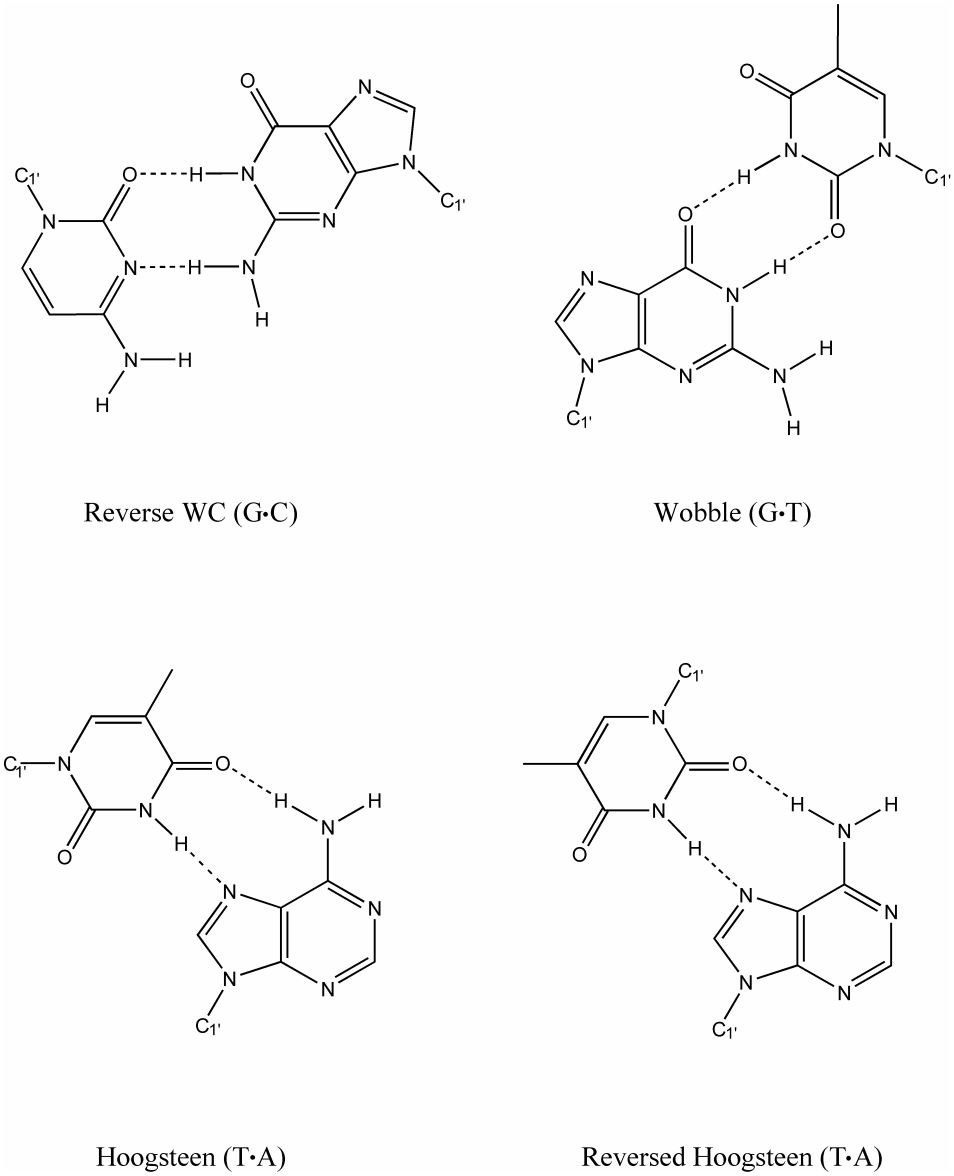

Figure 1.7 Examples of base pairing schemes found in DNA. The top pair represents a reverse WC pair with a 180° rotation of the pyrimidine base resulting in antiparallel orientation of the sugars and a wobble base pair in which the pyrimidine has been shifted slightly resulting in only two hydrogen bonds between the nucleotides. On the bottom is a Hoogsteen base pair in which the pyrimidine uses it WC surface to pair with the C6 amino group and the N7 of the purine base. A 180° rotation of the pyrimidine results in the formation of a reversed Hoogsteen base pair.

Although base pair hydrogen-bonding depends on composition, base stacking energies depend on composition and the sequence of the DNA (Ornstein *et al.*, 1978). For example, in unpaired bases, stacking interactions between purine and pyrimidine bases have the following trend (Solie and Schellma, 1968).

$$\begin{matrix}\text{Pur}\\\text{Pur}\end{matrix} > \begin{matrix}\text{Pyr}\\\text{Pur}\end{matrix} > \begin{matrix}\text{Pyr}\\\text{Pyr}\end{matrix}$$

This results from a greater degree of overlap between two purine bases compared to two pyrimidine bases. For base-paired dinucleotides, although more complex, in general the stacking is more stable for sequences rich in GC base pairs and weaker for those composed of AT base pairs (Ornstein *et al.*, 1978). However, the stacking energy is also influenced by the general sequence. For instance, a 5'dCG-3' dimer is more stable than a 5'-dGC-3' dimer (Saenger, 1984).

The structure of dsDNA is defined by the relative conformations of the bases in the base pair and the orientations of the neighboring base-pairs relative to one another (Figure 1.8). Although all of this flexibility allows DNA to adopt a variety of conformations, the predominant structure found under physiological conditions is the DNA double helix referred to as the B-form. The conformation of B-DNA contains two antiparallel polynucleotide chains connected by complementary WC base-pairing. The overall structure of B-DNA has two distinct helical grooves, the minor and the major. The minor groove is narrow, while the major groove is wide, with both grooves possessing a moderate, nearly equivalent depth. In this fashion, B-DNA adopts a right-handed helical structure containing a hydrophobic interior of base pairs stacked perpendicular to the axis at 0.34 nm intervals (Wing *et al.*, 1980; Dickerson *et al.*, 1982). Each base-pair plane of B-DNA is rotated with a twist of approximately 34.3° relative do the one preceding it. This results in a complete right-handed helical turn for every 10.5 contiguous base pairs and therefore a helical pitch of approximately 3.4 nm (Figure 1.9). In B-DNA, the deoxyribose ring adopts a C2′-*endo* conformation, while the N-glycosidic bond angle is in an *anti*-configuration.

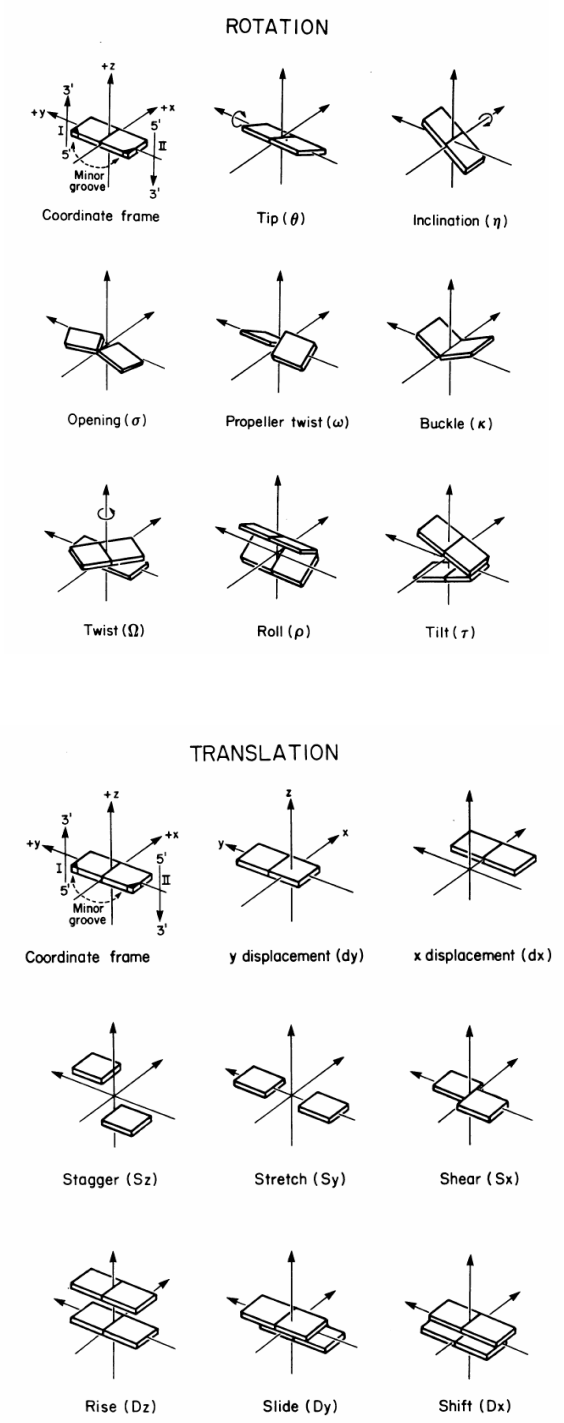

Figure 1.8 Base-pair and base-step parameters for duplex DNA. Taken from (Dickerson, 1989)

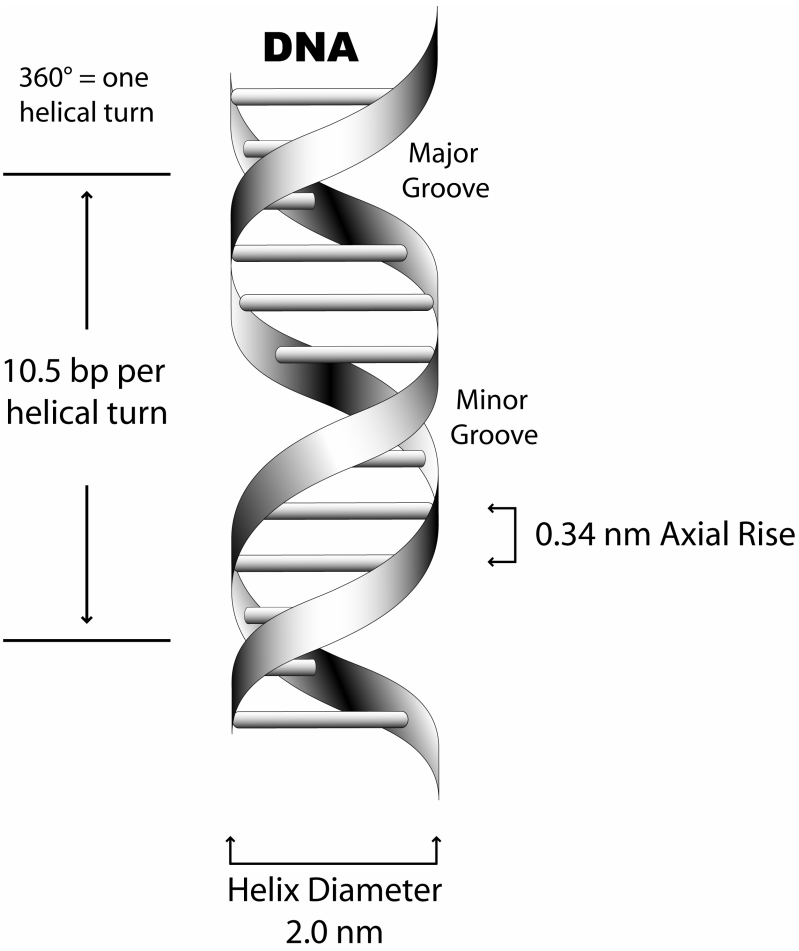

Figure 1.9 The major structural features of a WC base paired DNA duplex in the B-conformation.

1.1.3 Physical Properties of Double-Stranded DNA

The aromatic nature of the bases allows DNA to absorb ultraviolet light (UV) at a wavelength of approximately 260 nm (A_{260}). This allows the concentration of dsDNA to be measured, as an absorbance of 1 A_{260} equals approximately 50 μg/ml. This also provides a convenient way to monitor the formation and breakdown of double helices as dsDNA has 40% less absorbance compared to ssDNA. The decrease in absorbance is a result of the strong overlap between the π-orbitals caused from base stacking interactions which leads to less π- π* transitions and therefore a decrease in molecular absorbtivity (Voet *et al.*, 1963).

The denaturation of DNA is a cooperative process where the strands are either fully formed or completely dissociated (Porschke, 1971). Therefore the observed change in absorbance occurs over a very narrow temperature range at which the midpoint of this transition is referred to as the melting temperature (T_m) (Doty *et al.*, 1959). The nature of this melting transition is affected by several factors including nucleotide composition, chain length and sequence affects. As mentioned previously, stacking interactions are more stable for GC rich regions compared to AT rich regions (Ornstein *et al.*, 1978). Indeed, there is a linear dependence of melting temperature on the number of guanine and cytosine content in the DNA (Marmur and Doty, 1962). The melting temperatures of double-helical nucleic acids increase not only with their GC/AT ratio but also with the length of the polynucleotide. With increasing chain length, T_m increases and the slope at the melting point becomes steeper which is synonymous with enhanced cooperativity (Porschke, 1971; Filimonov and Privalov, 1978). Understandably, the strength of base-stacking mentioned in section 1.12 also correlates very well with the melting of DNA duplexes (Gotoh and Tagashira, 1981).

The renaturation of DNA can be explained by the cooperative zipper mechanism in which the helix requires three base-pairs to create a stable starting point from which further addition of stacked base-pairs occurs spontaneously leading to a stepwise construction of a helix similar to a zipper being closed. (Porschke, 1977). This nucleation event is also sequence dependent. Therefore, since CG base pairs are more

stable than AT base pairs, we expect the nucleation event to be more probable at stacked cytosine or guanine nucleotides.

1.1.4 Electronic Properties of DNA

Soon after the discovery of DNA by Watson and Crick, it was proposed that DNA could have conducting properties though the π- electron system of the staked bases (Eley and Spivey, 1962). In 1993, Jacqueline Barton's group reported photoinduced electron transfer between metallointercalators attached to opposite ends of a 15-base pair DNA duplex (Murphy *et al.*, 1993). Following investigations suggested an electron transfer rate of approximately $1x10^{10}$ s^{-1} over distances up to 40 angstroms (Arkin *et al.*, 1996; Hall *et al.*, 1996). This idea was further substantiated by showing that the repair of a thymine dimer was accomplished through the electron transfer from an intercalator through a 16-base pair DNA duplex (Dandliker *et al.*, 1997). A reevaluation of these results has been given (Fahlman *et al.*, 2002) and although there has been much debate with regards to this subject, the dominant mechanisms appear to be both short-range quantum mechanical tunneling (Dekker and Ratner, 2001) and long-range thermally activated hopping (Kandaswamy and Henderson, 1962; Lewis *et al.*, 2000; Giese *et al.*, 2001). According to many models, the electron transfer can occur through a multistep hopping reaction in which a positive charge migrates between guanine bases having the lowest ionization potential. In this mechanism, there is a shallow distance dependency on the rate of electron transfer. In the tunneling mechanism, the charge tunnels through high energy bases without formally occupying them, in which cases the rate decreases exponentially with distance between the charge donor and acceptor (Giese, 2002).

Although there is agreement that electron transfer indeed happens through DNA, there is still debate on whether DNA is intrinsically conducting. DNA electrical properties remain questionable due to the uncertainty in experimental procedures. For example, the contacts between the electrode and the DNA molecules will most likely affect the total conductivity of the DNA-electrode system (Otsuka *et al.*, 2002). Also, there are many differences in the DNA molecules and their environment which can

influence DNA conductivity. For instance, variations in the base composition and sequence may have consequences as it has been shown that positive charge is more stable on a GC base pair compared to an AT base pair (Endres *et al.*, 2004). The length and the character of the DNA molecules (bundles or single molecules) also will affect the conductivity. Temperature and humidity may change the conformation of DNA as the number of water molecules is critical in determining the overall structure of the DNA. For example, drying of the DNA with nitrogen tends to leave only two to three water molecules per nucleotide. This results in a transition from B- to A-DNA (see later section) (Warman *et al.*, 1996). As well, the presence of tightly bound water or counterions attached to the DNA even in vacuum environment can not be completely ruled out and may lead to the enhanced conductivity (Fink and Schonenberger, 1999). In conclusion, it seems that electron transfer is possible for short scale length under certain conditions. However, it is still unclear whether DNA itself is the conductor or if it needs help from the solvent to become conductive.

1.2 DNA-Metal Ion Interactions

Many factors affect DNA-metal interactions including the nature of the ligand and the metal ion, the pH of the surrounding environment as well as the accessibility of certain binding sites. Such interactions are very important as it has previously been shown that metal ions can dramatically affect both the stability and conformation of DNA (Kazakov, 1996). In many cases, completely new structures are formed which possess very unique and useful properties.

1.2.1 Interaction Sites on DNA

At physiological pH, the negative charge on the phosphate oxygens result in an ideal location for nonspecific electrostatic interaction with positively charged metal ions. Although all metal ions can typically bind here, Pearson generalized that metal ions which are more difficult to polarize such as the alkali and alkaline earth metals

Na^+, K^+, Mg^{2+}, Mn^{2+} and Ca^{2+} have a greater preference for these oxygen ligands (Pearson, 1963).

For many other metal ions, initial nonspecific binding can be followed by more specific interactions with the nitrogen and exocyclic keto substituents on the nucleobases. Generally, metal ions that have a larger radius and are easier to polarize, such as the transition metals Cu^+, Ag^+, Au^+, Cd^+, Pt^+ and Hg^+, tend to favour more covalent interactions with the nucleobase substituents (Pearson, 1963). However, there are also some transition metals such as Cu^{2+}, Zn^{2+}, Ni^{2+} and Co^{2+} that can bind equally well to both ligands (Cowan, 1997).

The association of metal ions with the nitrogens in the nucleobases is much more complex as there are many factors that can influence the availability of the metal ion binding sites. For example, the formation of the glycosyl link in DNA renders the N9 of purines and the N1 of pyrimidines unavailable. As well, the N3 position on the purine bases becomes less attractive due to the steric hindrance created from the sugar moiety when orientated in the *syn* conformation. Changes in the glycosidic torsion angle could, however, make this site more attractive for metal ions (Martin, 1979).

As well, since the ring nitrogens are potential protonation sites, the pH of the surrounding environment is quite relevant to the availability of binding sites for metal ions. Therefore a preference for metal ions to interact with these sites correlates closely to the pK_a values shown in parenthesis. At neutral pH, the principle metal-binding sites are on the nucleosides of guanosine (N7, 2.0), adenosine (N7 and N1, 3.8) and cytidine (N3, 4.2). However, at elevated pH, the nitrogen atoms in thymidine (N3, 9.9) and guanosine (N1, 9.3) become the preferential binding sites (Martin, 1979).

The base keto substituents are also able to complex with metal ions directly through the keto group or indirectly through the interaction of hydrogen bonds from other ligands (Saenger, 1984). The amino groups on the bases are not directly involved in metal ion coordination because the lone electron pair is delocalized over the π-bonding ring system giving the attached nitrogen a partial positive charge and thereby effectively repelling any positively charged metal ions from this location (Martin, 1979).

1.2.2 Effect of Metal Ions on DNA Stability

Although most metal ions can stabilize double helixes, this property is not universal. Generally, an interaction of metal ions with the phosphate backbone leads to stabilization of the DNA double helix whereas metal ions binding to the bases causes destabilization and eventual denaturation (Eichhorn and Shin, 1968; Yamada *et al.*, 1976). Therefore, metal ions can be placed in the following sequence which indicates the magnitude of their influence on DNA stability (Eichhorn and Shin, 1968).

$$Mg^{2+} > Co^{2+} \sim Ni^{2+} > Mn^{2+} > Zn^{2+} > Cd^{2+} > Cu^{2+} > Hg^{2+}$$

The affinity for the base compared to the phosphate backbone increases from left to right. Therefore, correspondingly, the first three metal ions in this list usually provide only stabilizing effects, whereas the others provide an initial stability as they bind the backbone followed by destabilization of the double helix at higher concentrations where they bind to the nucleobase (Eichhorn, 1973).

1.2.3 Alternative DNA Conformations Containing Metal Ions

Although the standard structure of DNA is in the B-form, there is an alphabet of alternative structures and conformations that are all heavily influenced by metal ions (Saenger, 1984; Wells *et al.*, 1988; Ghosh and Bansal, 2003). Since A-DNA and Z-DNA conformations are currently the best characterized, these will be discussed in further detail. Along with the linear duplexes described above, DNA can also adopt various other unusual structures such as triplex and quadraplex DNA structures consisting of three and fours strands of DNA respectively. Finally, there will be a review of DNA containing novel nucleotide analogues which have been engineered specifically to incorporate various metal ions.

1.2.3.1 A-DNA

B-DNA transforms into an A-form helix under low humidity and high salt concentrations (Franklin and Gosling, 1953). Although A-DNA is still a right handed helix, there are 11 base-pairs per helix turn with a rise of 0.25 nm per base pair, a helical pitch of 2.8 nm and a diameter of 2.3 nm resulting in a shorter, broader version of B-DNA as illustrated in figure 1.10 (Dickerson *et al.*, 1982; Frederick *et al.*, 1989). The most pronounced feature of this structure is the 20° tilting of the base-pairs and their net displacement away from the central axis (Sinden, 1994). This results in a deep and narrow major groove and a very shallow and wide minor groove. Looking down the central axis of A-DNA there is hollow core distinctly different from that of B-DNA. The A-form also adopts a C3′-*endo* sugar pucker conformation as opposed to the C2′-*endo* conformation present in B-DNA. The A-form is also commonly adopted by RNA-DNA hybrids (Milman *et al.*, 1967) as well as dsRNA (Arnott *et al.*, 1973) as the C2'-OH substituent forces the sugar to assume the C3'-endo conformation.

1.2.3.2 Z-DNA

A drastic conformational change was detected by circular dichroism with poly[d(GC)] in the presence of 700 mM Mg^{2+} or 2.5 M Na^{+} (Pohl and Jovin, 1972). Following this discovery, a crystal structure was solved and showed major structural differences in the sugar pucker, rotations about the glycosidic bond, and orientation of base pairs within the helix compared to the native B-DNA form (Wang *et al.*, 1979). The newly-discovered structure, called Z-DNA, was discovered with its unique ability to adopt a left handed helical structure. This conformation contains a wide and shallow major groove with a narrow and extremely deep minor groove. Z-form DNA also adopts sugar puckering and N-glycosidic torsion angles that alternate between C2′-*endo* and C3′-*endo* and between *anti* and *syn*, respectively making the actual repeating unit for the Z-form helix two base pairs in contrast to the single-base-pair repeat unit of the A- and B- form DNAs.

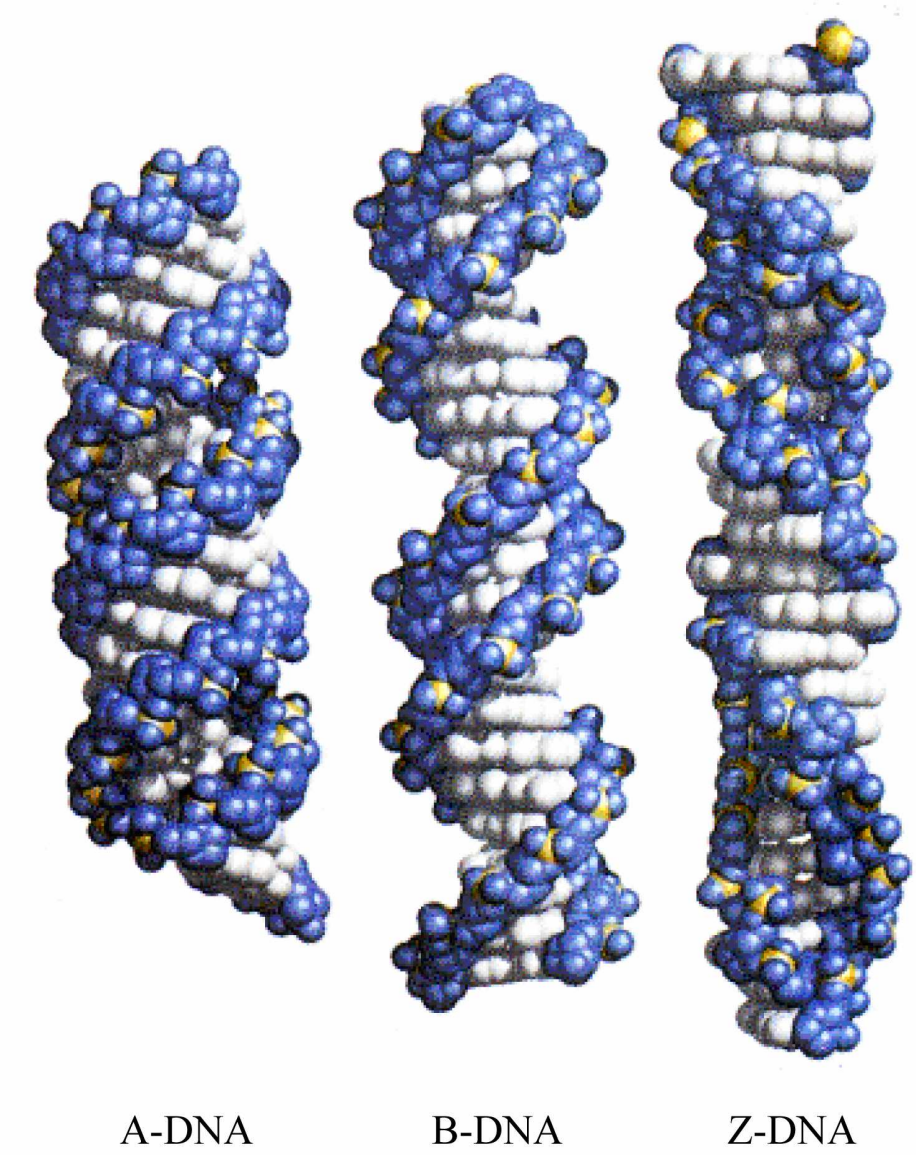

Figure 1.10 A Comparison of the overall structures of A, B and Z forms of DNA. There are 24 base pairs in each of the structures shown. The bases are shown in gray, the phosphate atoms in yellow, and the riboses and phosphate oxygens in blue. Taken from (Lehninger, 1993)

The alternating pattern, in combination with the 180° rotation of the bases about the glycosidic bond, results in a left handed helix with a phosphate backbone that appears to zigzag around the helical structure. There are 12 base pairs per helical turn, a helical rise of 0.37 nm per base and a helical pitch of 4.5 nm resulting in a longer narrower version of B-DNA (Figure 1.10). Although there is an increase in the rise per residue, the alternating sugar puckers orientate the phosphate residues of subsequent bases so that they are actually closer to each other than in B-DNA. Therefore, the proximity of the negatively-charged phosphate residues explains the dependence on the high ionic strength needed to stabilize this conformation (Sinden, 1994).

Although, the Z-DNA conformation can be induced by high concentrations of both Mg^{2+} and Na^{+} as previously mentioned, less than 5 mM of transitions metals such as Co^{2+}, Ni^{2+} or Mn^{2+} is required to obtain the same response (van de Sande *et al.*, 1982). Whereas alkaline and alkali-earth metals are able to stabilize the conformation by binding to the negatively charged phosphate groups, transition metal ions bind to the bases. For instance, previous investigations have shown that both Ni^{2+} and Co^{2+} are able to bind to the N7 of G stabilizing the *syn* conformation which is required for Z-DNA (Taboury *et al.*, 1984).

This conformation can also be induced or further stabilized by chemical modification of the bases. Bromination of the G residues on C8 or the C residues on the C5 both lock the molecule in the Z conformation as the new bulky substituent holds the G residue in the *syn* conformation preventing its rotation back to the *anti* conformation found in B-DNA (Moller *et al.*, 1984). The methylation of C8 of G residues also favours the Z conformation (Xu *et al.*, 2003). The methylation of cytosine at the C5 position also stabilizes Z-DNA as the hydrophobic methyl group in this position is less exposed to the solvent in the Z-DNA form than in the alternative B-form (Behe and Felsenfeld, 1981; Rich *et al.*, 1984).

The discovery that Z-DNA forms under conditions of negative superhelical stress (Klysik *et al.*, 1981; Peck *et al.*, 1982; Singleton *et al.*, 1982) raised excitement as it suggested the existence of Z-DNA in a biological context as negative supercoils form behind actively transcribing RNA polymerase (Liu and Wang, 1987). A number of experiments have been performed that demonstrate the existence of Z-DNA *in vivo*.

For example, the formation of Z-DNA in *E. coli* was assessed by creating fragments of DNA containing the *Eco*RI site. In the presence of *Eco*RI methylase, this fragment becomes methylated when the DNA is in the B- conformation. However, when the DNA is in the Z- conformation, this fragment becomes resistant to methylation (Jaworski *et al.*, 1987). Evidence for the existence of Z-DNA in eukaryotic systems is more indirect. Antibodies against Z-DNA have been shown to bind to eukaryotic chromosomes and proteins have been isolated from eukaryotic systems that are able to bind Z-DNA (Herbert and Rich, 1996; Rich and Zhang, 2003). Various possible biological roles have been suggested. For instance, Z-DNA may function to regulate gene expression as it could act as an alternative binding location for transcription factors. Also, the conformation may be important in recombination as alternating purine•pyrimidine tracts, which are very conducive to forming Z-DNA, have been found in recombination sites.

1.2.3.3 Triplex

In 1957, it was discovered that a WC duplex consisting of homopurine•homepyrimidine tracts had the ability to incorporate an additional third strand into the major groove (Felsenfeld *et al.*, 1957). Shortly after, a crystal structure was solved by Karst Hoogsteen which revealed that triplex formation was possible through the interaction with the N7 and C6 amino group of a purine base (Hoogsteen, 1963). This type of base interaction, referred to as Hoogsteen base-pairing, is shown in figure 1.7. In order for triplex formation to occur, the central strand must be a purine to provide the necessary sites for a WC base-pair and an additional Hoogsteen base-pair as illustrated in figure 1.11. The additional third strand, which is written in italics, may consist of either pyrimidines (PyPu•*Py*) or purines (PyPu•*Pu*) (Frank-Kamenetskii and Mirkin, 1995). If the third strand consists of a pyrimidine tract, it will form Hoogsteen bonds which result in a parallel orientation with the WC purine strand. As demonstrated in figure 1.11, if the third tract is purine rich, it forms reverse Hoogsteen hydrogen bonds resulting in an antiparallel orientation with the purine strand of the WC helix.

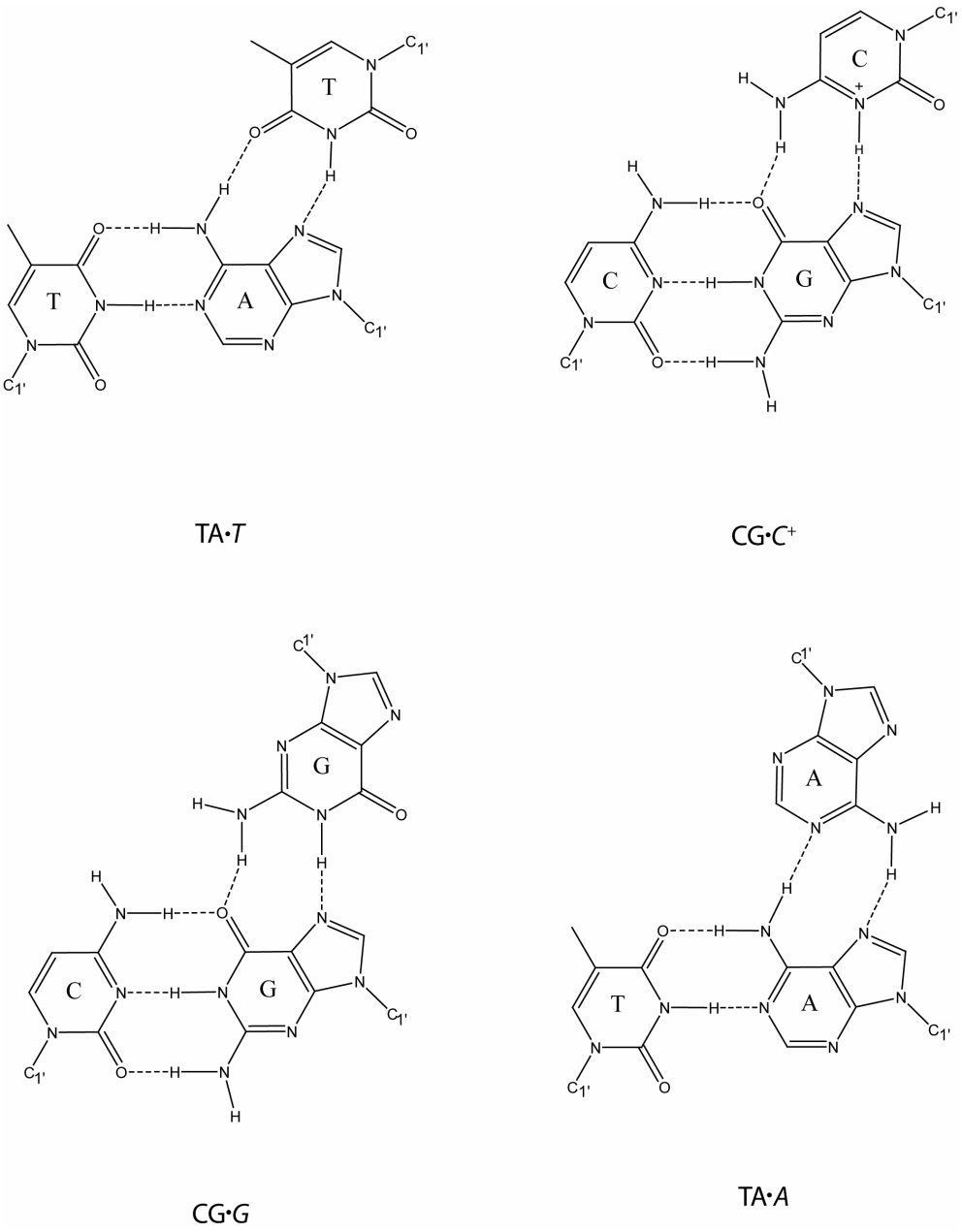

Figure 1.11 Hydrogen bonding pattern of the various triplex formations. Shown on the top are WC base-pairs containing a third pyrimidine strand and on the bottom, WC base-pairs contain a third purine residue.

In either case, the third strand always runs anti-parallel to the WC strand with the same type of base. As previously discussed with the above DNA conformations, triplex formation is also dependent on metal ions, pH, sequence effects and the incorporation of novel nucleotides.

Compared to dsDNA, triplexes have a relatively higher charge density and therefore require metal ions to stabilize the triplex by neutralizing the negatively charged phosphate groups. However, it is evident that the relationship is much more complex as different metal ions have drastically different effects on triplex formation, conformation and stability. For example, alkali metal ions are sufficient for the stabilization of PyPu•*Py* triplexes, however PyPu•*Pu* triplexes require divalent metal ions such as Mg^{2+} or Ca^{2+} for complete stabilization (Rougee *et al.*, 1992; Singleton and Dervan, 1993). Also, other metal ions like K^{+} and Rb^{+} interfere with PyPu•*Pu* triplex formation all together (Cheng and Van Dyke, 1993). In contrast, the transition metal ions Zn^{2+}, Ni^{2+}, Co^{2+}, Mn^{2+} and Cd^{2+} enhance the stability of the structures containing both the CG•*G* and TA•*T* triplets (Malkov *et al.*, 1993).

Triple-stranded DNA formation is also affected by pH as well as the incorporation of novel nucleotides. For instance, both CG•C^{+} and CG•A^{+} triplexes are stabilized at low pH since the protonation of the C or A residue enables the bases to participate in the Hoogsteen base-pairing (Lee *et al.*, 1979). On the other hand, substitution of 7-deazaadenine ($z^{7}A$) or 6-methyladenine ($m^{6}A$) with A in the central strand renders triplex formation impossible as it eliminates the essential hydrogen bonds needed for Hoogsteen interactions (Lee *et al.*, 1984).

Initial investigations showed triplexes containing three separate polynucleotide strands. However, it was later suggested (Lee *et al.*, 1984) and demonstrated that it was possible to form intramolecular triplexes from a double-stranded helix (Mirkin *et al.*, 1987; Kohwi and Kohwi-Shigematsu, 1988). This type of triplex structure was referred to as H-DNA as initial results showed the formation occurred at low pH. Alternatively the name originated because the structure involved Hoogsteen base-pairs. Regardless, in order for a dsDNA sequence to form H-DNA, it must contain mirror repeats of Py-Pu (Lyamichev *et al.*, 1985; Lyamichev *et al.*, 1986).

As is apparent from figure 1.12, due to the presence of the mirror repeat, there are four possible ways for a given intramolecular triplex to form.

Although any of the four intramolecular triplex structures are possible within a given mirror repeat, the conditions under which each one forms varies. Formation of Hy3 GC•C^+ triplex by $d(G)_{30}$•$d(C)_{30}$ at acidic pH can be converted to Hu3 GC•*G* by addition of Mg^{2+} or by increasing the pH (Kohwi and Kohwi-Shigematsu, 1988). Thus, as with intermolecular triplexes, formation of H-DNA can be modulated by adjusting the pH, the addition of different metal ions and changing the DNA sequence.

As discussed above, PyPu•*Py* triplexes are formed under acidic pH, while PyPu•*Pu* triplexes require divalent cations. However, under neutral pH, there is unlikely such a high level of metal ions in solution. One alternative method of stabilization for both inter- and intramolecular triplexes was from polyamines spermine and spermidine. This stabilizing effect was most likely a result of the decreased repulsion between the phosphate backbones after binding to polyamine (Hampel *et al.*, 1991).

The widespread occurrence of polypurine•polypyrimidine tracts in the eukaryotic genome (Birnboim, 1978) combined with ability of intramolecular triplex formation to occur within a single duplex DNA region (Mirkin *et al.*, 1987), have sparked great interest towards what potential role triplexes might have on biological functions. Initial experiments showed that GATC *dam* methylation sites adjacent to or between intramolecular-triplex forming regions were under-methylated *in vivo* (Parniewski *et al.*, 1990). Also, triplex-specific monoclonal antibodies, Jel 318 and Jel 466, have been shown to bind the cell nuclei and chromosomes. The binding could be inhibited by adding competing triplex DNA, but not by the addition of *E. coli* DNA to which the antibodies will not bind (Lee *et al.*, 1987; Agazie *et al.*, 1994; Agazie *et al.*, 1996).

Intramolecular triplex DNA could influence gene expression by affecting the level of DNA supercoiling (Sinden, 1994). The duplex to triplex transition could also act as a molecular switch by regulating which proteins are able to bind (Lee *et al.*, 1984). As well, studies have indicated that triplexes may act as a termination site for DNA replication both *in vitro* and *in vivo* (Baran *et al.*, 1991; Rao, 1994).

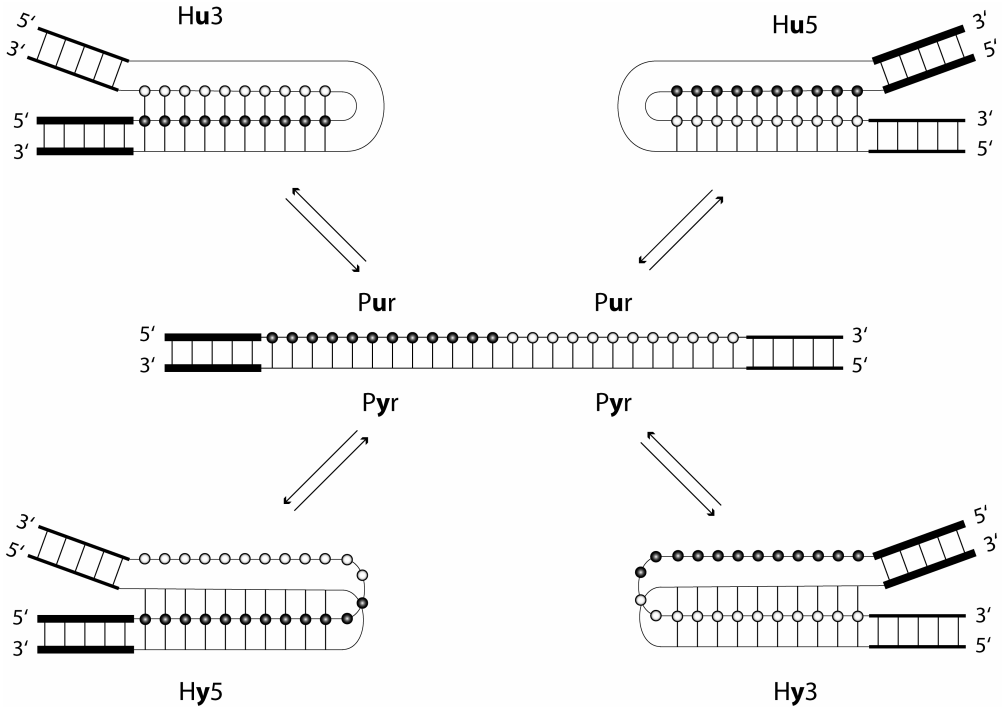

Figure 1.12 The various folding patterns adopted for intramolecular triplex formation. There are four possible isomers labeled Hu3, Hu5, Hy5 and Hy3. In all instances, the H refers to H-DNA, which is the term coined by (Mirkin *et al.*, 1987) to represent intramolecular triplex structures. The y and u represents a pyrimidine or purine rich region respectively acting as the third strand. The number 5 and 3 refers to which end (5' or 3') of the purine or pyrimidine-rich strand is acting as the third strand. Adapted from (Sinden, 1994).

1.2.3.4 Tetraplex

Oligonucleotides containing guanine rich sequences are able to adopt novel conformations in the presence of monovalent cations. The fundamental structural unit consists of four guanines arranged in a planar configuration (Figure 1.13a). Each guanine interacts with each of the two adjacent guanines through Hoogsteen-like hydrogen bonds where the N1-H and N2-H of one guanine pair with the N7 and O6 of the neighboring guanine (Gellert *et al.*, 1962; Fresco and Massoulie, 1963; Zimmerman, 1976). It has previously been shown that the alkali-metal cations were able to promote and stabilize such conformations (Pinnavaia *et al.*, 1978). As can been seen from figure 1.13a, the G-quartet has four oxygen atoms clustered in its center. Therefore, it is logical that cations will not only stabilize this structure, but without a bound cation in this cavity, the cyclic arrangement would be electronically unfavorable and would collapse (Spackova *et al.*, 1999; Sessler *et al.*, 2000). In particular, Na^+, K^+ and Rb^+ all were able to promote this conformational change while Li^+ and Cs^+ showed almost no ability to do so. It was also found that Ca^{2+} and Ba^{2+} are even more effective at stabilizing polypurine tetraplexes (Lee, 1990). Therefore, it can be seen, that the cavity made by the G-guartet is size discriminatory. If an ion is too large it is excluded sterically and if it is too small it is unable to bridge the distance between the ligand residues in the cavity. Although G-quadraplexes are made from the same basic structural subunit, they can differ in their orientation. As shown in figure 1.13b, tetraplex formation may occur either as a parallel intermolecular association of four separate strands (Sen and Gilbert, 1988; Sen and Gilbert, 1990) or as an association of two hairpin-forming strands (Sundquist and Klug, 1989) or as a single strand that is folded back on itself to comprise three loops (Williamson *et al.*, 1989). In the proposed models, the strands are either parallel to each other in which all of the glycosidic torsion angles adopt the same *anti* orientation within the tetrad or antiparallel to each other in which case the glycosidic bonds alternate between *syn* and *anti* orientations along each strand of the quartet (Zimmerman *et al.*, 1975; Sundquist and Klug, 1989).

A

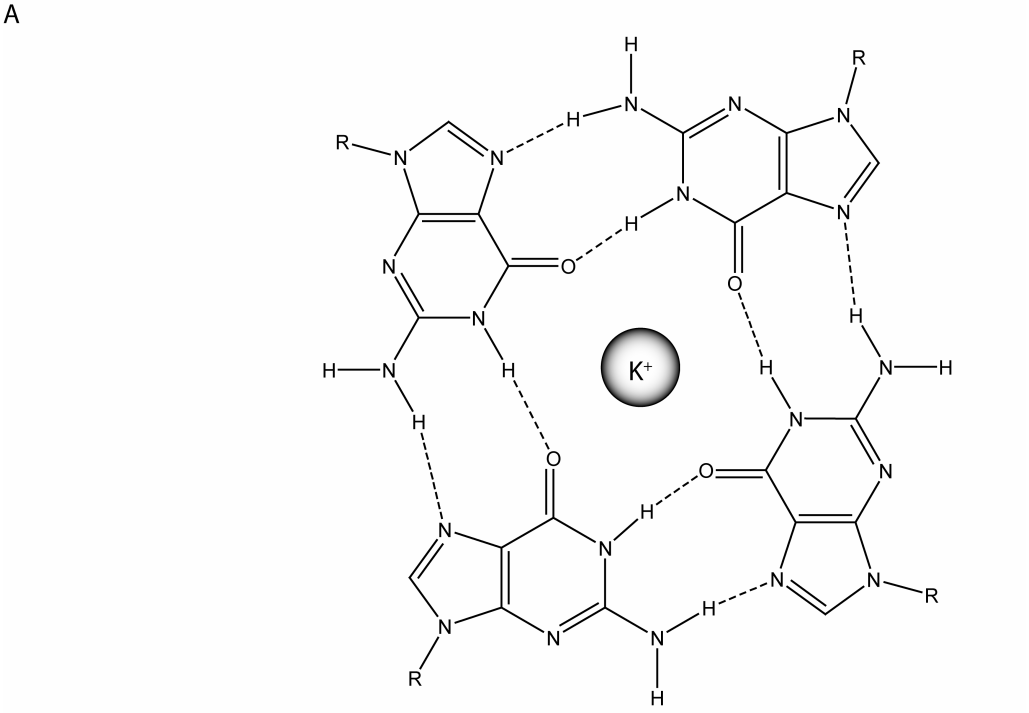

B

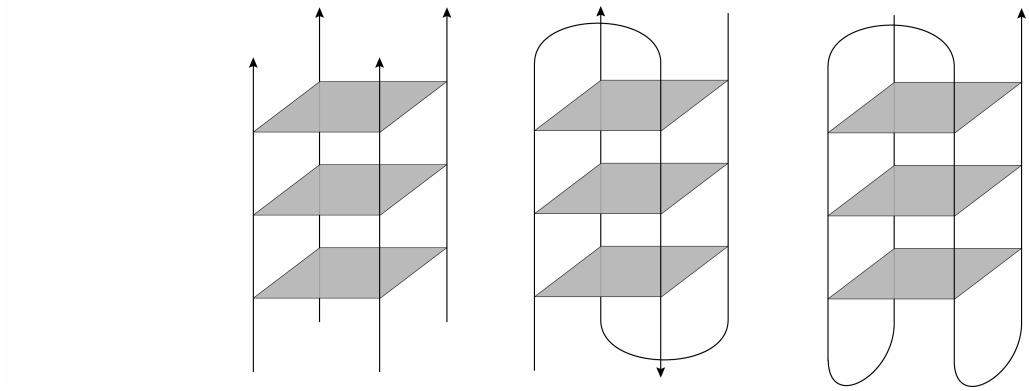

Figure 1.13 **A)** Guanine tetraplex shown with a coordinated potassium ion. **B)** Tetraplex formation can occur through a number of different oligoguanine associations. Four separate strands can assemble as a parallel-stranded tetraplex. Oligonucleotides containing two oligoguanine repeats can form hairpin structures (only one example of this isomer is shown). A single strand containing a number of oligoguanine repeats could also adopt a foldback structure (only one possible isomer shown).

The presence of G-rich sequences found in eukaryotic centromeres and telomeres suggest a fundamental role of quadraplex formation in these regions. Formation of quadraplexes has been shown to inhibit telomerase (Zahler *et al.*, 1991) and have been suspected in playing a role in tethering of chromosomes for meiosis (Sen and Gilbert, 1988).

1.2.3.5 Synthetic Metallized DNA

It was realized that metal interaction with DNA not only provided stabilization and conformational changes, but also improved the conductivity of native DNA. Therefore, there has been a growing interest to broaden the structural variety of DNA and to change its natural structure to incorporate metal ions. This has led to some promising new approaches including structural changes to the bases as well as the incorporations of completely new base pairs (Braun *et al.*, 1998; Aich *et al.*, 1999; Tanaka and Shionoya, 1999; Meggers *et al.*, 2000; Atwell *et al.*, 2001; Weizman and Tor, 2001; Zimmermann *et al.*, 2002; Tanaka *et al.*, 2003).

In order to incorporate metal complexes into oligonucleotides the hydrogen-bonding usually seen in WC base pairing is replaced by metal–assisted base pairing through the use of artificial nucleosides such as o-phenylenediamine, catechol or 2-aminophenol shown in figure 1.14a (Kawasaki *et al.*, 2000; Tanaka *et al.*, 2001; Tanaka *et al.*, 2003). Ligandosides, such as 2,2'-Bipyridine in figure 1.14b, also have a higher affinity for metal ions compared to the regular heterocyclic bases and are able to form complexes with comparable dimensions to a DNA base pair (Weizman and Tor, 2001). Alternative approaches shown in figures 1.14c and 1.14d respectively include the design of a base pair between pyridine-2,6-dicarboxylate nucleobase (Dipic) and a pyridine nucleobase (Meggers *et al.*, 2000) as well as artificial guanine which can still bind effectively to cytidine (Mancin and Chin, 2002). However, such strategies represent a significant synthetic challenge. As well, drastically changing the structure to incorporate metals may improve the conductivity, but it may unfortunately destroy the desirable molecular recognition properties of DNA.

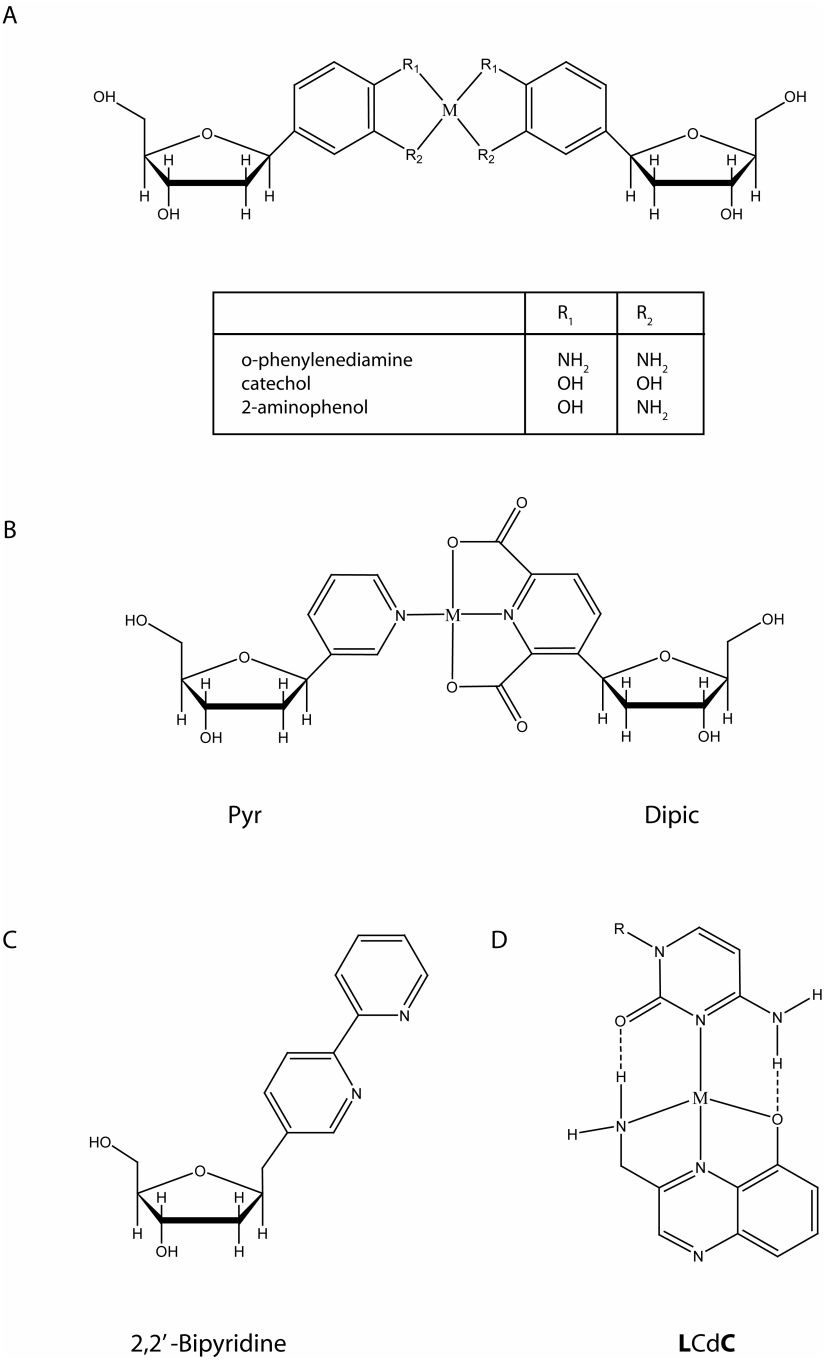

	R_1	R_2
o-phenylenediamine	NH_2	NH_2
catechol	OH	OH
2-aminophenol	OH	NH_2

Figure 1.14 Alternative DNA bases to allow the incorporation of metal ions. Adapted from (Tanaka and Shionoya, 1999; Tanaka *et al.*, 2001; Tanaka *et al.*, 2003; Tanaka *et al.*, 2002; Weizman and Tor, 2001; Meggers *et al.*, 2000; Mancin and Chin, 2002.)

A promising alternative is a new metal-DNA conformation discovered at the University of Saskatchewan by Dr. Jeremy Lee called M-DNA.

1.3 M-DNA

1.3.1 Structure

M-DNA is considered a modified B-type helix of duplex DNA in which metal ions such as Zn^{2+}, Ni^{2+} and Co^{2+} replace the imino protons of G and T at every base pair (Lee *et al.*, 1993; Aich *et al.*, 1999). The coordination of the metal ion is distorted square planar with the solvent providing the fourth ligand. Although unusual, a propeller twist of the bases could give rise to this geometry. From electrophoretic mobility assays, it can be estimated that this new helix is shorter and more compact than B-DNA containing approximately 5% fewer base pairs per turn. Although not all of the features of the usual Watson-Crick base pairs are retained in the structure of M-DNA, A still pairs with T and G with C (Lee *et al.*, 1993) (Figure 1.15).

In the presence of Zn^{2+} at pH 9.0, Calf Thymus (CT) DNA shows an increase in melting temperature of approximately 12 degrees compared to DNA in the absence of metal ions. Since previous research shows a destabilizing effect caused by zinc (Eichhorn and Shin, 1968), this unexpected stabilization may suggest that a possible metal ion complex or structural rearrangement is occurring.

There are several results that indicate M-DNA formation involves the replacement of the imino protons of both G and T with divalent metal ions. The H^1 NMR imino proton signal for $d(TG)_{15} \bullet d(CA)_{15}$ disappears in the presence of 2.4 mM Zn^{2+} at pH 9.0 which is equivalent to one metal ion per base pair (Lee *et al.*, 1993). As well, titration experiments also revealed that one proton is being released per metal ion per base pair upon Ni^{2+} M-DNA formation (Aich *et al.*, 1999). Not only is the high pH reflective of the high pKa for the imino proton on G and T, but results also indicate that by reducing the base pKa, M-DNA formation is able to occur at a lower pH as well (Wood *et al.*, 2002).

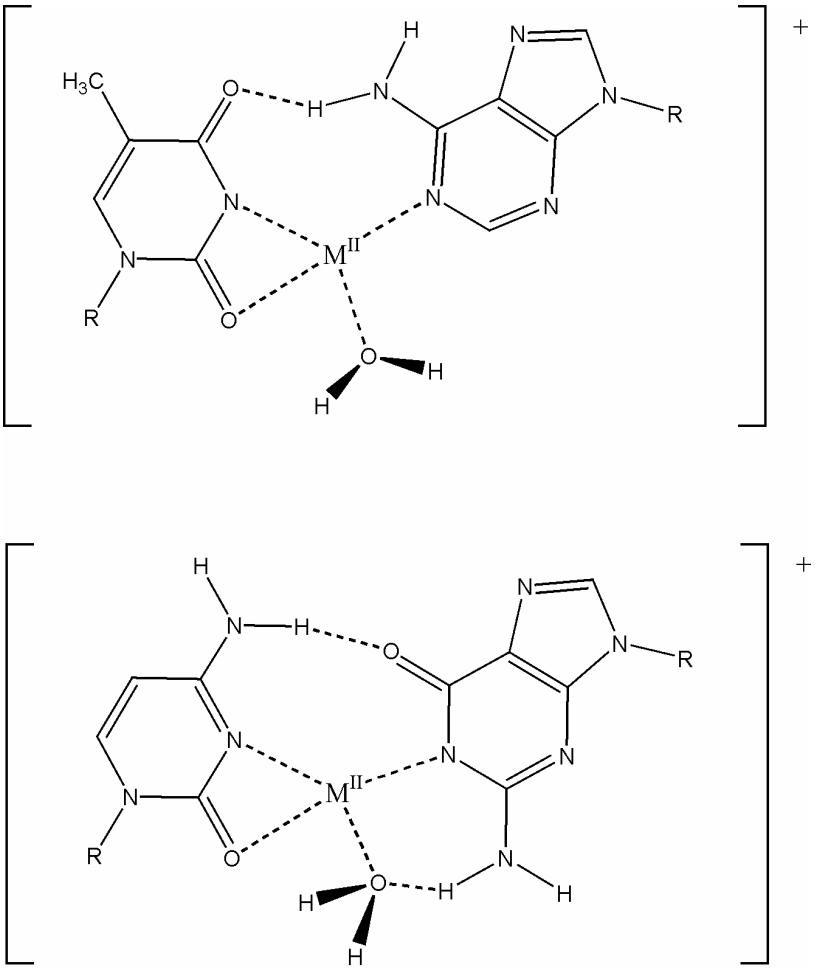

Figure 1.15 Proposed structures for the base pairs of M-DNA where M represents the Co^{2+}, Ni^{2+} or Zn^{2+} and R represents the atom C1' of the 2'-deoxyribose sugar. Adapted from (Aich *et al.*, 1999)

Bacterial DNA ranging in various GC content shows M-DNA formation at equivalent rates demonstrating formation is independent of DNA composition. However, a large degree of sequence dependence is observed in synthetic polymers with a repeating sequence. The effect of different repeating sequences on the rate of Zn^{2+} M-DNA formation was measured and it was determined that $d(TG)_n \bullet d(CA)_n$ was fully formed the quickest whereas $d(AT)_n$ remained mostly in the B-DNA conformation even after one hour (Lee *et al.*, 1993).

A second critical experiment was performed using the intercalator, ethidium bromide (EtBr). EtBr binds strongly to both B- and A-type duplexes with a large increase in fluorescence which will be discussed in further detail in section 1.4.2. However, on addition of Zn^{2+} at high pH the fluorescence of EtBr was quenched suggesting that a novel conformation was being formed. Since EtBr does not bind to M-DNA, a rapid EtBr fluorescence assay was developed which allowed many of the basic properties of M-DNA to be elucidated. Ethidium presumably does not intercalate because the metal ion repels the positively charged molecule similar to triplexes containing CGC^+ base triads that will also not accommodate ethidium (Morgan *et al.*, 1979; Lee *et al.*, 1984; Scaria and Shafer, 1991). However, Hoogsteen or other types of hydrogen bonding can be eliminated as the cause because replacing the adenosine with m^6A and z^7A did not inhibit the dismutation.

Various metal ions were assessed for their ability to facilitate M-DNA formation. Generally, only the metal ions that have ionic radii of about 0.70 Å or less favoured M-DNA formation. These include Zn^{2+}, Ni^{2+} and Co^{2+} while Mg^{2+}, Mn^{2+}, Cu^{2+}, Ca^{2+} and Ag^+ were all ineffective. Mn^{2+}, Cu^{2+}, and Ca^{2+} are all ineffective most likely as a result from their increased ionic radii of 0.80, 0.92 and 0.99 Å respectively. Although Mg^{2+} has an ionic radius of 0.65, previous results show that it is unable to form stable complexes with nitrogen bases and therefore does not form M-DNA. The ionic radius of Ag^+ is 1.13 Å and is most likely too large and therefore causes denaturation of the helix rather than M-DNA formation.

Zn^{2+} is one of the few metal ions which can coordinate well to both oxygen and nitrogen. Therefore, together with its small ionic radius, it is ideally suited for specific interaction with the bases of nucleic acids.

1.3.2 Properties of M-DNA

The proposed structure of M-DNA consisting of metal-metal distance of 0.4 nm suggest that electron transfer could occur within the helix and the molecule could behave as a molecular wire. Therefore, the conductivity of M-DNA has been examined by three methods.

First, duplexes were constructed in which the donor fluorophore (fluorescein) was attached to one end of the oligonucleotide and the acceptor fluorophore (rhodamine) was attached at the opposite end. Upon formation of M-DNA the fluorescence of fluorescein is quenched which is attributed to electron transfer of the excited electron from fluorescein down the helix to the rhodamine where it is absorbed (Aich *et al.*, 1999). More recently, a similar system was designed using a DNA Y-branched junction in which the fluorescein was attached to one arm and the electron acceptors rhodamine and anthraquinone were attached to the other two arms. Not only was it shown that electron transfer could occur through the junction, but that the quenching could be modulated by chemical reduction of anthraquinone thereby mimicking a chemical switch (Wettig *et al.*, 2003a). Interestingly, if a protein was bound to the duplex preventing M-DNA formation or the duplex was simply cleaved using a restriction enzyme no quenching was observed in either case (Aich *et al.*, 1999). Unfortunately, it has been suggested that the quenching could occur through fluorescence resonance energy transfer (FRET) opposed to the proposed electron transfer mechanism (Spring and Clegg, 2007). However, quenching was still observed using a different electron acceptor whose absorption spectrum did not overlap with the donor fluorescence (Wettig *et al.*, 2005), a system in which FRET is no longer a reasonable mechanism (Aich *et al.*, 2002).

Second, direct measurements of the conductivity of B- and M-DNA have been performed with phage λ DNA which is about 15 μm in length (Rakitin *et al.*, 2001). The DNA was placed between two gold electrodes separated by a deep physical gap. B-DNA showed semiconducting behavior with a bandgap of a few meV. M-DNA, on the other hand, showed a linear relationship between current and applied voltage with no

apparent bandgap providing direct evidence for metallic-like conduction (Rakitin *et al.*, 2001).

Third, electrochemical techniques have been developed to probe self-assembled monolayers (SAMs) of short duplexes attached to gold electrodes (Herne and Tarlov, 1997; Yang *et al.*, 1998; Kelley *et al.*, 1999; Petrovykh *et al.*, 2003). The rate of electron transfer through an M-DNA duplex was 1.2 x 10^{-4} cm/s whereas for B-DNA it was too slow to be measured (Li *et al.*, 2003).

1.4 Stability and Formation Analysis of M-DNA

Various methods have been developed to assess the stability and formation of DNA. Unfortunately, commonly applied methods such as UV absorbance and Circular Dichroism are rendered ineffective as large changes are not observed for the conversion of B-DNA to M-DNA. However, the formation of M-DNA can be characterized effectively by thermal denaturation profiles. As well, M-DNA does not bind ethidium which allows the formation of M-DNA to be monitored using fluorescence.

1.4.1 Denaturation Profiles

As mentioned previously the denaturation of DNA can be easily followed spectroscopically. Original characterization of M-DNA showed that the T_m of calf thymus DNA only increased slightly in the presence of Zn^{2+} at pH 6.5. Surprisingly, the T_m increased by as much as 12 °C when the pH was raised to 9.0 (Lee *et al.*, 1993). This result suggested the possibility of a novel metal-DNA complex. Other results have also shown that the increase in T_m seen in the presence of Zn^{2+} was even greater than that seen for Mg^{2+} at pH 9.0 (Wood *et al.*, 2002). This also suggests that the Zn^{2+} is not simply binding to the backbone and most likely is attributed to the conformational change to M-DNA. In this capacity, DNA containing various sequences and novel bases were compared at different pH values in the presence of various metal ions using thermal denaturation profiles.

1.4.2 Ethidium Bromide Assay

Ethidium Bromide (EtBr) is a positively-charged planar aromatic compound which has the ability to intercalate between the stacked base pairs of double helical DNA. Although it was originally used as a trypanocidal drug (Kandaswamy and Henderson, 1962; Waring, 1965), its enhanced fluorescence upon binding to dsDNA has made it an attractive agent for identifying and visualizing nucleic acid bands in molecular biology techniques such as agarose gel electrophoresis (Sharp *et al.*, 1973).

Although EtBr will form a complex with most dsDNA it does exhibit preferential binding to pyrimidine (3'-5') purine deoxydinucleotides as compared to purine (3'-5') pyrimidine isomers (Krugh and Reinhardt, 1975; Reinhardt and Krugh, 1978). Although it as been shown that the apparent binding affinity of ethidium is not very dependent upon the overall base composition (Waring, 1965; Lepecq and Paoletti, 1967; Muller and Crothers, 1975), ethidium fluorescence has been reported to be slightly higher for AT rich strands (Morgan *et al.*, 1979; Latimer and Lee, 1991).

As demonstrated in the crystal structure shown in figure 1.16, the planar phenanthridinium ring of the ethidium molecule intercalates between adjacent base pairs on the double helix. The DNA becomes saturated at one drug for every two base pairs. This binding pattern is referred to as the neighbor exclusion model and has been attributed to alternating sugar puckers hindering the binding at every base pair (Crothers, 1968; Bresloff and Crothers, 1981).

In its unbound form, EtBr has a very low fluorescence intensity which is attributed to quenching of the excited state molecule by proton transfer to the water or solvent molecules. However, EtBr fluorescence is enhanced approximately 25 fold after intercalating with dsDNA (Lepecq and Paoletti, 1967). This increase in fluorescence is a result of the hydrophobic environment found between the base pairs. As the ethidium moves into this environment it sheds away any water molecules that were associated with it and therefore slows down the proton exchange leading to a longer life time for the excited state and an overall increase in fluorescence (Olmsted and Kearns, 1977).

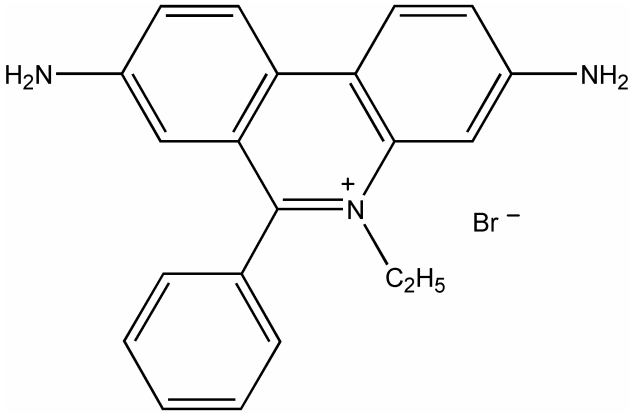

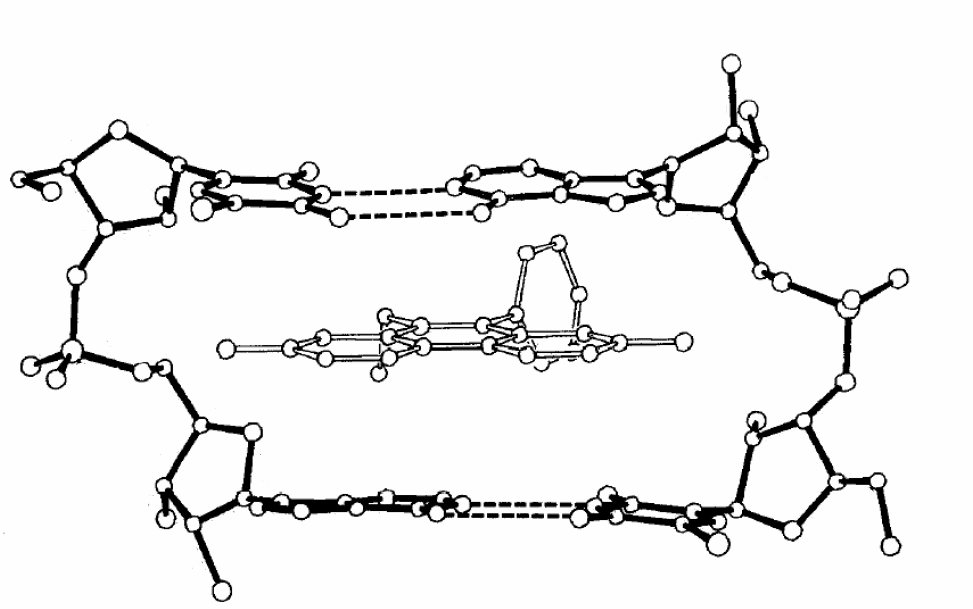

Figure 1.16 Structure of Ethidium molecule (top) and the crystal structure of ethidium intercalated between 5-iodo-UA (bottom). Taken from (Tsai *et al.*, 1975).

This effect is supported further by the fact that EtBr bound to a triplex is better protected from the solvent and consequently has increased fluorescence (Scaria and Shafer, 1991). However, if a triplex carries a positive charge no fluorescence is observed in the presence of EtBr (Morgan *et al.*, 1979). The lack of fluorescence has been attributed to the presence of a positive charge on the DNA effectively repelling the positively charged ethidium ions and preventing them from binding to the DNA (Morgan *et al.*, 1979; Lee *et al.*, 1984).

Similarly, EtBr does not bind to M-DNA presumably because the metal ion repels the positively-charged molecule (Morgan *et al.*, 1979; Lee *et al.*, 1993). This property allows for a convenient assay to measure the conversion of B-DNA to M-DNA. (Lee *et al.*, 1993).

1.5 Characterization of B-DNA and M-DNA Monolayers on Gold

As discussed above, denaturation profiles and EtBr assays have been used extensively to investigate the physical properties of M-DNA. In this research, surface techniques such as XPS and electrochemistry were also developed. DNA was also immobilized onto a gold substrate through Au-S linkages in order to examine the effects of Zn^{2+} ions on the XP spectra of elements such as nitrogen which is only found on the bases and is projected to directly interact with the Zn^{2+} ion in the M-DNA conformation. As well, detailed information such as the elemental ratios, DNA coverage, density and thickness are all able to be investigated through the use of XPS. Finally, the electronic properties of M-DNA will be assessed through the use of cyclic voltammetry, chronocoulometry and electrochemical impedance spectroscopy.

1.5.1 Preparation of the Gold Substrate

Polycrystalline gold was the chosen substrate as it is a relatively inert metal and has the capacity to easily attach DNA through thiol or disulfide adsorption as they coordinate very strongly to gold (Finklea, 1996). Although a well-defined single crystal face is important for many surface analytical techniques, there is no consistent evidence

that pinhole-free SAMs require a single crystal surface. The presence of impurities, grain boundaries, or large steps between atomically smooth planes may have more effect on the electrochemical properties of the SAM-coated electrode than the degree of crystallinity (Finklea, 1996).

However, before the substrate can be used, the gold must be cleaned. The two procedures, used in this thesis, for cleaning the gold substrate include immersion of the substrate in a powerful oxidant called "piranha" solution and electrochemical cycling in dilute sulfuric acid. These will be discussed in further detail in the Material and Methods. Both procedures lead to hydrophilic gold surfaces which are completely wetted by water. Any partial dewetting of the gold surface by water indicates incomplete cleaning and the presence of organic contaminants (Whitesides and Laibinis, 1990).

1.5.2 Preparation of Self-Assembled Monolayers

Although organized monolayers can be deposited in a number of ways using various substrates, this discussion will focus on self-assembled monolayers formed by strong adsorption of thiols and disulfides onto a gold substrate (Nuzzo and Allara, 1983; Nuzzo *et al.*, 1987a). The chemisorption of alkanethiols or dialkyl disulfides on gold are easily obtained by exposing a clean gold surface at room temperature to a 0.1 mM solution of the organosulfur compound. The organosulfur species formed from both alkanethiols and dialkyldisulfides at the Au^0 surface is a Au^I thiolate (Nuzzo *et al.*, 1987b). In the case of dialkyl disulfides, this surface gold thiolate is undoubtedly formed by oxidative addition of the sulfur-sulfur bond to Au^0. Formation of a gold thiolate from a thiol requires loss of hydrogen, but whether this hydrogen is lost as H_2 or lost as water through reactions with trace oxidants in the system is presently not known.

$$2RSH + 2Au^0 \longrightarrow 2RS^-Au^+ + 2H_2$$

$$RSSR + 2Au^0 \longrightarrow 2RS^-Au^+$$

The absorption time is roughly equal for both processes and the energy of the bond between the organic thiolate and the gold surface is approximately 40-45 kcal/mol (Nuzzo *et al.*, 1987b). A number of studies indicate the alkyl chains are largely trans extended, with the axis of the chain tilted approximately 30° from the surface normal (Porter *et al.*, 1987). Also the sulfur atoms rest in threefold hollows of the gold surface (Fenter *et al.*, 1994; Love *et al.*, 2005). Therefore the overall organization is obtained from the affinity of the sulfur to the gold substrate combined with the favorable interactions between close-packed tail groups.

1.5.3 X-Ray Photoelectron Spectroscopy

Photoelectron spectroscopy is a common technique used to examine the composition and electronic state of species at the surface or near-surface region. The photoelectric effect is the foundation of this technique. As illustrated in figure 1.17, incident photons are absorbed by various atoms or molecules leading to the ionization and the emission of a photoelectron (Einstein, 1905).

$$M + h\nu \rightarrow M^{+} + e^{-}$$

Based on the principles of conservation of energy, the above equation can be interpreted as follows:

$$h\nu - E(e^{-}) = E(M^{+}) - E(M)$$

where E(M) and E(M^{+}) are the energies of the atom or molecule M and the ion M^{+} formed by the ionization, and E(e^{-}) is the kinetic energy of the photoelectron. Since $h\nu$ is known and E(e^{-}) can be measured, the difference between the energies of the ion and the original molecule is obtained.

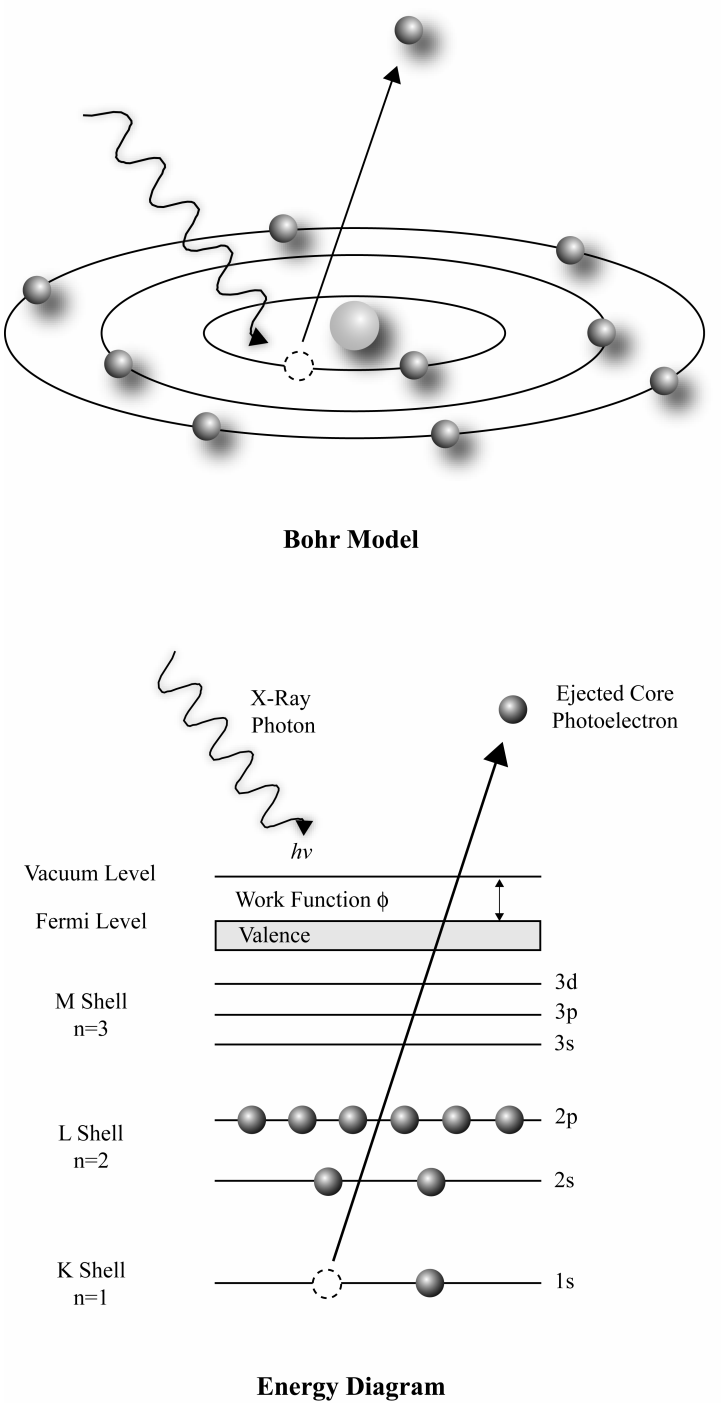

Figure 1.17 (Top) Classic Bohr model illustrating the transfer of energy from the initial X-ray photon to a core-level electron leading to photoemission. **(Bottom)** Energy Diagram showing ejection of inner 1s electron.

The difference in energy between the ionized and neutral atoms is generally referred to as the binding energy (BE) which leads to the following equation.

$$KE = h\nu - BE$$

However, the BE's in solids are measured with respect to the Fermi-level of the solid, rather then the vacuum level. As illustrated in the energy diagram in figure 1.17, an additional energy is required to raise an electron from the solid to the energy level corresponding to an electron at rest in vacuum. This energy difference is referred to as the work function (Φ) and is incorporated into the above equation as follows.

$$KE = h\nu - BE - \Phi$$

Photoelectric emission occurs if a photon with energy greater than the work function is applied. Any excess energy is given to the electron as kinetic energy. Depending on the energy of the incident photons, photoelectron spectroscopy can be classified as either ultraviolet photoelectron spectroscopy (UPS) or x-ray photoelectron spectroscopy (XPS). UPS uses photons in the ultraviolet spectral range of 10-50 eV and is used to study valence electrons. Conversely, XPS uses x-rays in the range of 100 eV – 10 keV in order to examine the inner core electrons. Since only XPS experiments were performed for this thesis, UPS will no longer be discussed.

XPS instrumentation consists of an x-ray source, a sample, an electrostatic lens system, an electron energy analyzer, an electron detector and a computer system for data collection and processing (Riviere, 1990; Riviere, 1998) (Figure 1.18) . Analysis is done in an Ultra-High Vacuum so as to remove adsorbed gases and eliminate adsorption of contaminants on the sample. The x-rays are generated by bombarding a metallic anode with high energy electrons (10-15 keV) and are then focused onto the sample though use of a monochromator. The energy of the generated x-rays is determined by the anode material which is usually Al or Mg. When x-rays strike the sample, a core electron can absorb the energy and be emitted with a range of energies.

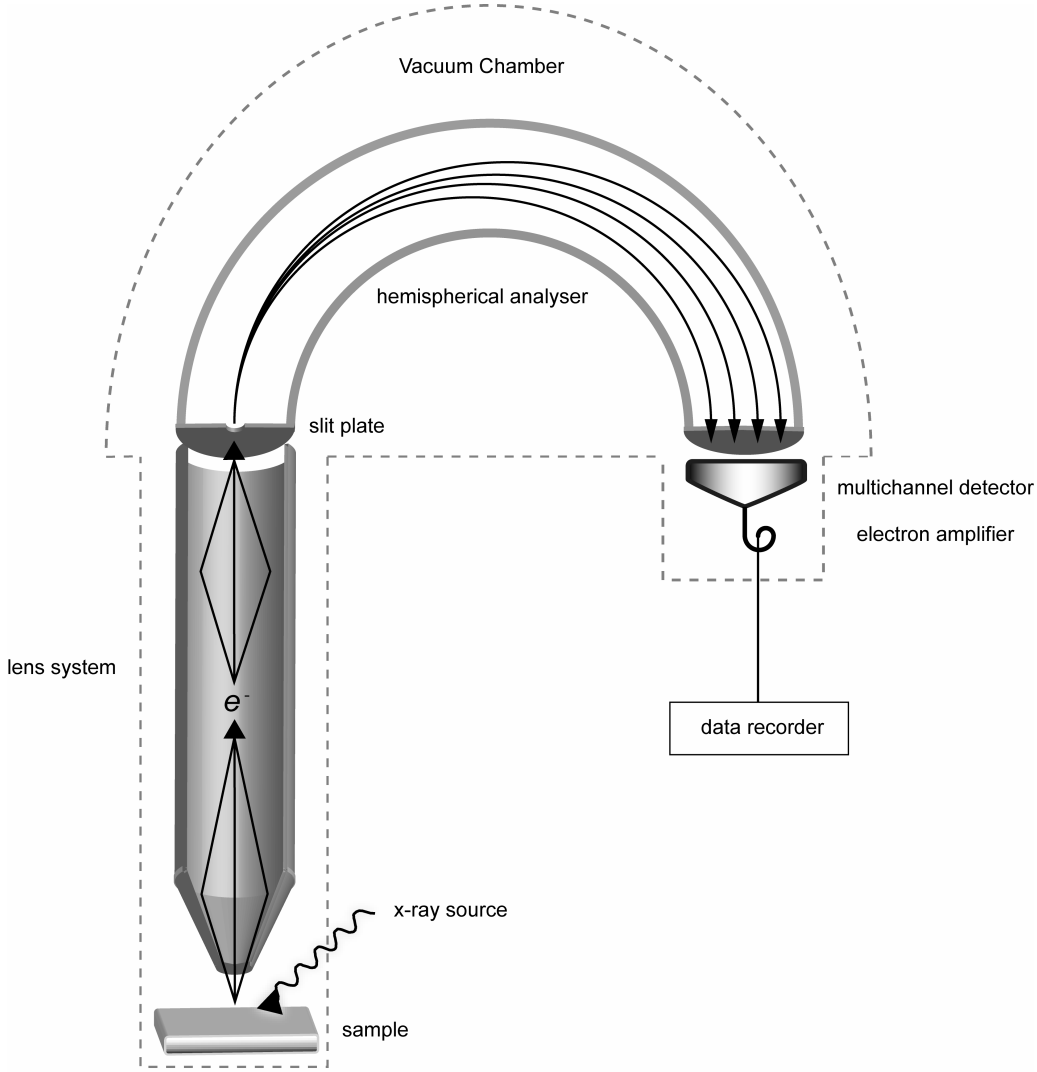

Figure 1.18 Schematic diagram of X-ray Photoelectron Spectrophotometer. The key components include X-ray source, collection lens, hemispherical analyzer, detector and computer analyzer.

An electrostatic lens system collects a portion of these emitted electrons and focuses them into an electron energy analyzer called a concentric hemispherical analyzer (CHA). This analyzer consists of two plates. Different voltages are applied to each plate creating an electric field between them. Electrons entering the analyzer with a high energy will contact the outer plate while those with low energy will be attracted to the inner plate. In this capacity, only electrons in a narrow energy region, referred to as the pass energy, are able to travel the distance of the analyzer and reach the detector. A variable retarding voltage is applied to a deceleration element in the transfer lens of the CHA. Therefore, only electrons that leave the target with a specific energy enter and pass through the analyzer to the detector. The commonly used electron detector is referred to as a channeltron. This consists of a bent tube coated with an insulating material which when struck by an electron emits a number of secondary electrons that are accelerated through the channeltron. This process is repeated throughout the length of the tube producing a large number of secondary electrons and therefore an amplified signal. The spectrum is obtained by recording the numbers of electrons as a function of the retarding voltage. This allows the energy resolution to be constant over the entire spectrum.

1.5.3.1 XPS Spectra Analysis

The intensity of a peak depends on how efficiently the x-ray interacts with the specific electron to cause the photoemission process to occur. The efficiency of the photon interaction with the electron is determined by the photoelectron cross section, σ (Scofield, 1976). Each spectral line also has a specific width or resolution which is usually defined as the full-width at half maximum. There are three main contributors that affect the photoelectron line width in an XPS spectrum. First, the Heisenberg uncertainty principle states that if the lifetime of an atom or molecule in an electronically excited state is quite short, there is consequently a greater variability in its energy and therefore a broadening of the spectral line will be observed (Heisenberg, 1927).

$$\Delta E \Delta t < h / 4\pi$$

Secondly, the natural line-width of the anode material used as the x-ray source usually limits the overall energy resolution. However, the use of a monochromator does reduce line width and therefore improves the resolution. Finally, the resolution is also affected by the pass energy and slit width of the analyzer. Therefore the peaks are fitted using a convolution of a Gaussian function to account for the principal x-ray line and instrumental response and a Lorentzian function to model the lifetime broadening due to the uncertainty principle.

Not only is the line shape important, but the background shape must be considered as well. Since X-rays penetrate far into the material compared to the depth from which electrons of a given kinetic energy can escape from the surface, there are changes to the background resulting from energy loss occurring as the photoelectrons are ejected from the surface material. Therefore, XPS spectra characteristically show an increase in the intensity of the background level on the high energy side of all peaks in an XPS spectrum. This phenomenon is a result of inelastic scattering. For instance, only electrons close to the surface can escape without energy loss. Electrons deeper in the surface lose energy from inelastic scattering and emerge from the sample with reduced KE, and therefore increased BE. Electrons very deep in the surface lose all energy and cannot escape at all. Inelastic scattering is caused from photoelectrons traveling though the solid and interacting with other electrons in the material. The energy loss can result from the primary photoelectron losing energy from a single scattering event as it leaves the sample or multiple scattering events causing secondary low energy electrons to be ejected from the material (Shirley, 1972; Tougaard and Sigmund, 1982)

Since electrons have spin, those ejected from core levels with primary quantum numbers p, d, f show two observable peaks. The separation between the two peaks is referred to as spin-orbit coupling (Laidler and Meiser, 1995). These doublet states are characterized by total angular momentum given by *j*.

$$j = \left| l \pm \tfrac{1}{2} \right|$$

The relative intensities of these doublet pairs can be calculated from 2j + 1. Thus for p electrons where the angular momentum equals one, the relative intensities are 1:2, while for d electrons the doublet pairs are in the proportion 2:3 and for f electrons the ratio is 3:4.

1.5.3.2 Variable angle XPS

Variable angle XPS (VAXPS) can be used in order to investigate the depth distribution of different chemical species. In VAXPS, the effective sampling depth is dependent on the angle of the sample relative to the detector. As shown in figure 1.19, as the Take-Off Angle (TOA) goes from 90° to 30° the sampling depth decreases and detection becomes more sensitive towards species at the surface. Therefore, by comparing intensities at low and high take-off angles the approximate location of the species can be determined.

1.5.4 Electrochemistry

Electrochemistry investigates the transfer of charge between a metallic electrode and a species in a conductive solution. Therefore, in a simple scenario, this involves the transport of the reactant to the electrode surface where electron transfer is able to occur. Through oxidation or reduction, the product is produced and returned back to the bulk solution. Although the reaction of interest only occurs at the surface of the working electrode (WE), an auxiliary or counter electrode (CE) must be included in order to complete the circuit allowing the flow of current. The CE is most commonly an inert metal to prevent any interfering reactions and whose electrochemical properties do not affect the behavior of the WE. In most cases, a reference electrode (RE) is also included to monitor or maintain a specific potential at the WE. The reference electrode has a high impedance to prevent current from passing through it and consequently retains a constant potential (Bard, 2001). As well, trace amounts of chloride ions might adsorb onto the electrode surface changing its electrochemistry. Therefore a salt bridge is also used to electrically connect the reference electrode to the main body of the cell to prevent the leakage of ions. A typical three electrode cell setup is shown in figure 1.20.

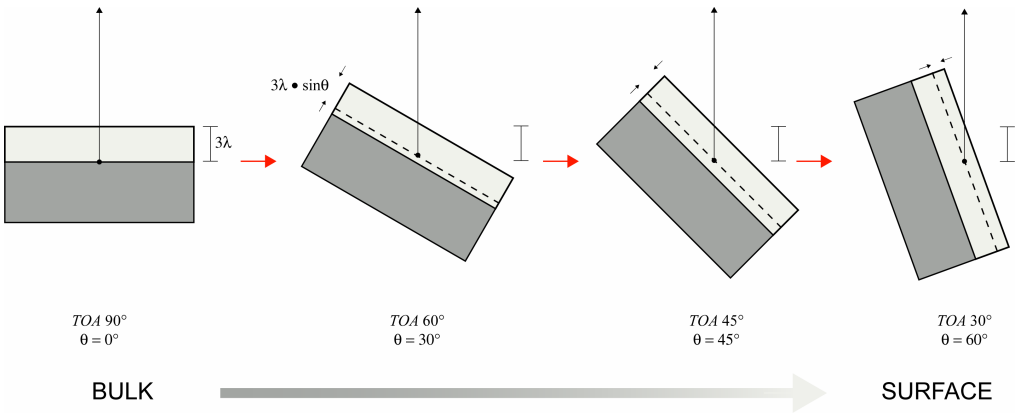

Figure 1.19 As the sample is rotated, maintaining the X-ray source and detector in fixed positions, the effective sampling depth decrease by a factor of sinθ. The sample angle, θ, is defined relative to the surface normal.

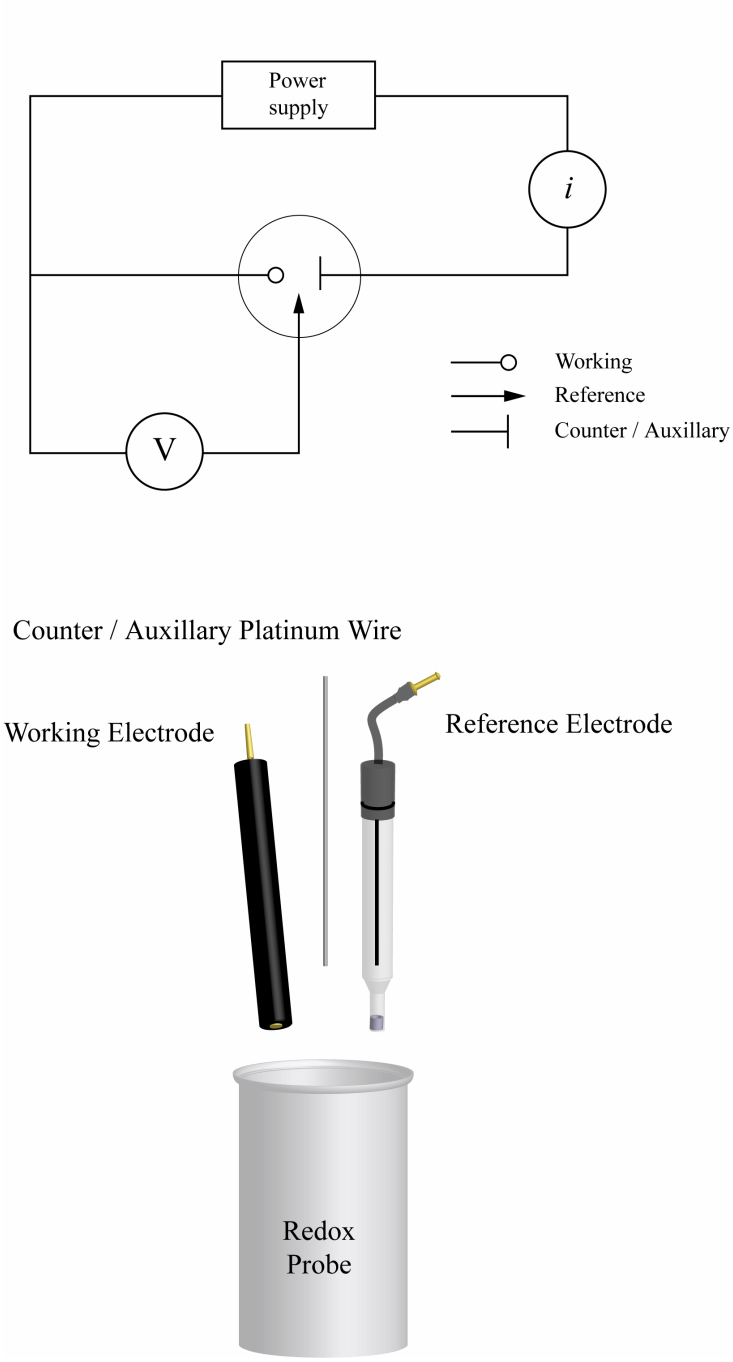

Figure 1.20 Typical experimental setup of three-electrode cell. Circuit schematic taken from (Bard, 2001)

1.5.4.1 Cyclic Voltammetry

In cyclic voltammetry, a potentiostat is used to direct the flow of electrons by controlling the potential at the WE. As illustrated in figure 1.21, if the potential at the electrode becomes increasingly negative, the energy of the electrons increases until they reach a level high enough that it is thermodynamically favorable to transfer into vacant electronic states on species in the electrolyte. Therefore electrons flow from the electrode to the solution resulting in the reduction of the species in the electrolyte. In this instance, the electrode is referred to as the cathode. Similarly, the energy of the electrons can be lowered to a positive potential in which the electrons from the species in the solution will find it more energetically favorable to transfer to the electrode. The flow of electrons from solution to the electrode will result in the oxidation of the species in the electrolyte and therefore the electrode is considered to behave as an anode.

In this manner CV experiments are performed by linearly sweeping the potential between two values at a fixed scan rate. A typical CV recorded for a reversible single electrode transfer reaction for $[Fe(CN)_6]^{3-/4-}$ is shown in figure 1.22. As the voltage is swept from a positive to negative potential, a current begins to flow as Fe^{III} is being reduced to Fe^{II} at the surface of the electrode. However, for the reaction to continue a constant supply of reactant must approach the surface which is accomplished through diffusion. As more products are created over time, the concentration of reactant approaches zero at the electrode surface and a maximum (I_{pc}) eventually occurs. At this point, the diffusion layer becomes too thick to sustain the transfer of enough reactant to the electrode surface and the current begins to drop off according to the Cottrell equation (Bard, 2001). When the scan is reversed, the Fe^{II} which has been accumulating at the electrode surface from the preceding reduction reaction can now be oxidized back to Fe^{III} in an identical manner. The most important parameters for a CV are labeled in figure 1.22 and include the cathodic peak current (I_{pc}) and potential (E_{pc}) as well as the anodic peak current (I_{pa}) and potential (E_{pa}). The peak potentials provide information regarding the identity of the analyte and the kinetics of the redox process where as the peak currents supply information about the analyte concentration and stability of the electrogenerated species (Bard, 2001).

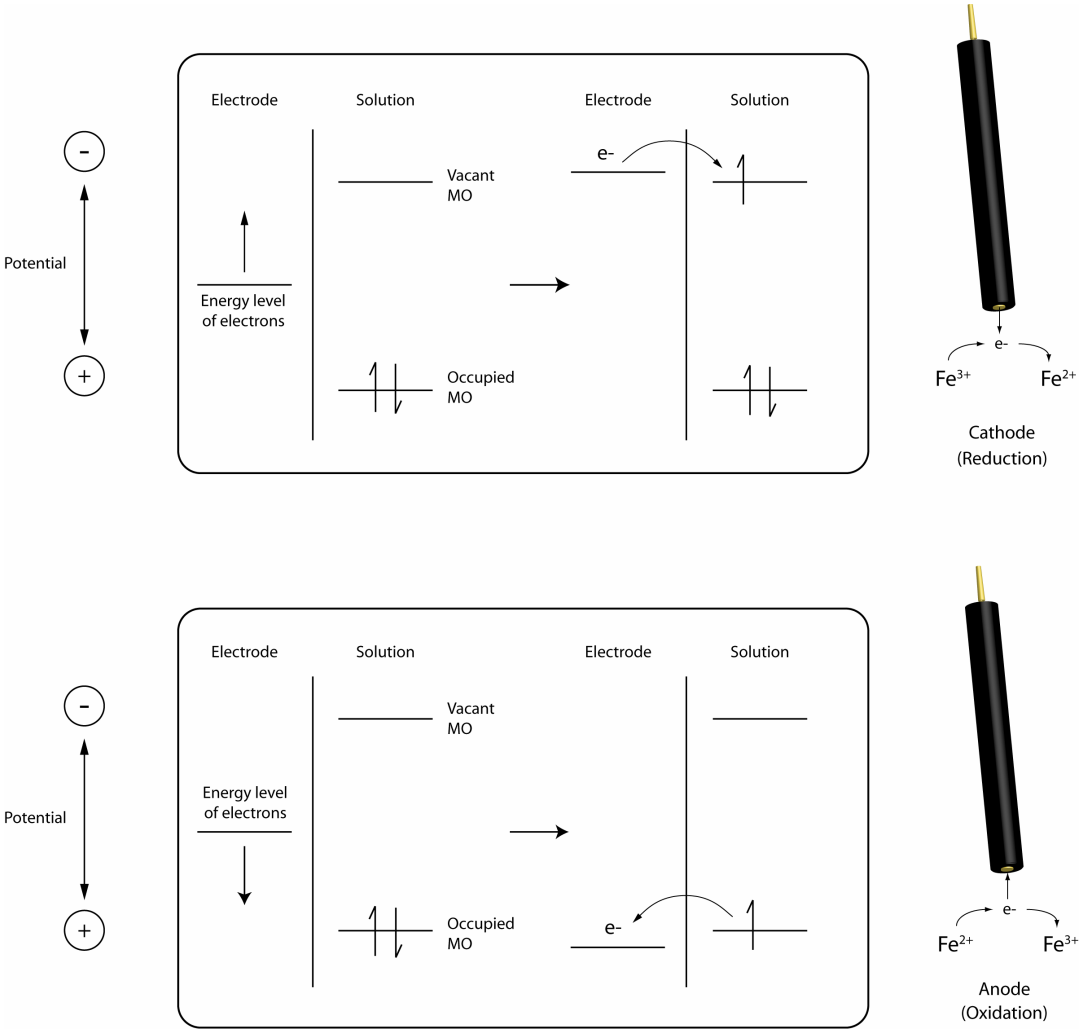

Figure 1.21 Representation of the oxidation and reduction process at an electrode-solution interface. Adapted from (Bard, 2001)

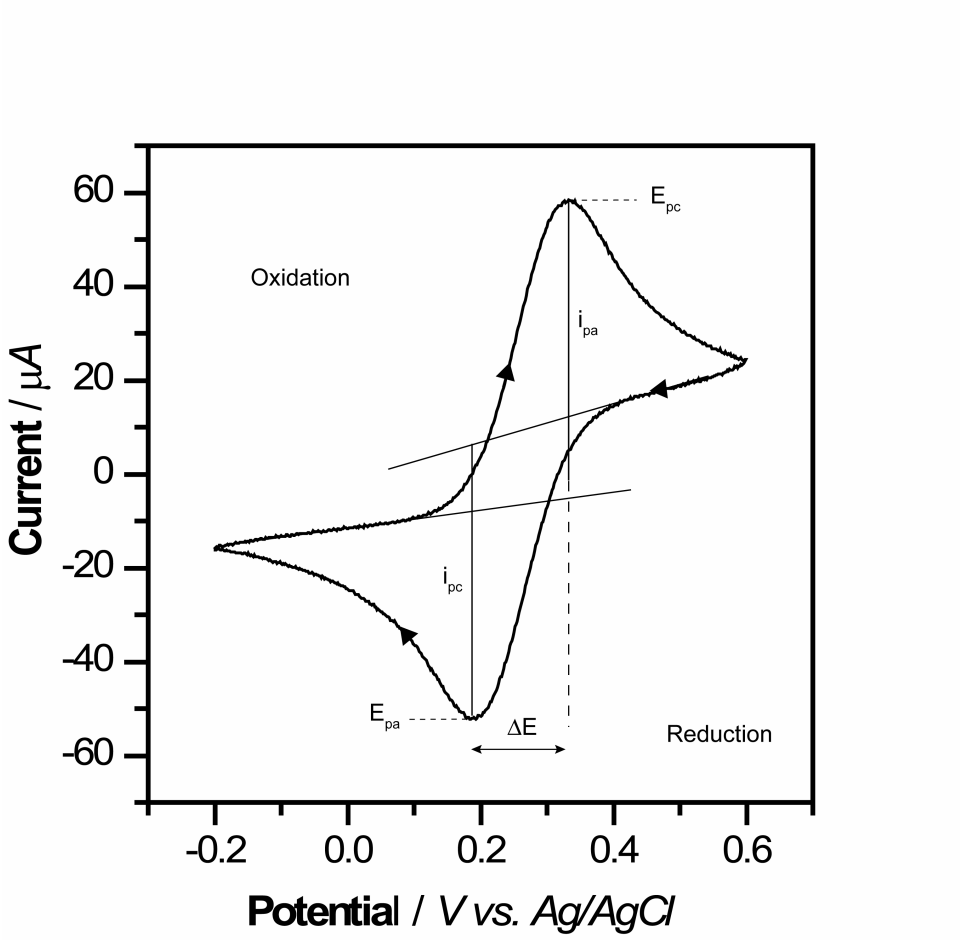

Figure 1.22 A typical cyclic voltammogram showing reversible electron transfer. Anodic and cathodic current (I_{pc}, I_{pa}) and potentials (E_{pc}, E_{pa}) are indicated.

1.5.4.2 Electrochemical Impedance Spectroscopy

EIS offers several advantages over cyclic voltammetry because the effects of solution resistance, double-layer charging and current due to diffusion or to other processes occurring in the monolayer are observed more explicitly (Bard, 2001).

Impedance is measured by applying an AC potential to the electrochemical cell and measuring the resulting current. As the name implies, the impedance is the ability of a circuit to oppose the flow of current. There are two components that contribute to the total impedance in our system and will be discussed further. The simplest of these components is the common resistor as it is not dependent on frequency. Therefore at any specific voltage, the current can be easily predicted by Ohms Law. However, the capacitance is more complex as it is dependent upon the frequency. Therefore, to investigate the behavior of our electrochemical system, the impedance was measured over a range of frequencies.

EIS is advantageous because a model based purely on electronic components can be used to represent the electrochemical system. For example, the impedance of an electrode undergoing electron transfer through a DNA self-assembled monolayer is usually described on the basis of the model developed by Randles (Randles, 1947). The circuit components in the Randles cell can easily be compared with familiar physical phenomena (Figure 1.23). The solution resistance term, R_S, represents the resistance of the solution between the counter and the working electrode. The charge transfer resistance term, R_{CT}, results from the transfer of electrons from the redox probe to the DNA monolayer, through the base pairs of the DNA helix and from the helix to the surface of the gold electrode. The array of charged species and oriented dipoles existing at the metal-solution or DNA-solution interface create an electrical double layer which has been shown to resemble a capacitor (Cdl). As well, at low frequency, diffusion begins to dominate the electrochemical reaction and this mass transfer is referred to as Warburg Impedance (W).

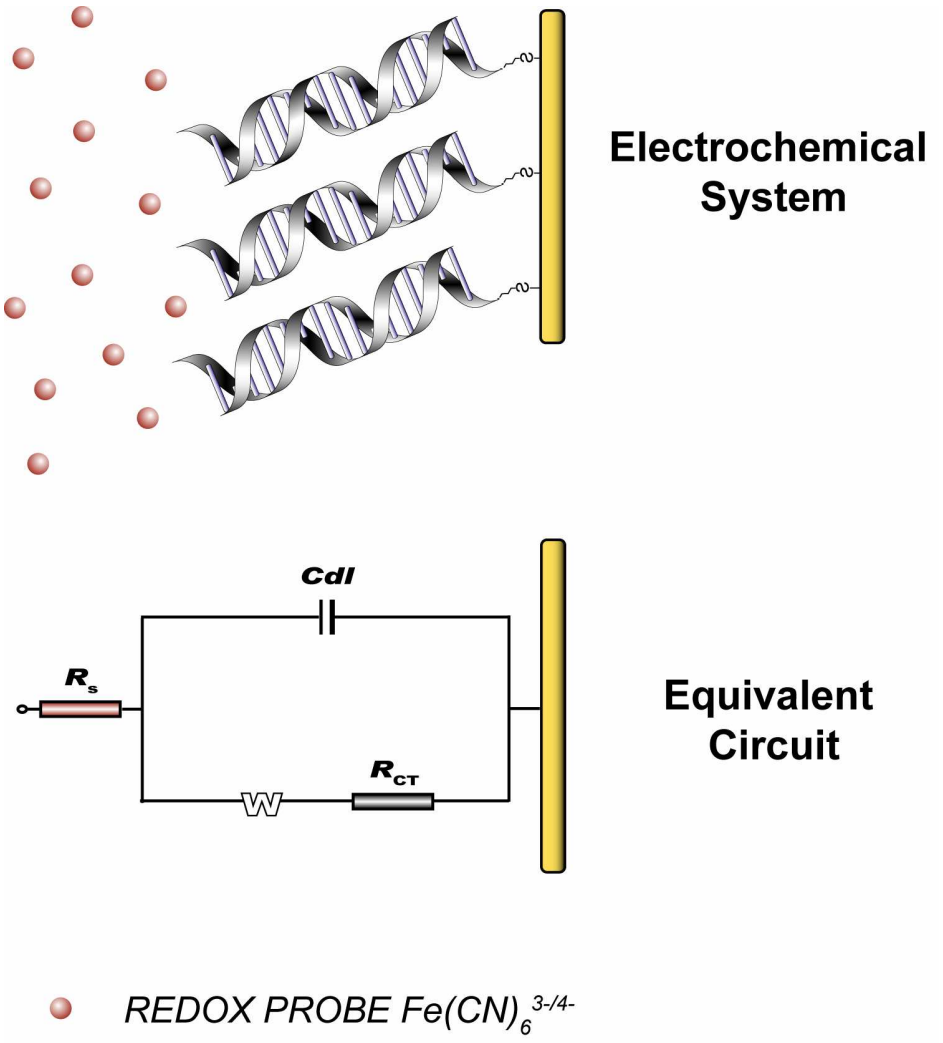

Figure 1.23 Randles equivalent circuit consists of the solution resistance through the redox probe (R_S), the charge transfer resistance through the DNA (R_{CT}), the double layer capacitance (Cdl) and the Warburg constant (W).

If a circuit is comprised of only a resistor, the sinusoidal waves for the current and voltage are in the same phase and differ only in amplitude. However, when a capacitor is added to the circuit, the waves differ in both amplitude and phase. This can be represented graphically, by using x,y coordinates, magnitude and phase angle, or by using a complex number. In order to graph both components on the same graph, the capacitance term is simply calculated as a complex or imaginary number which is plotted on the y-axis and the resistance is then plotted on the x-axis and labeled as the real component. This popular format for evaluating electrochemical impedance data is referred to as the Nyquist plot. Figure 1.24 illustrates the expected response for the simple Randles circuit shown above the graph. Each point represents the impedance value at a specific frequency which decreases from left to right. At high frequencies, there is not enough time for charge to build up on the plates of the capacitor as the charges are constantly being added and removed as the current direction changes. Therefore, there is no electric field to resist the flow of current and the impedance through the capacitor approaches zero. Thus at high frequencies, the cell is controlled almost entirely by the initial resistance term. At very low frequencies, charge is able to build up causing an electric field. Eventually, it becomes so large that it is unable to be further charged resulting in no voltage drop across the plates preventing any flow of current. Therefore, it is effectively removed from the circuit and the impedance of the cell becomes a combination of both the resistors. Therefore, only at intermediate frequencies does the capacitor begin to have an effect which is evident from the increased imaginary values on the y-axis. Although the capacitance is difficult to calculate from such a graph, this plot format is advantageous as the charge transfer resistance of the system can be easily read and compared.

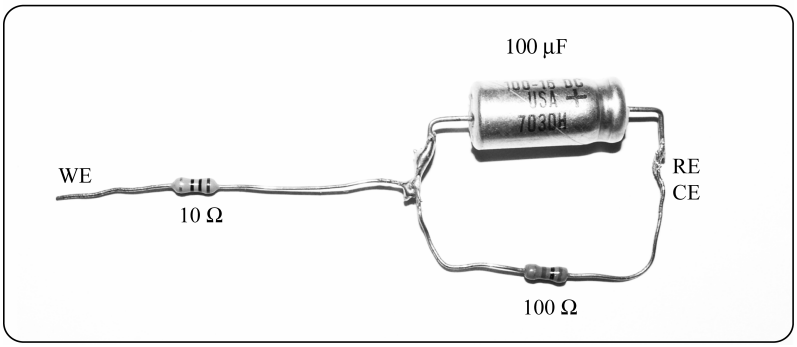

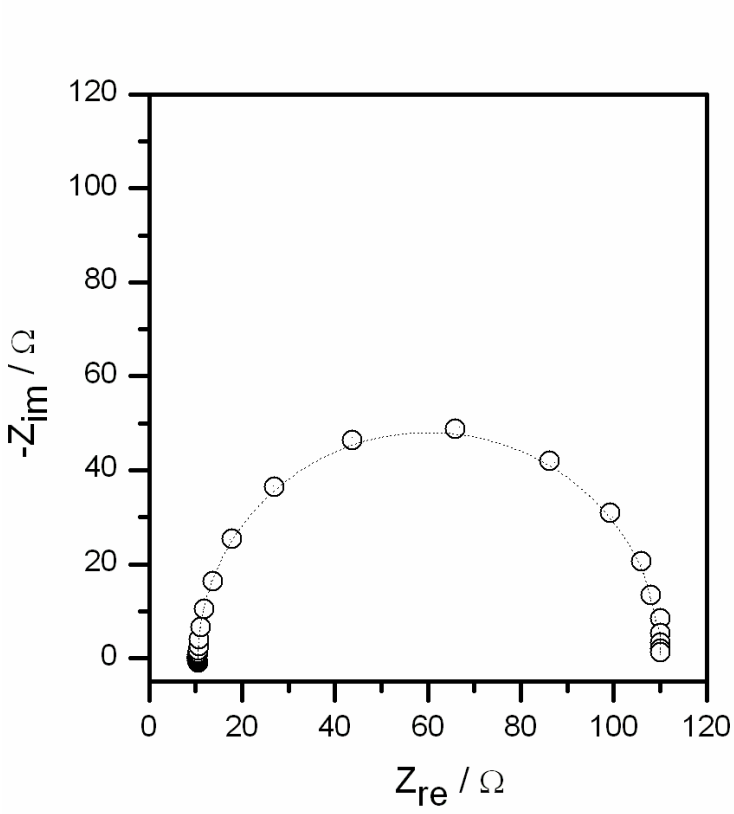

Figure 1.24 Randles circuit comprised of a 10 Ω resistor followed by a 100 Ω resistor and 100 µF capacitor in parallel. Below is the corresponding Nyquist plot showing the resistance plotted along the x-axis and the capacitance comprising the y-axis component.

1.6 Objectives

The potential utility of M-DNA is restricted by the narrow pH range under which it will form (Lee *et al.*, 1993). Therefore, the first objective of this thesis was to incorporate novel nucleotides into DNA and examine their effect on the formation and stability of M-DNA in the presence of Zn^{2+}. Using thermal denaturation profiles and the ethidium fluorescence assay, it was successfully shown that both sequence and base composition were able to lower the pH at which M-DNA formation could occur.

As previously mentioned in section 1.2.3.5, there has been continued interest in the development of DNA scaffolding that can localize metal ions to specific locations. Therefore, it was our second goal to use sequence effects and base replacements in order to localize metal ions at specific locations throughout the M-DNA helix. Convincing results were obtained in solution using the ethidium fluorescence assay. Therefore, the next step was to use DNA self-assembled monolayers to examine how these gaps in the helix would alter the conductance through the DNA. First, detailed characterization of B- and M-DNA monolayers were examined using X-ray photoelectron spectroscopy followed by the examination of the electronic properties using various electrochemical techniques including cyclic voltammetry and electrochemical impedance spectroscopy.

2.0 MATERIALS AND METHODS

2.1 Chemical and Biological Reagents, Supplies and Equipment

Table 2.1 contains a comprehensive list of all chemical and biological reagents, supplies and equipment used for research experiments described throughout this thesis. All chemicals were ACS grade or better. A list of DNA primers used for PCR as well as the names and sequence for all synthetic oligonucleotides can be found in Table 2.2.

2.2 Nucleic Acids

2.2.1 Production of Synthetic Repeating-sequence DNA

Duplex DNAs were synthesized by methods described previously with slight variations to the reaction conditions in order to improve synthesis (Morgan *et al.*, 1974). Reaction mixtures were prepared in 50 mM potassium phosphate (Kpi) buffer pH 7.0 with 5mM $MgCl_2$, 2 mM NTPs, 50 µg/mL albumin, 15 µM double-stranded poly[d(AT)] or poly[d(TG)•d(CA)] as primer and 2 units of *Escherichia coli* DNA polymerase in a final volume of 2 mL. Since the sequence is repetitive, there is strand slippage creating overhangs which allow polymerase a template to elongate the DNA. Reactions were incubated at 37 °C, and the synthesis was followed by the ethidium fluorescence assay (Lepecq and Paoletti, 1967; Morgan *et al.*, 1974). The fluorescence measurements were made on a Hitachi F-2000 fluorescence spectrophotometer set at 525 nm excitation and 600 nm emissions. The spectrofluorometer was calibrated with 10 µL of a 50 µg/mL Calf Thymus DNA standard in 2 mL of ethidium buffer (5 mM Tris-HCl pH 8.0, 0.5 mM EDTA, and 0.5 µg/ml ethidium bromide). At various times during the reaction, 10 µL of sample was removed and measured.

Table 2.1 Chemical and Biological Reagents, Equipment and Supplies

Item	**Supplier**
Chemical and Biological Reagents	
(1,3-bis[tris(Hydroxymethyl)-methylamino]propane) (Bis-Tris)	Sigma
2'-deoxyadenosine-5'-triphosphate (dATP)	Pharmacia
2'-deoxycytidine-5'-triphosphate (dCTP)	Pharmacia
2'-deoxyguanosine-5'-triphosphate (dGTP)	Pharmacia
2'-deoxythymine-5'-triphosphate (dTTP)	Pharmacia
2'-dexoxyuridine-5'-triphosphate (dUTP)	P-L Chemicals
2-thio-2'-deoxythymine-5'-triphosphate (s^2T)	Trilink
2-(*N*-cyclohexylamino)ethanesulfonic acid (CHES)	Sigma
2-(*N*-Morpholino)ethanesulfonic acid (MES)	Sigma
3-(*N*-Morpholino)propanesulfonic acid (MOPS)	Sigma
4-thio-2'-deoxythymine-5'-triphosphate (s^4T)	Trilink
Agarose (ultra pure)	Gibco BRL
Argon (gas)	Praxair
Bacteriophage Lambda DNA (λ DNA)	Pharmacia
Bromophenol blue	Pharmacia
Calf thymus DNA (type I: sodium salt)	Sigma
Cobalt Chloride hexahydrate ($CoCl_2 \cdot 6H_2O$)	Sigma
Concert ^{TM} Rapid PCR purification system	Gibco BRL
Copper (II) sulfate pentahydrate	Sigma
di-Potassium hydrogen orthophosphate (K_2HPO_4)	BDH
DNA molecular weight markers	Roche, NEB
Ethidium Bromide (EtBr)	Sigma
Ethylenediaminetetraacetic acid disodium salt (EDTA)	BDH
Hydrochloric acid (HCl)	BDH
Magnesium Chloride ($MgCl_2$)	Sigma
Magnesium Perchlorate hexahydrate $(MgClO_4)_2 \cdot 6H_2O$	Alfa Aesar

N-(2-hydroxyethyl)piperazine-*N*'-(2-ethanesulfonic acid) Sodium salt (HEPES)	Sigma
Nickel Chloride hexahydrate ($NiCl_2 \cdot 6H_2O$)	Sigma
Nitrogen (gas)	Praxair
Perchloric Acid, 70%	EMD
Potassium dihydrogen orthophosphate (KH_2PO_4)	BDH
Potassium hexacyanoferrate (II) $K_4[Fe(CN)_6]$	Sigma
Potassium hexacyanoferrate (III) $K_3[Fe(CN)_6]$	Sigma
Potassium hexachloroiridate (IV) (K_2IrCl_6)	Alfa Aesar
Sodium Chloride (NaCl)	Sigma
Sodium Hydroxide (NaOH)	BDH
Sodium Perchlorate ($NaClO_4$)	Sigma
Taq DNA polymerase	Amersham
Tris[hydroxymethyl]aminomethane (Tris)	Sigma
Tth DNA polymerase	Roche
Zinc Chloride ($ZnCl_2$)	Sigma
Zinc Perchlorate hexahydrate $Zn(ClO_4)_2 \cdot 6H_2O$	Sigma

Equipment and Supplies

0.20 μM filter discs	Nalgene
18- and 30-guage needles	Becton Dickinson
Accumet Basic pH electrode	Fisher
Absorbance Spectrophotometer 260	Gilford
Ag/AgCl Reference Electrode	BASi
Alumina Polishing Pads	BASi
Axis-165 (Kratos Analytical)	ACSES
Disposable fluorescence cuvettes	VWR
Double-junction reference electrode chamber	BASi
Eppendorf Tubes, 15 mL and 50 mL	VWR
F-2000 fluorescence spectrophotometer	Hitachi
F-2500 fluorescence spectrophotometer	Hitachi

Falcon tubes, 15 mL and 50 mL	VWR
Faraday Cage	VoltaLab
Gold-coated silicon wafers (1000 Å Au)	Platypus Tech.
Micropipettors and tips	Eppendorf
Millipore Q System	Millipore
Pasteur pipettes and bulbs	VWR
Platinum wire, annealed 0.5 mm	Alfa Aesar
Polishing alumina, 0.05 μM, 7mL	BASi
Potentiostat model 283	PAR
Quartz cuvettes (1 mL)	Fisher
Single block easy cycler system	Ericomp
Syringes, 60 mL, 20 mL and 1 mL	Becton Dickinson

Table 2.2 Names and Sequences of DNA Primers and Synthetic Oligonucleotides[a]

Name		Sequence
Primers		
λ-13		5'-GCG GGT TTT CGC TAT TTA TG-3'
λ-509		5'-CAG CGG AGT CTC TGG CAT TC-3'
Oligomers		
TG-30	HO-$(CH_2)_6$-SS-$(CH_2)_6$-	5'-TGT GTG TGT GTG TGT GTG TGT GTG TGT GTG-3' 3'-ACA CAC ACA CAC ACA CAC ACA CAC ACA CAC-5'
Mx-30a	HO-$(CH_2)_6$-SS-$(CH_2)_6$-	5'-ATA TAT ATA TAT ATA TGT GTG TGT GTG TGT-3' 3'-TAT ATA TAT ATA TAT ACA CAC ACA CAC ACA-5'
Mx-30b	HO-$(CH_2)_6$-SS-$(CH_2)_6$-	5'-TGT GTG TGT GTG TGT ATA TAT ATA TAT ATA-3' 3'-ACA CAC ACA CAC ACA TAT ATA TAT ATA TAT-5'
Mx(s^4T)-30a	HO-$(CH_2)_6$-SS-$(CH_2)_6$-	5'-ATA TAT ATA TAT ATA TGT GTG **T**G**T** G**T**G TGT-3' 3'-TAT ATA TAT ATA TAT ACA CAC ACA CAC ACA-5'
Mx(s^4T)-30b	HO-$(CH_2)_6$-SS-$(CH_2)_6$-	5'-TGT G**T**G **T**G**T** GTG TGT ATA TAT ATA TAT ATA-3' 3'-ACA CAC ACA CAC ACA TAT ATA TAT ATA TAT-5'

[a] Primers were purchased from the University of Calgary Regional DNA Synthesis Lab. Oligomers were purchased from the Plant Biotechnology Institute. The location of the incorporated 4-thiothymines in Mx(s^4T)-30 are indicated by the blocked characters in the sequence.

Reactions were allowed to continue linear synthesis until the reaction rate decreased at which time the synthesis was terminated by adding 25 mM EDTA (pH 8.0).

2.2.2 Production of Lambda DNA by PCR

A 496 bp duplex DNA fragment from the bacteriophage lambda genome was amplified using primers λ-13 and λ-509 listed in Table 2.2. Each polymerase chain reaction contained 20 μL of 10X PCR buffer (500 mM KCl, 15 mM $MgCl_2$, and 100 mM Tris-HCl pH 9.0), 15 μM of lambda template DNA, 9.6 μM of each primer, 0.25 mM of each dNTP, 10 U of *Taq* DNA polymerase and sterilized ddH_2O in a final volume of 200 μL. The reaction mixtures were covered with 1 drop of parafilm oil and run in an Ericomp thermocycler. Reactions were cycled 30 times with each cycle consisting of 30 sec (94°C), 30 sec (45°C) followed by 1 minute (72°C). Following purification (see below), the length of the PCR products were verified by agarose gel electrophoresis (Figure 2.1). The amplified DNA was run along side molecular weight markers on a 2% (w/v) agarose gel dissolved in running buffer (40 mM TRIS-Acetate pH 8.0, 20 mM sodium acetate, and 0.1 mM EDTA). The samples were electrophoresed at 80 V for 2 hours in a BioRad horizontally submerged gel apparatus and then stained with 2.0 μg/mL EtBr overnight on a shaker. The gels were then photographed under illumination by UV light at 365 nm.

2.2.3 Purification of Nucleic Acids

All synthesized DNA was purified with the Concert ™ rapid purification system as per manufacturers instructions (Gibco BRL) using 10 mM Tris-HCl (pH 7.5, 8.0, 8.5) or 10 mM 2-[N-Cyclohexylamino]ethanesulfonic acid (CHES) (pH 9.0) with 5 mM NaCl at 65°C to elute the final purified product.

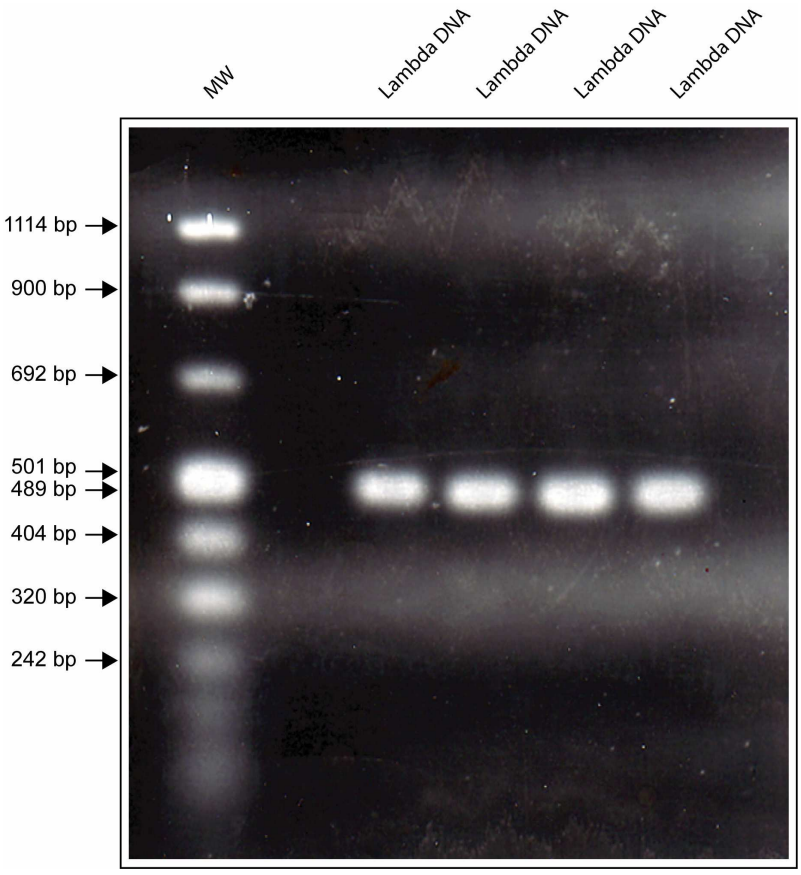

Figure 2.1 Ethidium Bromide fluorescence image showing the electrophoresis of PCR product for λ-496 DNA. The gel was run on 2.0% agarose. Roche DNA molecular weight marker VIII was loaded at 2 μL in the first lane. Five μL of PCR reaction was loaded into each of the lanes.

2.2.4 Oligonucleotides

The 30-mer oligonucleotides were synthesized in the Plant Biotechnology Institute (National Research Council, Saskatoon, Canada) with a DNA standard solid synthesizer, purified by HPLC and characterized by MALDI-TOF MS. DNA duplexes were prepared by adding 10 nmol of the disulphide-labeled DNA strands to 10 nmol of the complementary strands in a final volume of 100 μL in 20 mM Tris-ClO_4 and 100 mM $NaClO_4$ for at least 4 hrs at room temperature. The oligonucleotides were then electrophoresed on a 20% non-denaturing polyacryalamide gel in order to validate correct lengths and hybridization (Figure 2.2). Gels were poured and run in 1x TBE at low voltage to prevent denaturation of small fragments of DNA by heating. The gels were then stained with 2.0 μg/mL EtBr overnight on a shaker. The gels were photographed under illumination by UV light at 365 nm. Hybridization and concentration was confirmed using the ethidium fluorescence assay (Le Pecq and Paoletti, 1966). Although the presence of ssDNA can not be completely ruled out, the concentration of dsDNA calculated from both fluorescence and absorbance measurements were equivalent, indicating an undetectable concentration of ssDNA in solution.

2.3 Thermal Denaturation Profiles

The T_m measurements were recorded on a Gilford 600 spectrophotometer equipped with a thermoprogrammer using a 0.5 °C/min heating rate with a DNA concentration of 15 μg/mL. The buffer contained 10 mM Tris-HCl (pH 7.5, 8.0, 8.5) or 10 mM CHES (pH 9.0) and 5 mM NaCl with or without 0.2 mM metal ion.

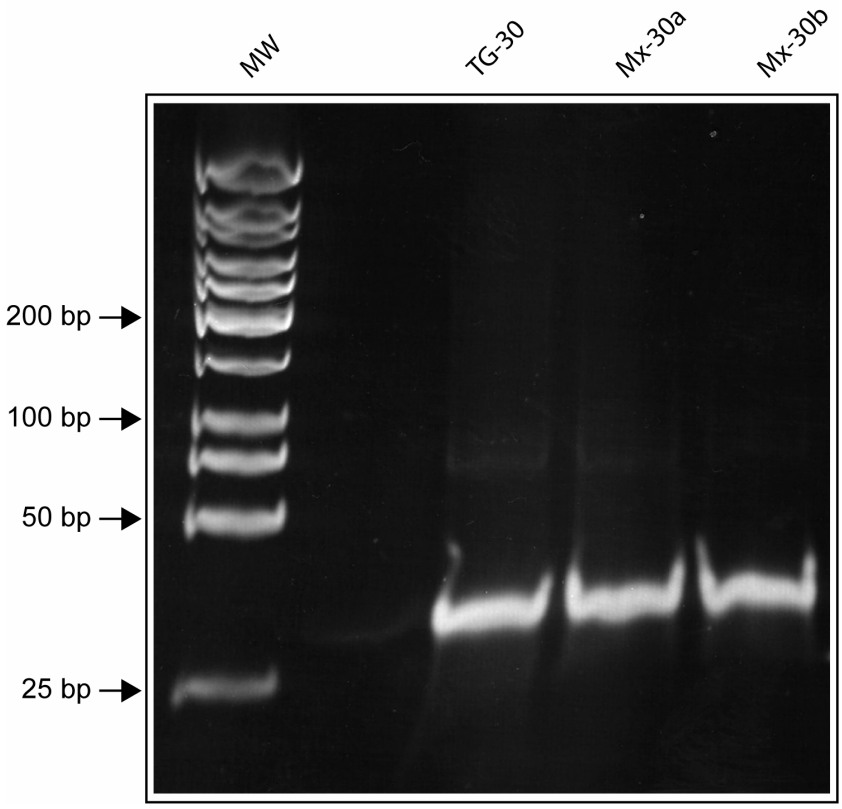

Figure 2.2 Ethidium bromide fluorescence image showing the electrophoresis of 30-mer oligonucleotides. The gel was run with 20% non-denaturing polyacrylamide gel for small DNA fragments. USB DNA low molecular weight marker was loaded at 2 μL in the first lane. Five μL of duplex oligonucleotide was loaded into each of the lanes.

Table 2.3 Experimental and Calculated Melting Temperatures of the Oligonucleotides[a]

NAME	T_m (°C)	Calculated
Mx-30a	58.9 ± 0.4	59
Mx-30b	59.6 ± 0.3	59
TG-30	73.4 ± 0.1	70

[a]The calculated melting temperatures were derived from the publicly available program MeltCalc.

2.4 Ethidium Fluorescence Assay

Briefly, if B-DNA is added to a pH 8.3 buffer containing ethidium and 0.2 mM Zn^{2+}, the ethidium will bind and the fluorescence will be enhanced. If M-DNA is added to the same buffer the conversion to B-DNA is very slow, ethidium does not bind and there is no enhancement of fluorescence (Lee *et al.*, 1993). By addition of EDTA, the M-DNA is converted back to B-DNA and the fluorescence is restored. The addition of EDTA also serves to distinguish between M-DNA and denatured DNA since the later does not bind ethidium to yield high fluorescence with or without EDTA (Figure 2.3).

A modified form of the ethidium fluorescence assay was used in which the DNA and $ZnCl_2$ were incubated in the presence of ethidium bromide. This technique has been used previously and the ethidium bromide does not affect M-DNA formation (Wood *et al.*, 2002). Aliquots of 10 μL 150 μM DNA (in bases) in 10 mM, CHES (pH 9.0) with 5 mM NaCl were added to 2 mL of ethidium fluorescence buffer (EFB), giving a final DNA concentration of 0.71 μM. The EFB contained 10 mM buffer, 0.2 mM $ZnCl_2$ and 0.5 μg/ml ethidium bromide. Eight pHs of buffer were used: pH 6.0 with 2-[*N*-morpholino]ehtanesulfonic acid (MES) buffer, pH 7.0 and 7.2 with 3-[*N*-Morpholino]propanesulfonic acid (MOPS), and pH 7.6, 7.8, 8.0, 8.2, and 8.4 with Tris-HCl buffer. The aliquots were incubated in the EFB for 30 minutes then the emission at 600 nm following excitation at 525 nm was recording using a Hitachi F-2500 fluorescence spectrophotometer. EDTA was added to a final concentration of 1.0 mM following each measurement, and the fluorescence was again measured. All values are reported as percentage B-DNA normalized against the pH 6.0 reading taken as 100% B-DNA.

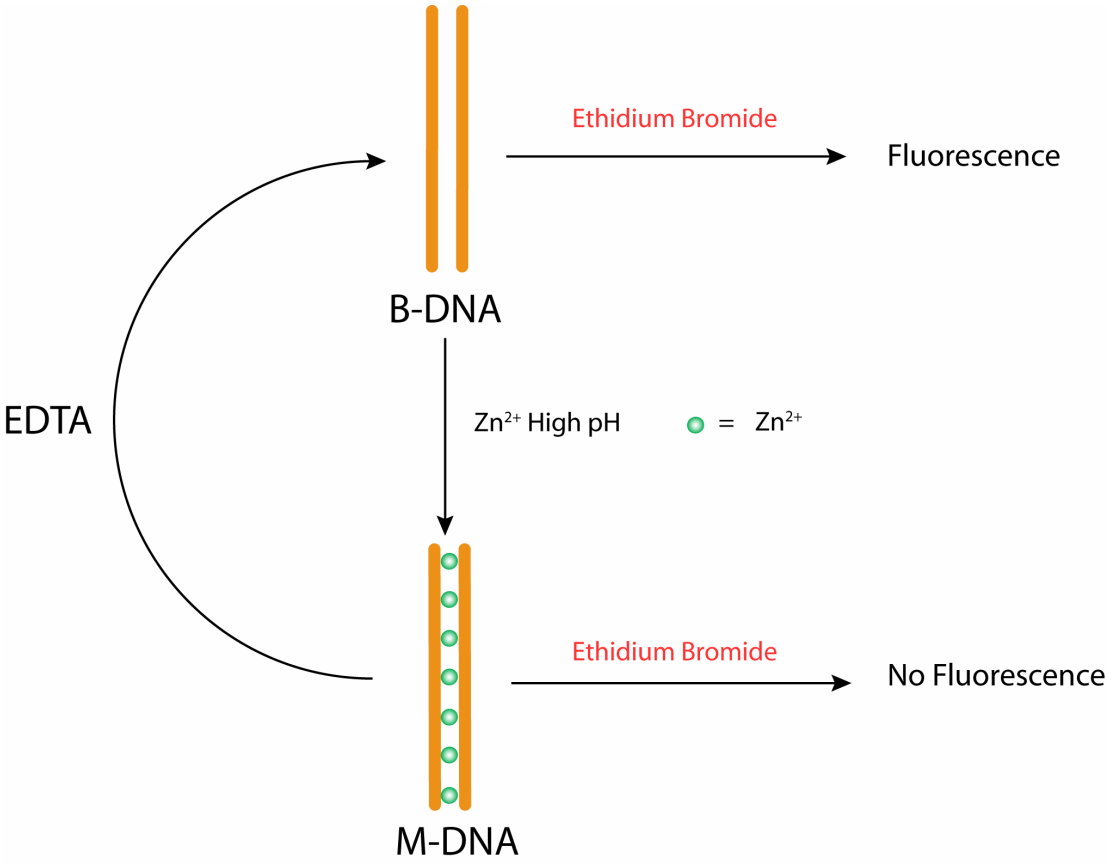

Figure 2.3 A schematic of the ethidium fluorescence assay

2.5 X-ray Photoelectron Spectroscopy

An Axis-165 (Kratos Analytical) photoelectron spectrometer equipped with a monochromatic Al-Kα X-ray source with an operating power of 210 W was used to collect photoemission spectra at the Alberta Centre for Surface Engineering and Science, University of Alberta. The size of the sample spot was 400 μm x 700 μm and an 8 channeltron multidetector was used to collect the energy spectra. The base pressure during measurements was maintained at 5 x 10^{-10} Torr. The take-off angles were 90, 70, 45 and 30 degrees from surface. The sample holder was rotated on an axis coplanar with the sample surface and intersecting the detector axis. Survey scans were measured from 0-1100 eV binding energy at 160 eV pass energy at a step increment of 0.33 eV and high-resolution spectra were measured at a pass energy of 40 eV and a step increment of 0.1 eV resulting in an energy resolution of 0.76 eV (measured as the FWHM for Ag $3d_{5/2}$ peak). The peaks were fit using the publicly available XPSPEAK v. 4.1. The film spectra were referenced to the Au 4f $_{7/2}$ at 84.0 eV and also checked against the Au $4d_{5/2}$ at 335. 2 eV as a secondary reference (Seah, 1989; Powell, 1995). Shirley and linear functions were used as a background and Gaussian-Lorentzian products were used to fit the individual peaks.

2.5.1 Preparation of DNA Modified Gold Electrodes

Prior to deposition of the films, gold-coated silicon wafers were cut into approximately 1cm x 1cm pieces and cleaned in a "piranha solution" consisting of 70% H_2SO_4 and 30% H_2O_2 (30% H_2O_2 in H_2O) for 10 minutes *(Caution! Piranha solution should be handled with extreme care and should never be stored in a closed container. It is a very strong oxidant and reacts violently with most organic materials).* The wafers were then rinsed thoroughly with Millipore water, dried with argon gas and immediately immobilized with 10 μL of 100 μM dsDNA dissolved in 20 mM Tris-ClO_4 buffer pH 8.5 with 20 mM $NaClO_4$. The DNA was deposited onto the freshly prepared gold electrode and manually spread to cover the entire gold surface area. The electrodes were placed in a sealed container and incubated for 5 days in a humidifier in

order to prevent evaporation of the samples (Galka and Kraatz, 2002; Long *et al.*, 2003). After the five day incubation, the wafers were then washed thoroughly with buffer in order to remove nonspecifically bound DNA and dried with Argon gas before measurements were taken (Yang *et al.*, 1998). The washing procedure was done using a glass Pasteur pipette in order to produce a reasonable amount of hydrodynamic force and was repeated using approximately 40 mL of buffer before drying with Argon gas. B-DNA was converted to M-DNA by the addition of 0.2 mM $Zn(ClO_4)_2$ to the gold surface for 2 hours (Li *et al.*, 2003; Long *et al.*, 2003). As above, the wafers were washed with buffer and dried with Argon. The bare gold control was cleaned with the same procedure as the other samples. After rinsing with Millipore water the wafer was dried with Argon and incubated for 5 days alongside the other samples.

2.5.2 DNA Coverage Calculations

In order to determine the DNA coverage, the atomic density of N relative to Au (N_N/N_{Au}) was first calculated using Equation 3.2, which will be discussed in detail in the Results section. This number was then multiplied by the film thickness in order to determine the relative N coverage and finally, was multiplied by 2.72 x 10^{13} molecules/cm^2 to obtain the DNA coverage. The numerical factor 2.72 x 10^{13} molecules/cm^2 was derived by dividing the atomic density of gold, calculated as 5.892 x 10^{22} atoms/cm^3 assuming a gold density of 19.28 g/cm^3, by the number of nitrogen (N=217) in one molecule of dsDNA and multiplying by a factor of 10^{-7} to account for the thickness being in nanometers rather than centimeters.

2.5.3 Density Calculations

In order to calculate the density of DNA in g/cm^3, the N_N/N_{Au} calculated from Equation 5 was multiplied by the following conversion factor [19.28 x (18616/217)/197] = 8.40 where 18616 g/mol and 217 are the atomic mass and the number of nitrogen respectively in one molecule of dsDNA. The atomic mass and density of gold are 197 g/mol and 19.28 g/cm^3 respectively.

2.6 Electrochemistry

2.6.1 Electrode Preparation

Stationary gold voltammetry electrodes (1.6 mm diameter) were purchased from Bioanalytical Systems. Before use, the electrodes were polished with alumina on fabric pads attached to glass plates and then rinsed thoroughly with Millipore water. Finally, they were electrochemical treated by cycling from a potential of 0.2 to 1.5 V versus Ag/AgCl in 0.5M H_2SO_4 solution (Finklea, 1996). The voltammogram in figure 2.4 shows two clearly defined peaks separated by a third less distinct peak. The three peaks observed in the anodic scan for bare gold in H_2SO_4 results from the chemisorption of OH species from the breakdown of water molecules at the electrode surface and proceed via the following three distinct steps (Woods, 1976).

$Au + H_2O \rightarrow Au_4OH + H^+ + e^-$
$Au_4OH + H_2O \rightarrow Au_2OH + H^+ + e^-$
$Au_2OH + H_2O \rightarrow AuOH + H^+ + e^-$

These formulas do not represent stoichiometric species, but only denotes the surface-site occupancy. The characteristics of clean gold includes a sharp rise in anodic current near 1.1 V, a single oxide stripping peak near 0.9 V and a reproducible cyclic voltammogram (CV) on successive scans (Figure 2.4). Any residue of organic contaminant left by the preceding cleaning treatments is removed during repeated oxidation and reduction of the gold.

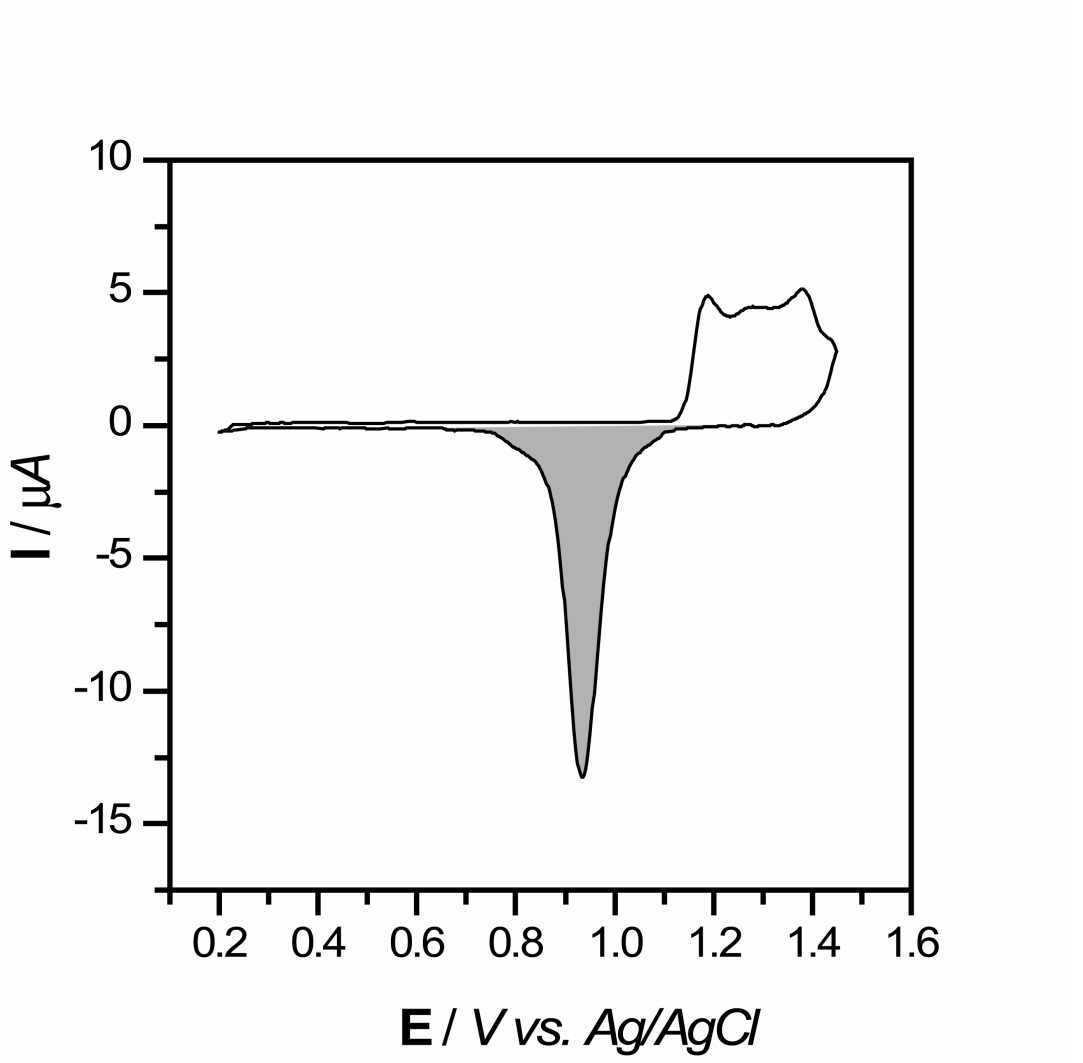

Figure 2.4 CV of a bare gold electrode cycled in 0.5 M H_2SO_4 at 100 mV/s. The shaded area represents the integration of the cathodic peak current.

2.6.2 Real Surface Area Determination

An added advantage of performing the above step is that the real surface area of the gold electrodes can be estimated from the oxygen adsorption measurements. After the three peaks, there should be an approximate monolayer. Therefore the coverage can be obtained by desorbing the layer on the cathodic potential sweep and calculating the amount of charge passed (Figure 2.4). This can be done by integrating the cathodic peak current vs. voltage and then dividing by the scan rate or simply graphing the current vs. time and directly integrating the charge. The charge corresponding to the adsorption of one oxygen atom per surface site was calculated to be approximately 386 μC cm^{-2} (Woods, 1976). Hence, the real area is given by the calculated charge of cathodic peak divided by 386 μC cm^{-2}. Importantly, it can be seen that the current begins to increase above ~1.5 V due to the onset of molecular oxygen evolution causing an increasingly larger cathodic peak (Figure 2.5). Therefore, care must be taken to stop the scan prior to this event in order to achieve a more accurate estimation of surface roughness. Also the charge created from the double layer capacitance should not be included when calculated the amount of charge passed.

Another approach to obtain the real surface area of the gold electrode is to perform CV experiments in solution containing a redox probe at various scan rates. The slope from the peak current vs. the inversed square root of the scan rate can be used in the Randles-Sevcik equation in order to obtain the area of the electrode.

$$I_p = \left(2.69 \times 10^5\right) n^{3/2} A D^{1/2} v^{1/2} C_0 \qquad (2.1)$$

Where the peak current (I_p) is in Amps, n is the number of electrons transferred, the diffusion coefficient (D) is in cm^2/sec, the scan rate (v) is in V/sec, the concentration is in mols/cm^3 and the area of the electrode surface (A) is in cm^2.

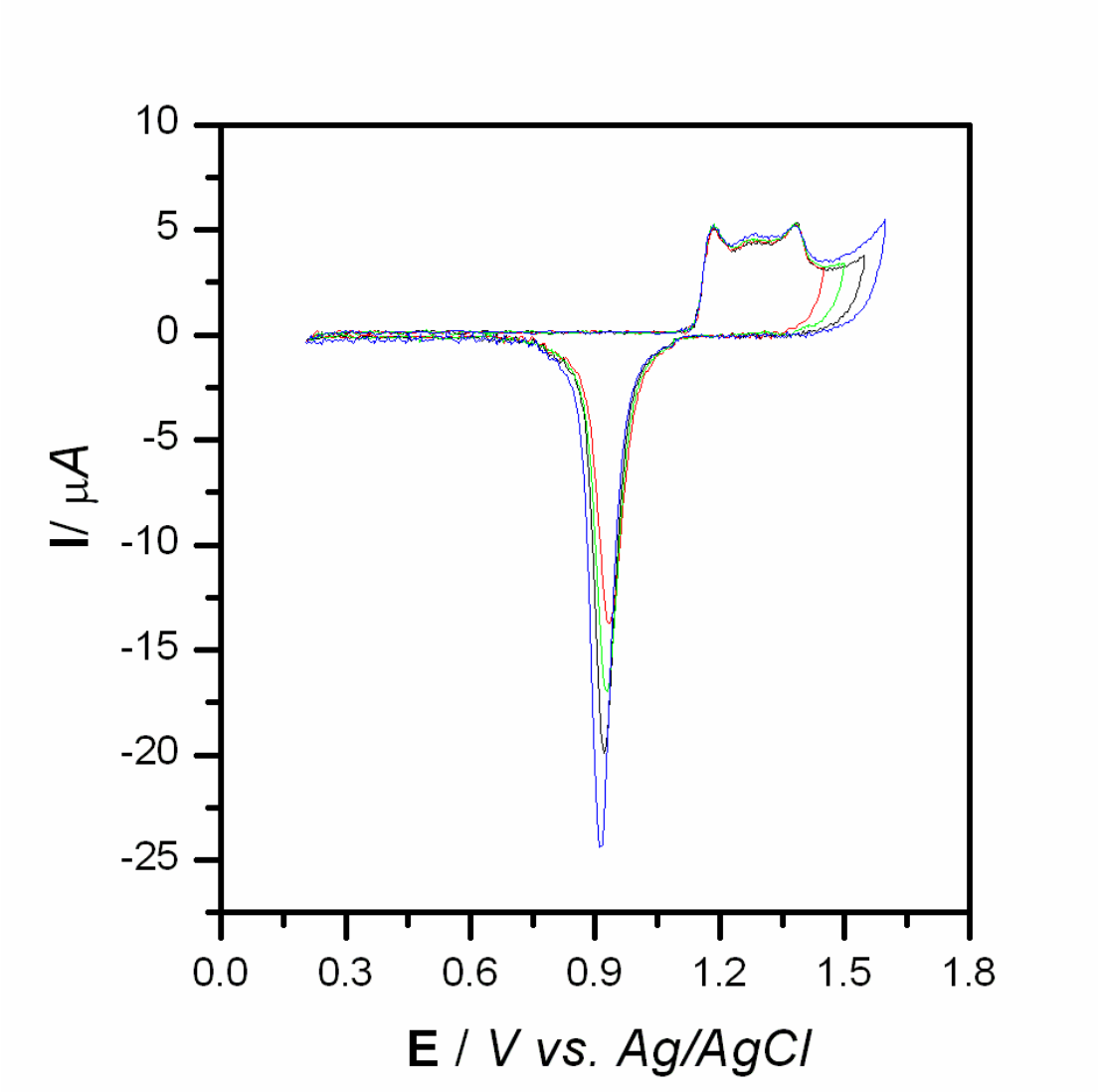

Figure 2.5 CV of a bare gold electrode cycled in 0.5 M H_2SO_4 to increasingly positive potentials.

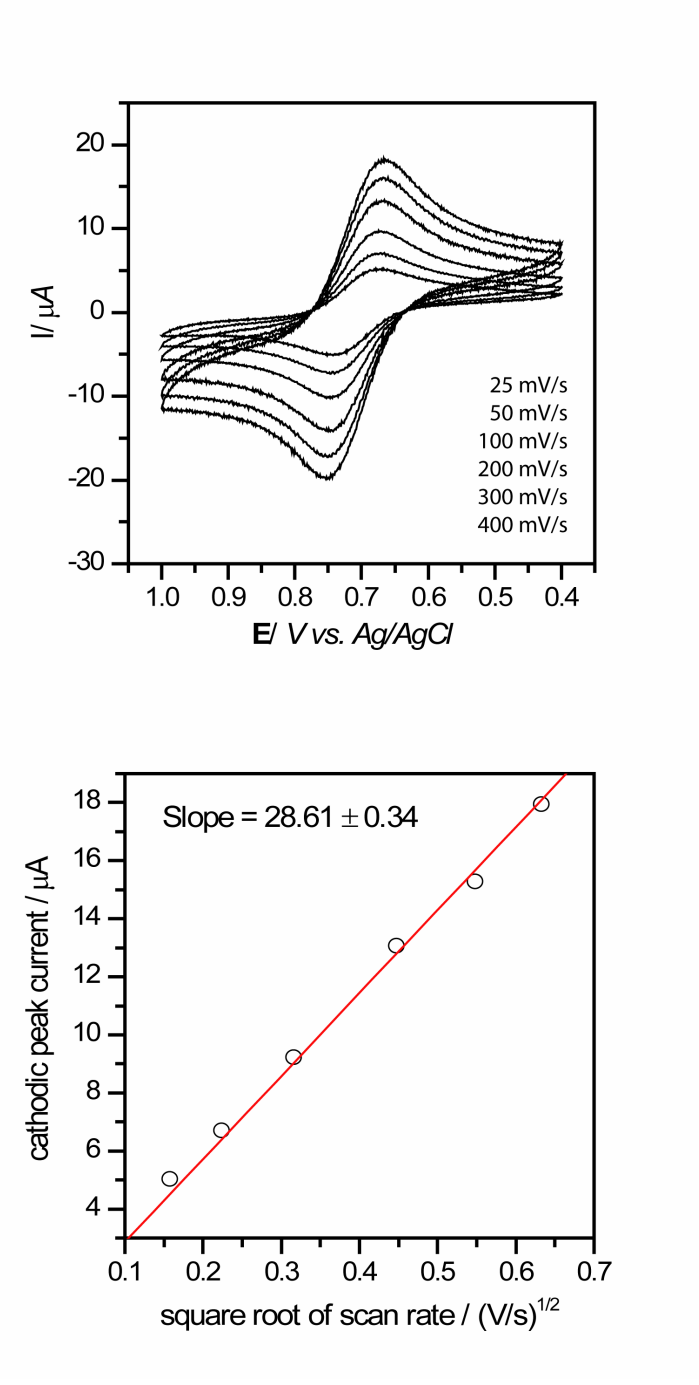

Figure 2.6 Cyclic Voltammetry of bare gold electrode performed in 1 mM $IrCl_6^{2-/3-}$ at various scan rates.

2.6.3 Monolayer Preparation

Immediately following the electrochemical treatment in H_2SO_4, the electrode was thoroughly rinsed with Millipore water, dried with argon and 5 μL of 100 μM dsDNA was deposited onto electrode. The freshly prepared electrodes were incubated for 5 days in a sealed humidifier in order to prevent evaporation of the samples (Galka and Kraatz, 2002; Long *et al.*, 2003). After 5 days, the electrodes were rinsed thoroughly with buffer solution in order to remove nonspecifically bound DNA and mounted into an electrochemical cell shown in figure 1.20 in section 1.5.4.1 of the Introduction (Yang *et al.*, 1998).

2.6.4 Electrochemical Measurements

All electrochemical experiments were performed in a conventional three electrode cell consisting of a gold working electrode with a geometrical area of 2.0 mm^2, a Ag/AgCl/3 M NaCl reference electrode encased in a double-junction electrode chamber containing 3 M KNO_3 and finally a Pt wire (0.5 mm diameter) as the auxiliary/counter electrode. The salt bridge was used in conjunction with the reference electrode in order to prevent the leakage of Cl^- ions which can result in etching of the gold surface or stripping of the DNA monolayer. All experiments were performed in a grounded Faraday cage at room temperature using a Princeton EG & G 1025 frequency response analyzer interfaced to an EG & G 283 potentiostat/galvanostat. All data was compiled using oligomers Mx-30a and Mx-30b unless otherwise specified.

Typical cyclic voltammetry experiments were done in 2 mM hexachloroiridate (IV) in 20 mM TrisClO_4 at a sweep rate of 100 mV/s. Impedance measurements were taken using an ac voltage amplitude of 5 mV with voltage frequencies ranging from 100 kHz to 25 mHz using an applied potential of 690 mV vs Ag/AgCl. Measurements were performed in 1 mM hexachloroiridate (IV) in 20 mM TrisClO_4. The chronocoulometry experiments were done using a 400 mV potential step experiment (900 to 500 mV) in 2 mM hexachloroiridate (IV) in 20 mM TrisClO_4. The initial potential of 900 mV was held for 0.1 sec and then stepped to 500 mV for 9.0 sec.

The dsDNA monolayer was converted to M-DNA by incubating the monolayer in a solution of 0.4 mM $Zn(ClO_4)_2$ in 20 mM Tris-ClO_4 buffer (pH 8.6). Bis-tris propane was used for experiments involving buffers at pH 6.0, 6.3, and 6.7. Denaturation of ds-DNA was achieved by exposing the monolayer to 10 mM NaOH for 10 minutes at 65 °C, thorough rinsing with Millipore water followed by an additional 10 minute soak in NaOH. Rehybridization was performed by exposing the film to 100 μM target strand in 20 mM Tris-ClO_4, 100 mM $NaClO_4$ (pH 7.1) for 3 hours.

2.6.4.1 Determination of DNA Surface Density

Chronocoulometry experiments were also performed in order to determine the DNA concentration on the gold surface (Steel *et al.*, 1998; Yu *et al.*, 2003). The measurements were done in Tris buffer (pH 8.5) in the presence and absence of 100 μM $[Ru(NH_3)_6]^{3+}$. Since $[Ru(NH_3)_6]^{3+}$ binds to the negatively charged phosphodiester backbone of DNA in a 1:3 ratio, the amount of charge-compensating redox marker can be used to determine the DNA surface density with the integrated Cottrell equation, which expresses charge Q as a function of t

$$Q = \frac{2nFAD_0^{1/2}C_0^{*}}{\pi^{1/2}}t^{1/2} + Q_{dl} + nFA\Gamma_0 \qquad (2.2)$$

where n is the number of electrons per molecule for reduction, F is the Faraday constant (C/equiv), A is the electrode area (cm^2), D_0 is the diffusion coefficient (cm^2/s), C_0* is the bulk concentration (mol/cm^2), Q_{dl} is the capacitive charge (C), and $nFA\Gamma_0$ is the charge from the reduction of Γ_0 (mol/cm^2) of adsorbed $[Ru\text{-}(NH_3)_6]^{3+}$. The surface excess term, Γ_0, is determined from the difference in chronocoulometric intercepts for identical experiments in the presence and absence of redox marker. The DNA surface density can then be calculated using the following relationship

$$\Gamma_{DNA} = \Gamma_0(z/m)(N_A) \qquad (2.3)$$

where Γ_{DNA} is the DNA surface density (molecules/cm^2), m is the number of bases in the immobilized DNA, z is the charge of the redox molecule, and N_A is Avogadro's number (Steel *et al.*, 1998).

3.0 RESULTS

3.1 Thermal Denaturation Profiles

The effect of metal ions on DNA stability has been extensively investigated previously using thermal denaturation profiles (Eichhorn, 1962; Eichhorn and Shin, 1968). Due to their ease of determination and the reproducibility of results, they were implemented in order to assess the effect of the sequence, modified base substitutions and pH on the thermal stability of M-DNA.

3.1.1 Denaturation Profile of Lambda DNA

As shown in figure 3.1, in the absence of metal ion, λ-496 DNA has three different melting transitions corresponding to A•T rich regions, mixed regions and G•C rich regions of DNA. However, upon the addition of Zn^{2+} at pH 7.5 only one melting transition is observed. This new T_m corresponds more closely to that of the A•T region in lambda DNA meaning the higher melting G•C regions have become less stable under these conditions. As the pH is increased to 8.0 and 8.5, the destabilization becomes much more prominent. However, upon the addition of Zn^{2+} at pH 9.0 there is an increase in temperature corresponding more closely to the mixed or G•C rich regions. This sudden increase in thermostability is associated with the structural transition to M-DNA. Interestingly, although the addition of Mg^{2+} (Table 3.1) increases the melting temperature at all pH values, there still remain three separate melting transitions. The drastic difference in the denaturation profiles between Mg^{2+} and Zn^{2+} support previous claims that Mg^{2+} is simply binding to the backbone whereas Zn^{2+} is binding to the nucleobases and affecting the hydrogen bonds. This may be responsible for the initial destabilization, but under high pH conditions the DNA is able to undergo a conformational change to M-DNA.

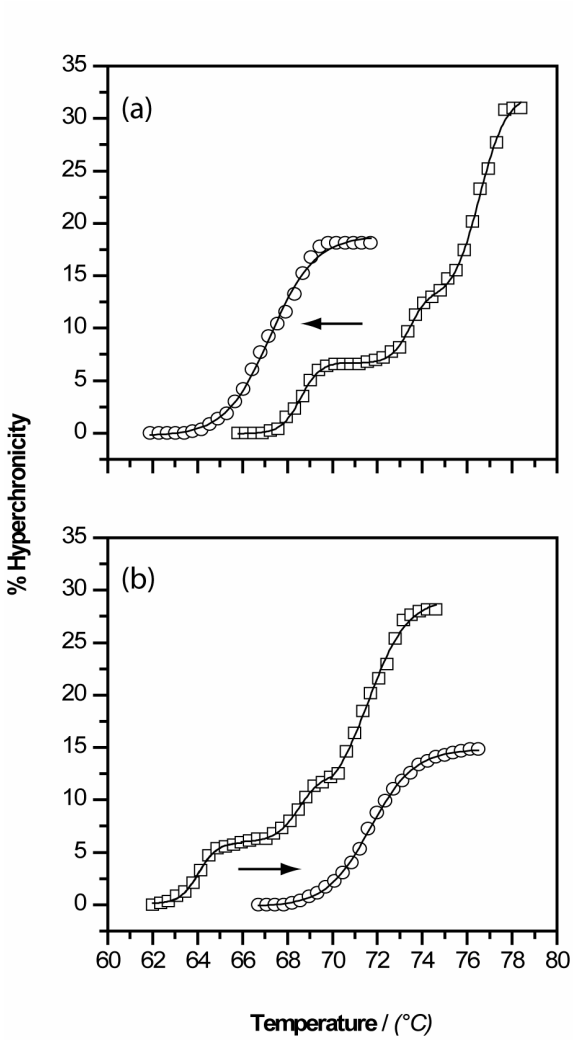

Figure 3.1 Thermal denaturation profiles for λ-496 DNA in the absence of metal ions (□) and in the presence of 0.2 mM $ZnCl_2$ (○) at pH a) 7.5 and b) 9.0. The solid lines represent calculated sigmoidal fits to the corresponding data.

Table 3.1 Melting Temperatures of λ-496 DNA in the Presence and Absence of Metal Ions

pH	DNA	DNA + Zn	DNA + Mg
7.5	(72 ± 3), (76 ± 3), (80 ± 2)	(69 ± 1)	(77 ± 1), (82 ± 1), (85 ± 1)
8.0	(70 ± 1), (74 ± 1), (77 ± 2)	(59 ± 1)	(78 ± 1), (83 ± 1), (85 ± 1)
8.5	(70 ± 4), (75 ± 4), (78 ± 4)	(59 ± 3)	(77 ± 1), (82 ± 1), (84 ± 1)
9.0	(66 ± 2), (71 ± 2), (74 ± 2)	(70 ± 3)	(77 ± 1), (82 ± 1), (84 ± 1)

These experiments demonstrate the importance of pH on the formation of M-DNA. However, in order to investigate the effects of sequence on M-DNA formation, repetitive sequence DNA was synthesized. Such DNA is extremely useful as its sequence repetition will amplify any effect that the particular sequence has on the conformation.

3.1.2 Synthesis of Repetitive Sequence DNA

An important aspect of the experiments described in this report was the synthesis of repetitive sequence nucleic acids. An example of the reaction kinetics for the synthesis of poly[d(AT)] is shown in figure 3.2. Initially, great care was taken to stop the reaction before synthesis was complete in order to inhibit the 5'→3' exonuclease activity of *E. coli* polymerase which would cause rapid degradation of the duplex, as demonstrated in figure 3.2. However, in the majority of subsequent experiments only the large fragment, called the Klenow fragment, of polymerase was used. The Klenow fragment is advantageous as it maintains the polymerase activity as well as the 3'→5' proofreading activity, but no longer has the 5'→3' exonuclease activity which is responsible for degrading the DNA. Therefore, synthesis reactions were allowed to continue to completion without the need to stop the reaction prematurely.

The effect of sequence on the rate of M-DNA formation was previously investigated and it was found that poly[d(TG)•d(CA)] formed Zn^{2+} M-DNA the quickest while poly[d(AT)] formed it at the slowest rate. After only a couple of minutes poly[d(TG)•d(CA)] was completely converted to M-DNA. However, even after one hour, the majority of poly[d(AT)] was still in the B-DNA conformation (Lee *et al.*, 1993). Therefore, these sequences were considered excellent candidates to study the effects of sequence in combination with the incorporation of novel nucleotides on the formation and stability of M-DNA.

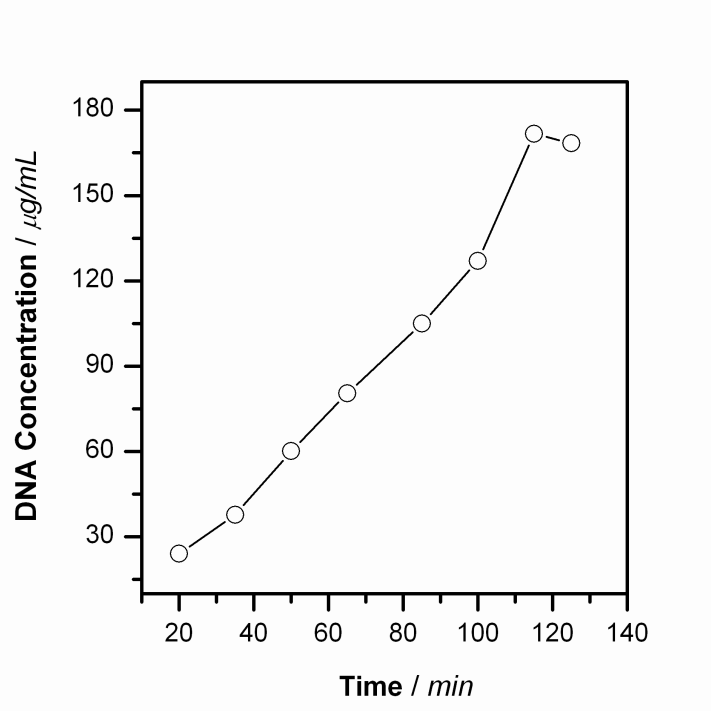

Figure 3.2 Synthesis of poly[d(AT)] in Kpi buffer system at 37ºC using DNA *E. coli* polymerase. Synthesis was followed by the ethidium fluorescence assay. Reactions were allowed to continue linear synthesis until the reaction rate decreased at which time the synthesis was terminated by adding 25 mM EDTA (pH 8.0).

Since transition metal ions such as Zn^{2+} form stable complexes with sulphur-containing ligands (Lee *et al.*, 1984; Maret, 2004), it was considered possible that incorporation of thiobases into the DNA helix might stabilize M-DNA at lower pHs. Therefore, the effects of the nucleotide analogues 2-thiothymine (s^2T) and 4-thiothymine (s^4T) on the stability of M-DNA was studied by preparing poly[d(As^2T)], poly[d(As^4T)], poly[d(s^2TG)•d(CA)] and poly[d(s^4TG)•d(CA)].

The synthesis of s^4T-containing duplexes proved to be much more difficult than those with s^2T. A possible explanation for this is that the thioketo group coordinated to the C4 position is directly involved in a hydrogen bond whereas the sulfur bond to the C2 position is not. Since the atomic radius of sulfur (109 pm) is almost twice as large as the oxygen atom (65 pm) it is replacing, a duplex with s^4T must be distorted with a widening of the major groove. However, it was discovered that synthetic reactions containing 50% s^4TTP and 50% TTP gave reasonable yields with approximately a 42% incorporation of s^4T. Since the incorporation of s^4T gives a characteristic UV maximum at approximately 345 nm which is clearly separated from the 260 nm maximum observed in native DNA, the proportion of s^4T residues was estimated by comparing our spectra with those reported elsewhere (Figure 3.3) (Connolly and Newman, 1989).

Interestingly, in the presence of 0.2 mM $ZnCl_2$ at pH 8.5, the 345 nm peak of poly[(As^4T)] shows a blue shift of approximately 10 nm as well as a slight decrease in the intensity at 260 nm (Figure 3.4). The 345 nm peak does not change with increasing pH in the absence of metal ion or in the presence of $MgCl_2$ as shown in figure 3.5. Only when the DNA is completely denatured is there a similar shift, which most likely results from the single stranded thiobases being in a state where they are free to interact with the Zn^{2+} or Mg^{2+}. However, the decrease in absorbance at 260 nm in the presence of Zn^{2+} at pH 8.5 clearly shows that the DNA is not denatured and that the Zn^{2+} must be interacting with the thiobases while maintaining the duplex conformation. All of these results suggest strongly that a conformational change such as that proposed for M-DNA is taking place.

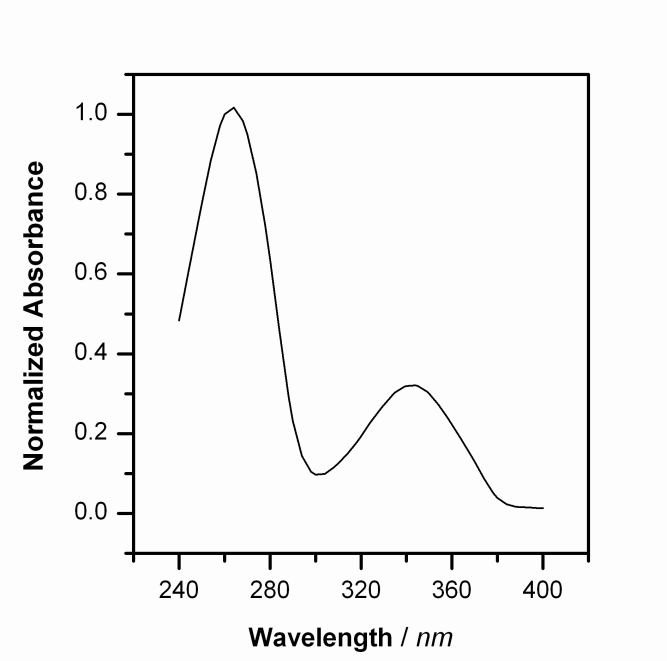

Figure 3.3 The UV absorption spectra of poly[d(As^{4}T)]. The percentage of s^{4}T incorporation was calculated based on the A_{260}/A_{345} ratio in comparison to published data from Connolly and Newman, 1989.

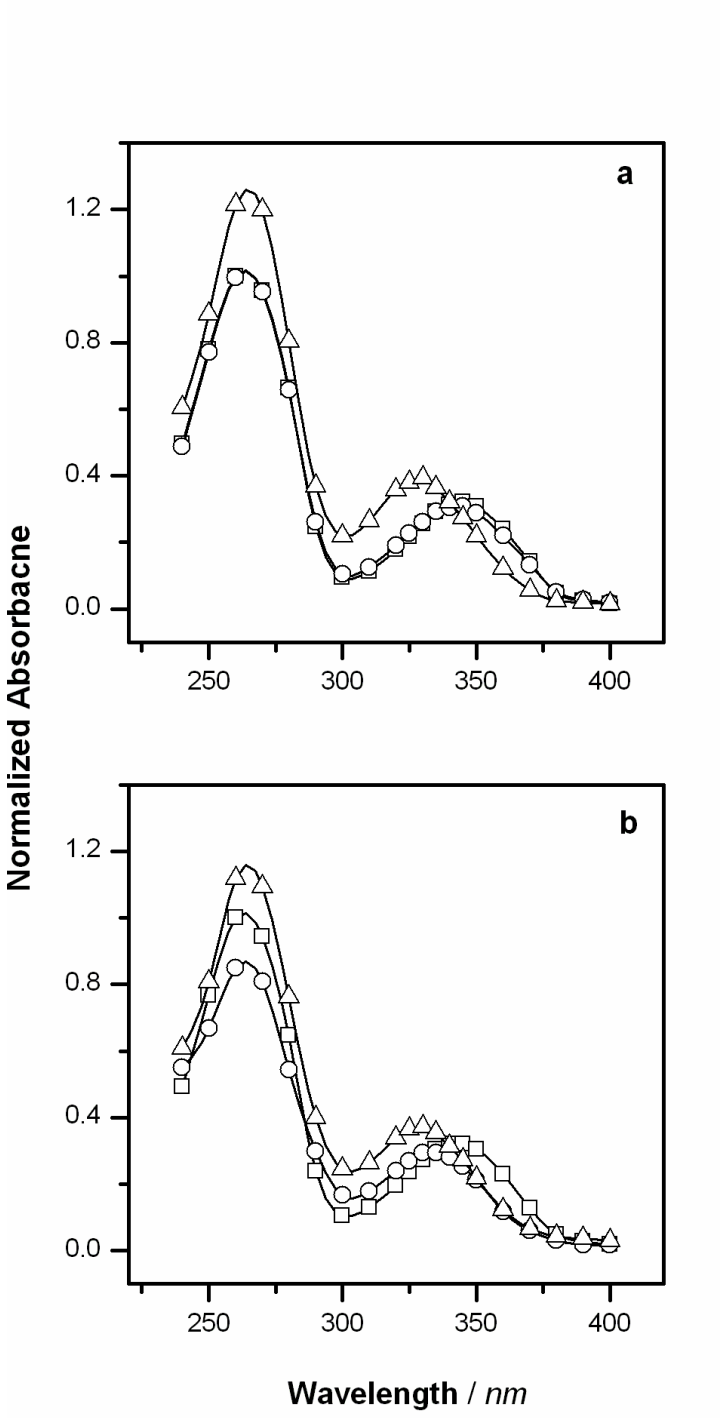

Figure 3.4 Absorption spectra of poly[d(As^{4}T)] in the absence of metal ion at 27ºC (□); with 0.2 mM ZnCl at 27ºC (○); with 0.2 mM ZnCl at 92ºC (△); in **(a)** 10 mM Tris-HCl buffer (pH 7.5) with 5 mM NaCl and **(b)** in 10 mM Tris-HCl buffer (pH 8.5) with 5 mM NaCl.

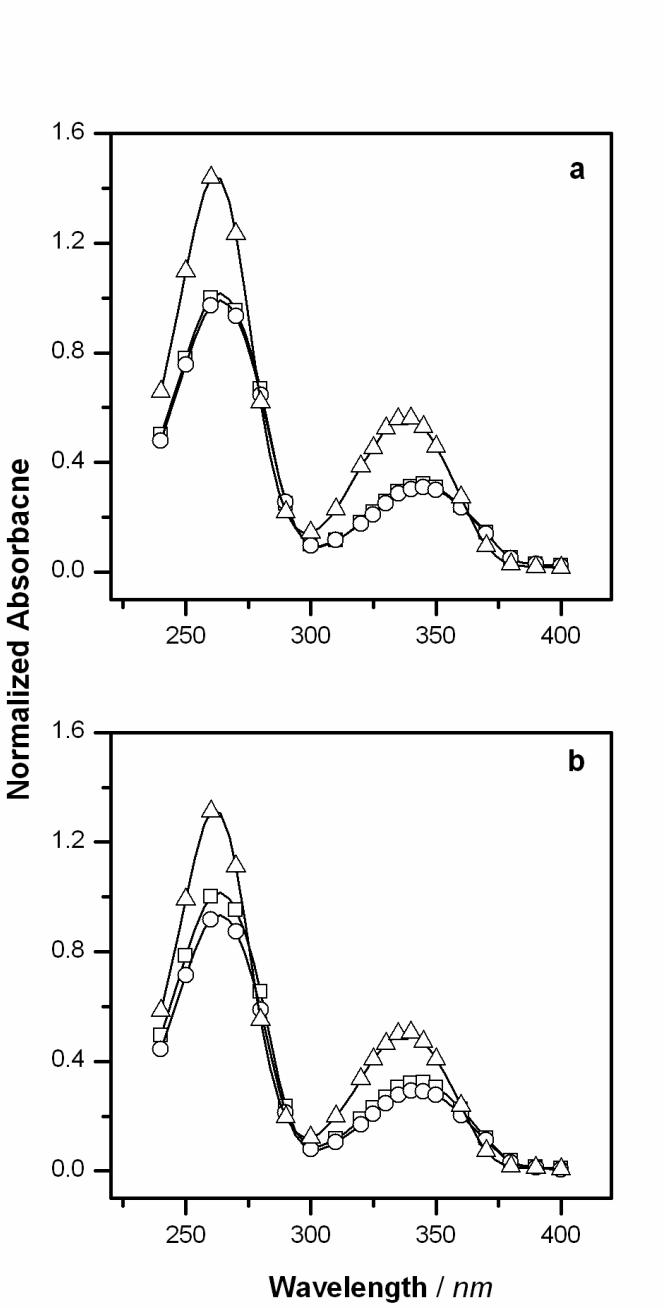

Figure 3.5 Absorption spectra of poly[d(As^{4}T)] in the absence of metal ion at 27ºC (□); with 0.2 mM MgCl at 27ºC (○); with 0.2 mM MgCl at 92ºC (△); in **(a)** 10 mM Tris-HCl buffer (pH 7.5) with 5 mM NaCl and **(b)** in 10 mM Tris-HCl buffer (pH 8.5) with 5 mM NaCl.

Although initially this discovery showed promise for the development of an additional assay to monitor the formation of M-DNA, further studies showed that the shift is far less dramatic when the s^4T is incorporated into λ-496 DNA. The decrease in sensitivity is most likely a result of sequence. Previously, it was shown that oligonucleotides GACGAs^4TATCGTC and GACGATAs^4TCGTC gave slightly different maximum UV values of 345 nm and 335 nm respectively (Connolly and Newman, 1989). Therefore, such a shift would mask any effects seen for the conversion of B-DNA to M-DNA. However, this development has clearly shown that there is a definite conformational change in the presence of Zn^{2+} as opposed to magnesium.

3.1.3 Effect of Base-Substitutions on Thermal Stability

Synthetic DNAs were studied by comparing thermal denaturation profiles at different pHs in the presence or absence of Zn^{2+}. Mg^{2+} was also included as a control since it does not induce M-DNA formation and stabilizes B-DNA at all pHs (Lee *et al.*, 1993). As shown in figure 3.6a, an expected increase of approximately 10 °C in the T_m for poly[d(AT)] in the presence of Mg^{2+} is observed at all pH values (Eichhorn and Shin, 1968). There is also a smaller increase observed upon the addition of Zn^{2+} at pHs 7.5, 8.0 and 8.5. However, there is an additional increase in T_m above that for Mg^{2+} observed for Zn^{2+} at pH 9.0. This increase in thermostability at high pH is attributed to the formation of M-DNA. As shown in figure 3.6b the T_m of poly[d(As^2T)] with Zn^{2+} seems thermally unstable and reaches a minimum of 38 ^oC at pH 8.5. Although an increase to nearly 50^oC at pH 9.0 does suggest the formation of M-DNA, the structure is very unstable in comparison to its B-DNA construct. In figure 3.6c, the T_m of poly[d(As^4T)] with Zn^{2+} reaches a minimum of 35^oC at pH 8.0 which begins to increases at pH 8.5 and continues to 55 ^oC at pH 9. Therefore, this analogue seems to aid in the early formation of M-DNA at a lower pH value but still remains thermally unstable until pH 9.0 at which point the melting temperature is similar to that for Mg^{2+}.

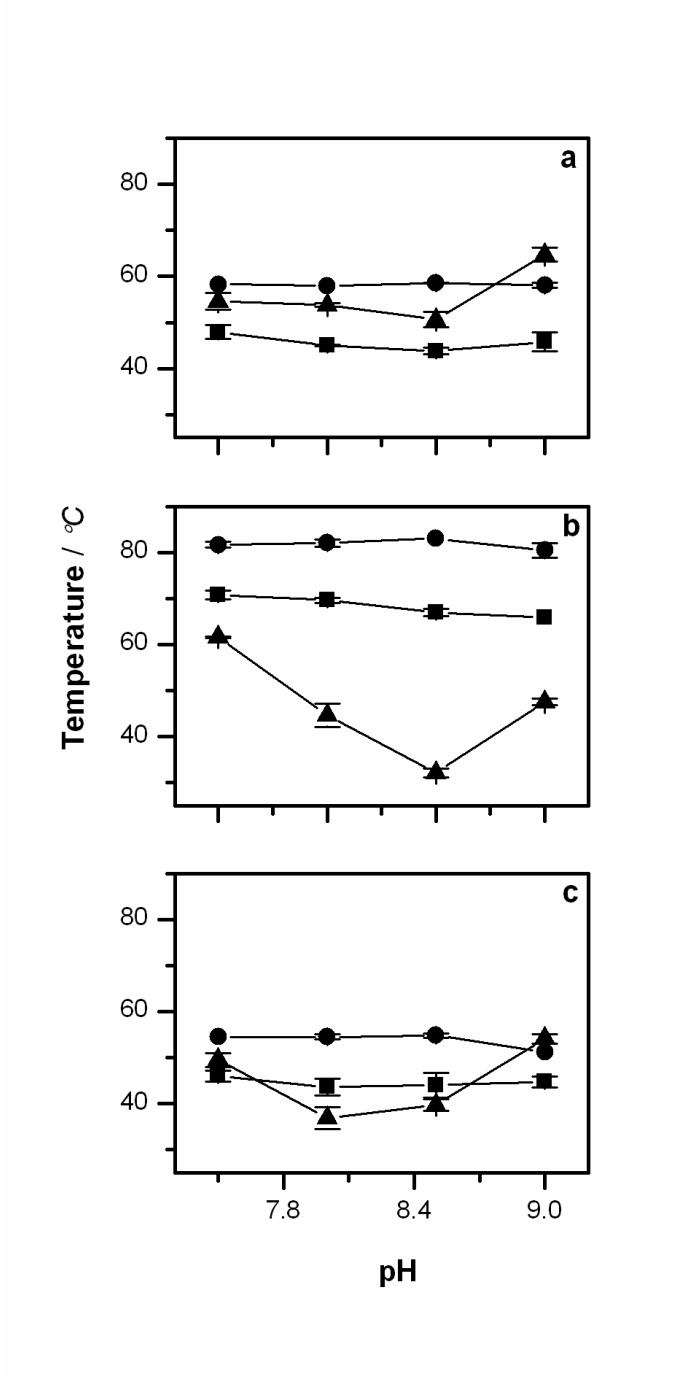

Figure 3.6 The effect of pH on the T_m of **(a)** poly[d(AT)]; **(b)** poly[d(As^{2}T)]; and **(c)** poly[d(As^{4}T)] in the presence of 0.2 mM $MgCl_2$ (●), 0.2 mM $ZnCl_2$ (▲), and in the absence of metal ion (■).

In figure 3.7a, an expected increase of approximately 5 °C in the T_m for poly[d(TG)•d(CA)] in the presence of Mg^{2+} is observed at all pHs. Similar to poly[d(AT)], there is an additional increase in the T_m of poly[d(TG)•d(CA)] above that seen for Mg^{2+} observed for Zn^{2+} at pH 9.0 which is attributed to the formation of M-DNA. The T_m of poly[d(s^2TG)•d(CA)] in figure 3.7b continues to decrease with higher pH values. Much like poly[d(As^2T)], poly[d(s^2TG)•d(CA)] is very unstable in the presence of Zn^{2+}, but shows even less propensity to forming M-DNA. However, the denaturation profile for poly[d(s^4TG)•d(CA)] in the presence of Zn^{2+} shows an additional increase above that for Mg^{2+} beginning as low as pH 8.0 (Figure 3.7c).

In order to investigate how thermal stability correlates with the ease with which the polymer will convert to M-DNA, the ethidium assay was used to examine the pH at which the transition occurs.

3.2 Ethidium Fluorescence Assay

3.2.1 Zn^{2+} M-DNA Formation on Repeating-sequence DNA

In the presence of 0.2 mM Zn^{2+}, poly[d(AT)] shows complete M-DNA conversion at pH 8.6 (Figure 3.8a). As expected from the thermal denaturation profiles, poly[d(As^4T)] is able to form M-DNA at an even lower pH and in fact, is fully converted by pH 8.2. Surprisingly, the thermal profile of poly[d(As^2T)] suggested a very unstable conformation, however, it was still able to incorporate Zn^{2+} at a lower pH than the unmodified poly[d(AT)]. A possible explanation can be found in the T_m data measured at pH 7.5 (Figures 3.6 and 3.7) where all the DNAs are in the 'B' conformation. The addition of Zn^{2+} increases the T_m of poly[d(AT)] but decreases the T_m of poly[d(As^2T)], poly[d(TG)•d(CA)], poly[d(s^2TG)•d(CA)] and poly[d(s^4TG)•d(CA)]. Therefore, the B-form of poly[d(AT)] may be unusually refractory to conversion to M-DNA and therefore in this sequence context, the unusual base plays an important role in M-DNA formation.

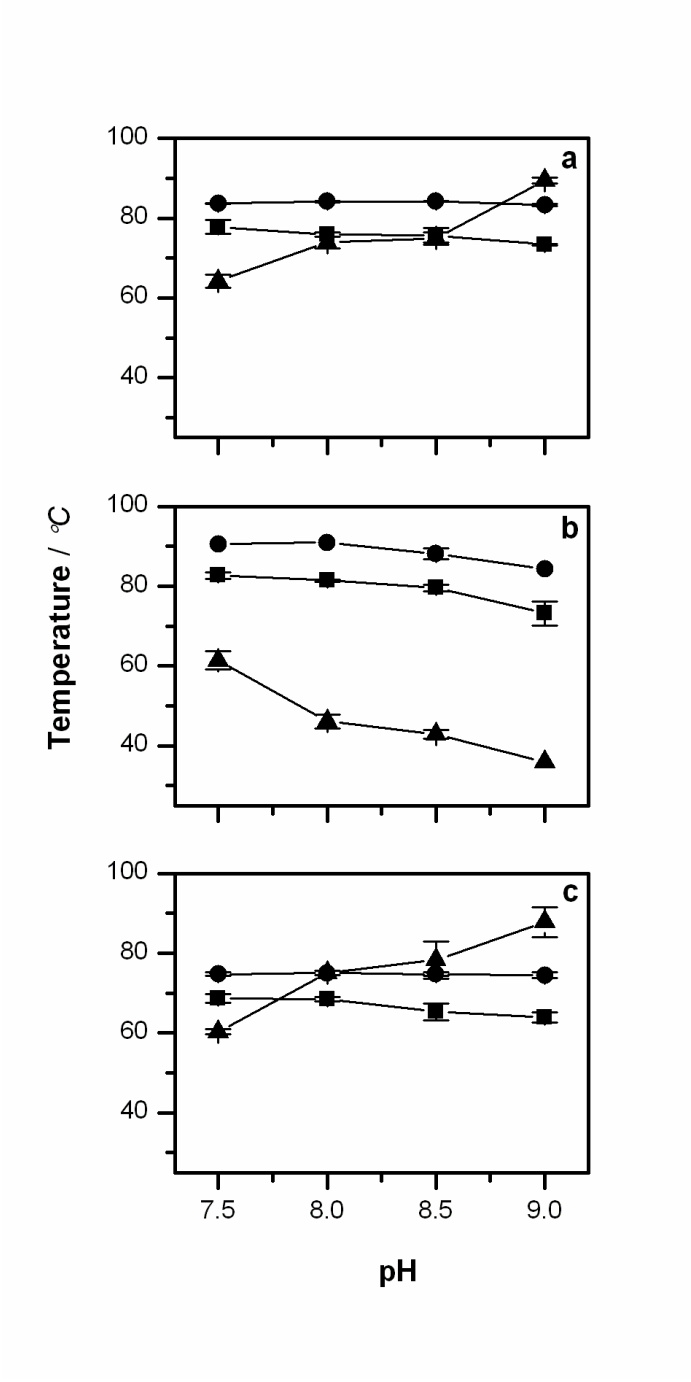

Figure 3.7 The effect of pH on the T_m of **(a)** poly[d(TG)•d(CA)]; **(b)** poly[d(s^2TG)•d(CA)]; and **(c)** poly[d(s^4TG)•d(CA)] in the presence of 0.2 mM $MgCl_2$ (●), 0.2 mM $ZnCl_2$ (▲) and in the absence of metal ion (■).

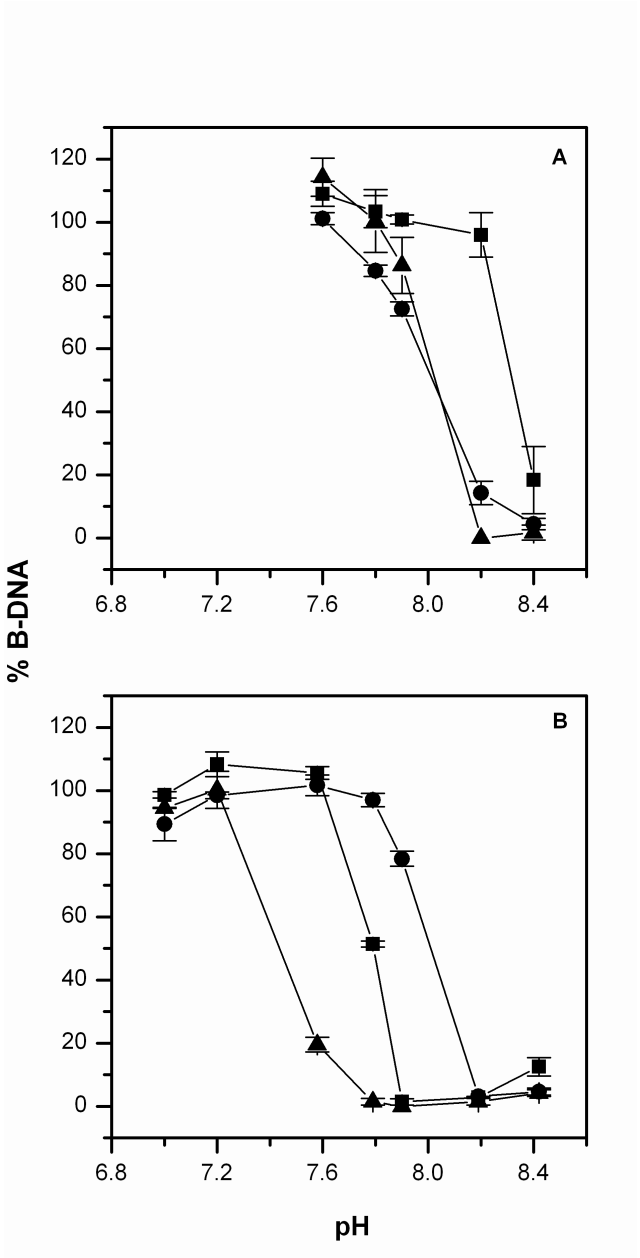

Figure 3.8 The conversion of B-DNA to M-DNA with 0.2 mM $ZnCl_2$ at ambient temperature. (A) poly[d(AT)], (■); poly[d(As^2T)], (●); poly[d(As^4T)], (▲). (B) poly[d(TG)•d(CA)], (■); poly[d(s^2TG)•d(CA)], (●); poly[d(s^4TG)•d(CA)], (▲).

The results in figure 3.8b are consistent with the previous T_m data. At pH 7.9, poly[d(TG)]•poly[d(CA)] is fully converted to M-DNA. However, upon the incorporation of s^4T, the polymer is almost completely converted at pH 7.6. In contrast, the pH of poly[d(s^2TG)]•poly[d(CA)] conversion increases to 8.2. Therefore, it can be clearly seen that poly[d(AT)] has the lowest propensity of forming M-DNA. In the presence of 0.2 mM Zn^{2+}, poly[d(TG)]•poly[d(CA)] shows complete conversion to M-DNA at pH 7.9 whereas poly[d(AT)] is still 100% B-DNA. As hypothesized from the thermal denaturation profiles, the pH at which M-DNA will form can be further reduced by incorporating s^4T into poly[d(TG)]•poly[d(CA)]. Therefore, the next step was to use these sequence effects in combination with the modified bases in order to design olignonucleotides that could localize metal ions at various regions according to the pH.

3.2.2 Zn^{2+} M-DNA Formation on 30-mer Oligonucleotides

Double stranded oligomers 30 nucleotides in length were synthesized containing the sequences $d(TG)_{15}$•$d(CA)_{15}$, a mixed sequence with 50% d(AT) and the other 50% d(TG)•d(CA) and another mixed sequence in which three terminal thymines on the d(TG)•d(CA) track where replaced with 4-thiothymines. All of the sequences and corresponding names can be found in Table 2.2 of the Material and Methods. As would be predicted from the previous experiments, figure 3.9 demonstrates that at pH 7.9 TG-30 is completely converted to M-DNA, but both mixed sequences show approximately only 50% M-DNA formation which accurately corresponds to the d(TG)•d(CA) tract forming M-DNA while the d(AT) tract remains as B-DNA . Also, as would be expected, the mixed sequence Mx(s^4T)-30 containing the incorporated 4-thiothymines begins to form M-DNA at a lower pH compared to both Mx-30 and TG-30. Once the d(TG)•d(CA) track forms M-DNA, Mx(s^4T)-30 starts to plateau at pH 7.9 and begins to follow the Mx-30 sequence more closely corresponding to the M-DNA conversion of the remaining d(AT) tract.

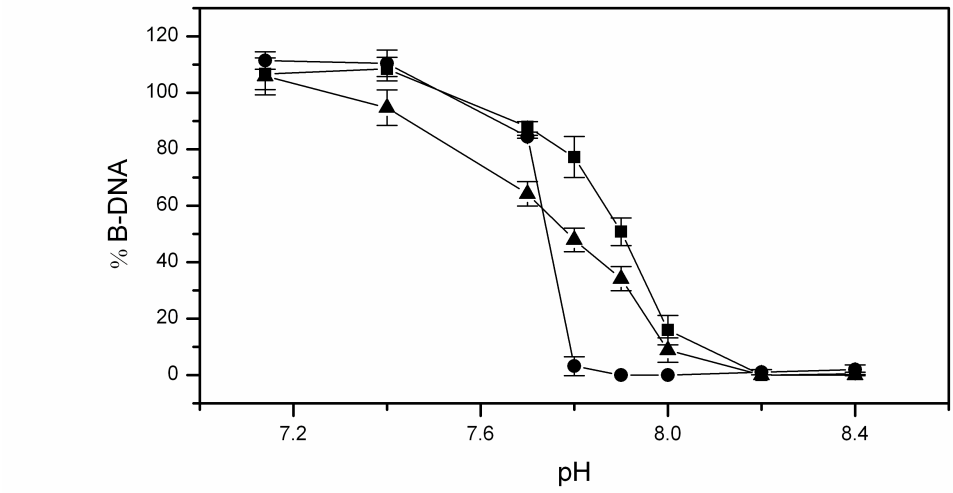

Figure 3.9 The conversion of B-DNA to M-DNA with 0.2 mM Zn^{2+}, TG-30 (●); average of Mx-30a and Mx-30b, (■); average of Mx(s^4T)-30a and Mx(s^4T)-30b (▲).

3.3 X-ray Photoelectron Spectroscopy

A continuing challenge in the investigation of M-DNA has been solidifying the proposed binding location of the metal ion. Therefore, XPS was employed to gain information on the electronic structure and chemical bonding of the molecules. In XPS, the incident x-ray photons are absorbed by various atoms in the surface layer leading to the ionization and the emission of an inner shell electron. Photoelectrons from each element will have a characteristic binding energy and relative intensity associated with each core atomic orbital providing an extremely powerful tool for quantitative analysis of the surface composition. Notably, the shape of the peak and the binding energy are slightly altered by variations in the electrostatic shielding of the inner shell electrons from all other electrons in the atom. Also, the removal or addition of electronic charge as a result of changes in bonding can also cause similar shifts in energy. Therefore, in order to gain more information on the structure and electronic properties of M-DNA, nucleic acids were immobilization onto a gold surface and analyzed using XPS.

Previous XPS studies of DNA have delineated the binding energies (BE) of the C 1s, N 1s, O 1s and P 2p electrons in ssDNA (Petrovykh *et al.*, 2003; Moses *et al.*, 2004; Saprigin *et al.*, 2005). Of particular interest are the N atoms which are only present in the bases and are presumed to interact directly with Zn^{2+} upon M-DNA formation. Therefore by examining these spectra, we were able to study the location of the metal ion location within the DNA helix.

3.3.1 Characterization of the DNA Monolayer

Duplex DNA, 30 base pairs in length, was assembled onto the gold surface as described in Materials and Methods and the resultant monolayer was characterized by XPS. Disulfides with an attached hexanol were chosen rather than simple thiol adsorption because previous results showed stable monolayers with improved dehybridization-rehybridization characteristics (Long *et al.*, 2003; Long *et al.*, 2004; Li *et al.*, 2006). A monolayer formed from ssDNA or a simple thiol linked duplex may position the molecules too close together to allow efficient rehybridization. Another

possible problem with ssDNA attachment is that the DNA may non-specifically bind through the bases so that it is unavailable for hybridization.

3.3.1.1 DNA Film Thickness

From the intensity of the Au $4f_{7/2}$ peaks, the thickness of each DNA monolayer was estimated using the following equation,

$$\ln(I) = -d/(\lambda \sin\theta) + \ln(I_0) \tag{3.1}$$

where λ is the inelastic mean free path (IMPF), θ is the takeoff angle between the sample surface and the photoelectron energy analyzer, I is the gold photoelectron intensity with the DNA sample present, and I_0 is the photoelectron intensity of the bare gold substrate. The value of λ was taken to be 3.980 nm which was the average effective attenuation length (EAL) from the gold substrate photoelectron in a DNA overlayer calculated using the NIST Standard Reference Database 82 (SRD-82) software (Powell, 2001). The EAL definition allows this term to be introduced in place of the λ(IMPF). A more detailed description and discussion on EAL formalism can be found in the following review (Jablonski and Powell, 2002). According to the above equation, ln(I) should be linearly related to 1/(sinθ) with the slope of –(d/λ).

Therefore, XP spectra were obtained at the takeoff angles 90°, 60°, 45°, 30° and the slope from the plot of ln(I) versus 1/(sinθ) was used to calculate the thickness of each monolayer (Figure 3.10) (Kondo *et al.*, 1998). Each monolayer was composed of 30-mer duplexes attached to the gold surface through an S-$(CH_2)_6$ linker. Therefore, a thickness of approximately 11.2 nm would be expected if the strands were stretched to full length and perpendicular to the surface assuming the DNA films do not collapse when the water is removed under vacuum. However, the average thickness calculated for the B-DNA monolayers was determined to be 5.2 ± 0.4 nm.

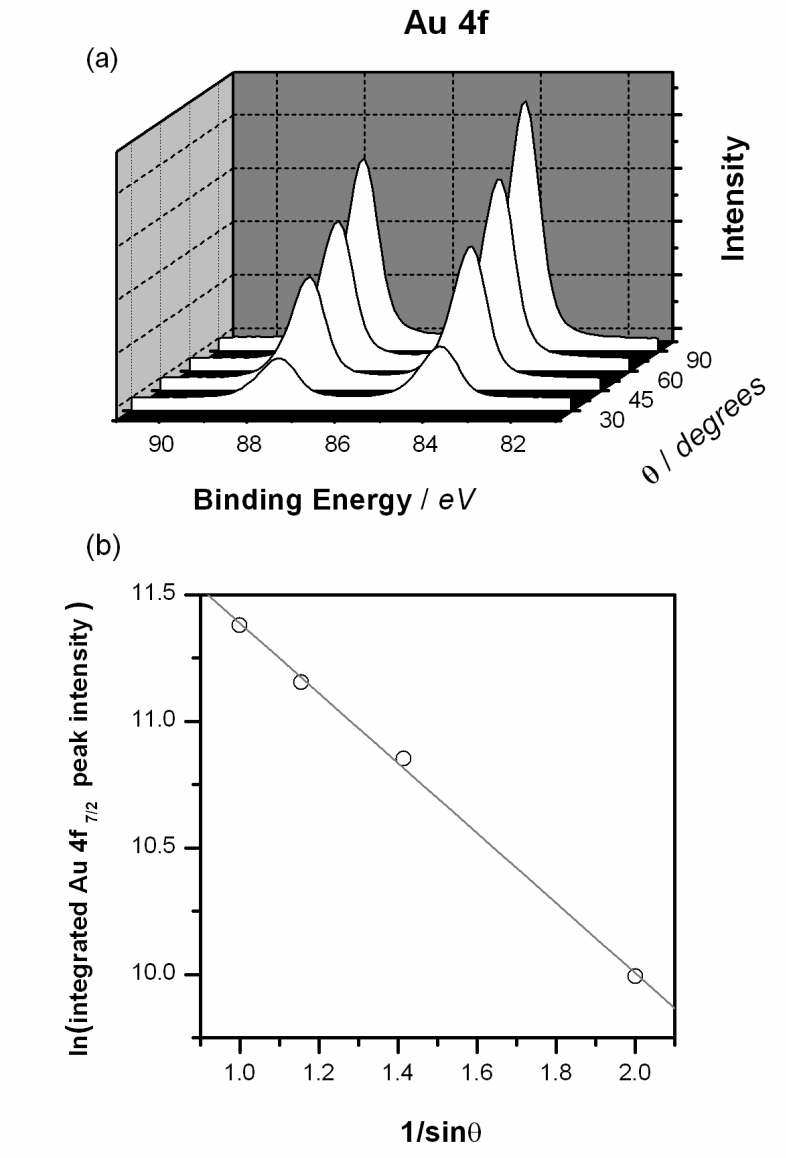

Figure 3.10 (a) Au 4f XP spectra of the DNA SAM on polycrystalline gold measured at various values of θ; (b) The relationship between 1/sinθ and logarithm of the integrated peak intensities from the Au 4f $_{7/2}$ XP spectra in figure A.

Therefore, for a completely rigid structure, the DNA chains would be orientated at approximately 30° to the surface (Figure 3.11). However, another possibility is that the long oligomers in conjunction with the measurements being done in a vacuum have lead to the hybridized strands forming kinks or bends leading to a decrease in thickness. As well, immobilization in the presence of a monovalent cation such as NaCl compared to a divalent cation such as $MgCl_2$ has been shown to decrease the monolayer coverage by approximately two fold (Petrovykh *et al.*, 2003). This would result in a lower surface density and most likely a decrease in thickness as well.

3.3.1.2 Elemental Analysis

All films analyzed showed distinct peaks for the principal elements in an immobilized thiol-linked DNA film (C, O, N, P, S). The N 1s (399.5 – 402.0 eV), P 2p (134.0 eV) and S 2p (162.0 eV) peaks are all evident in the spectra with immobilized DNA but are absent in the spectrum for bare gold providing good evidence for the attachment of DNA to the surface (Figure 3.12)(Table 3.2). The bare spectrum does show peaks for carbon (285 eV) and oxygen (531 eV) most likely as a result of atmospheric contamination. In order to analyze the composition and coverage of the monolayer, elemental concentrations were determined using the following equation suggested by Petrovykh *et al*., 2003.

$$\frac{N_X}{N_{Au}} = \frac{I_X}{I_{Au}} \frac{T_{Au}\sigma_{Au}L_{Au}^{Q}}{T_X\sigma_X L_X^{Q}} \frac{\exp[-d/L_{Au}]}{1-\exp[-d/L_X]} \tag{3.2}$$

where T is the analyzer transmission function, σ is the total photoelectric cross section in which Scofield coefficients were used (Scofield, 1976), d is the film thickness and L is the EAL for electrons in the film. More specifically, this equation utilizes two types of EALs: “average practical EAL” (PEALs) which refers to the attenuation of the electrons from the various elements caused by the DNA film and “EAL for quantitative analysis” (QEALs) which refer to the electrons originating in a material and attenuating within the material itself.

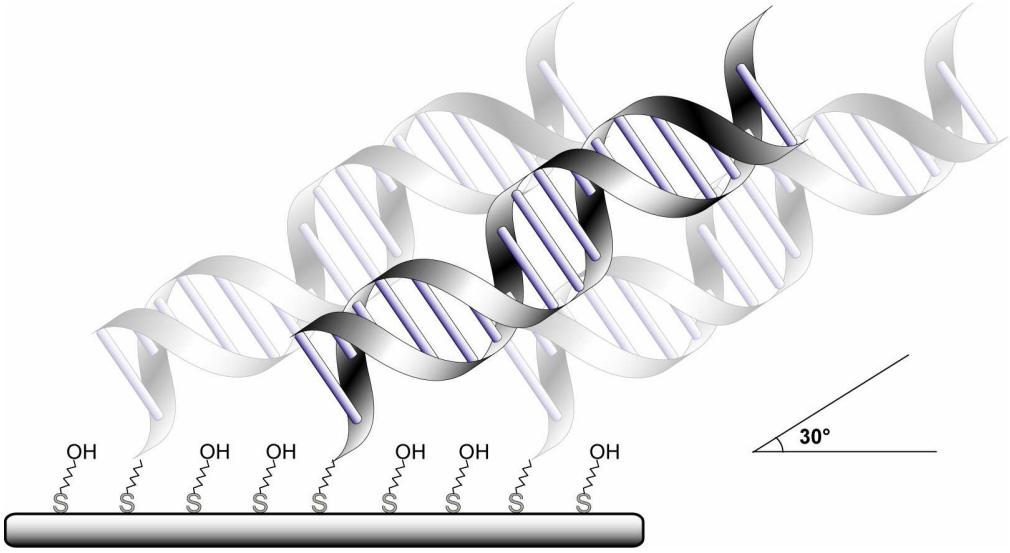

Figure 3.11 Schematic of dsDNA orientation at 30° to the surface.

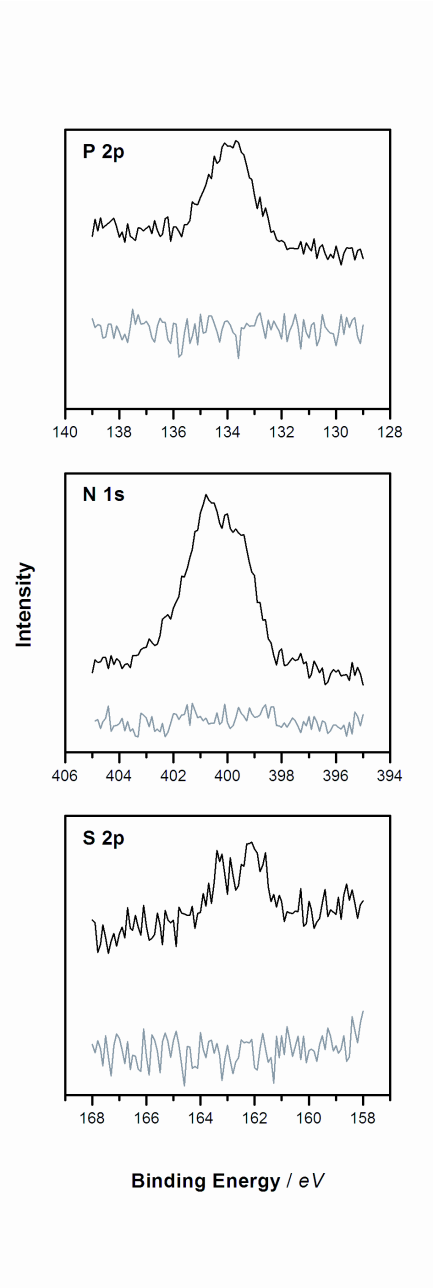

Figure 3.12 XP spectra of bare gold (bottom) and 30 basepair duplex B-DNA assembled on gold (top) for elements P, S and N.

Table 3.2 Average Elemental Compositional Data for DNA Monolayers on Gold in the Presence and Absence of Various Metal Ions

	Atomic Percent								Atomic Ratio		
DNA	**Au 4f**	**N 1s**	**P 2p**	**C 1s**	**O 1s**	**S 2p**	**Zn 2p**	**Mg 1s**	**P/N**	**C/N**	**O/N**
Bare Au	81.3 (4.8)	-	-	15.2 (2.9)	3.5 (1.9)	-	-	-			
DNA theoretical									0.28	2.7	1.7
B-DNA	28.5 (1.6)	6.1 (0.2)	2.1 (0.3)	33.7 (9.2)	29.0 (8.7)	0.5 (0.3)	-	-	0.34	5.5	4.8
M-DNA[a]	29.2 (3.6)	5.7 (0.1)	2.6 (0.1)	30.6 (2.7)	30.4 (6.7)	0.2 (0.0)	1.2 (0.4)	-	0.46	5.4	5.3
M-DNA[b]	36.9 (1.6)	5.6 (1.3)	2.4 (0.4)	31.5 (1.1)	19.6 (1.3)	0.5 (0.2)	3.5 (1.2)	-	0.43	5.6	3.5
Mg^{2+} (pH 8.6)	22.9 (2.2)	8.7 (1.6)	3.9 (0.5)	34.9 (1.8)	27.7 (3.5)	0.3 (0.1)	-	2.5 (0.2)	0.45	4.0	3.2
Zn^{2+} (pH 7.0)	23.2 (4.9)	7.0 (1.1)	2.8 (0.1)	29.7 (0.8)	36.9 (5.0)	0.1 (0.0)	0.2 (0.1)	-	0.40	4.2	5.3

After the monolayer was converted to M-DNA the electrodes were rinsed with [a] 20 mM Tris-ClO_4 and 20 mM $NaClO_4$ or alternatively [b] 20 mM Tris-ClO_4 and 20 mM $NaClO_4$ containing 0.4 mM $Zn(ClO_4)_2$. The values in parentheses represent the standard deviation.

In the above equation, L_{Au} and L_x represent the PEAL for electrons from Au and from DNA elements (X = C, N, O, P, Zn) in the DNA film respectively. Similarly, L^Q is used to assign the QEAL values all of which are listed in Table 3.3. More complete and comprehensive definitions of EALs and their appropriate use can be found in the review mentioned previously (Jablonski and Powell, 2002).

Since both P and N are located exclusively in DNA, their presence in the proper stoichiometric ratio reveals important information regarding the state of the film. Although the average P/N ratios are constant within the experimental ±10% error reported by Petrovykh (Petrovykh *et al.*, 2003), the ratios are higher than expected (Table 3.2). This result may be due to some desorption or preferential damage of the DNA bases compared to the phosphate backbone.

3.3.1.3 Determination of DNA Coverage

Since the DNA contains more N atoms than P atoms, and N has a higher XPS cross section the signal-to-noise was much higher and therefore was used to determine the DNA coverage. The DNA coverage was determined to be approximately 1.2 x 10^{13} molecules/cm^2 with a density of 0.702 g/cm^3 (Table 3.4). The DNA coverage is less than the value of 3.7 x 10^{13} molecules/cm^2 reported elsewhere for single stranded 25mer oligonucleotides (Steel *et al.*, 2000). However, this is most likely because the diameter is larger for dsDNA and there is possibly more repulsion between adjacent duplexes. Since there is limited data on the self-assembly of dsDNA, a surface coverage of approximately 4 x 10^{12} molecules/cm^2 was found for monolayers formed by the self-assembly of ssDNA followed by hybridization (Steel *et al.*, 1998). It is interesting to note the increase in surface coverage seen for dsDNA assembly in comparison to assembly through hybridization. This may be a result of the poor hybridization efficiency associated with the latter method.

Table 3.3 Calculated EAL Values for the Major Components in the DNA Monolayer

Peak	PEAL in DNA film L (nm)	QEAL L^Q (nm)
C 1s	3.497	3.646
O 1s	2.884	3.035
N 1s	3.213	3.364
P $2p_{3/2}$	3.862	3.968
S $2p_{3/2}$	3.793	3.900
Zn $2p_{3/2}$	1.600	1.726
Au $4f_{7/2}$	3.980	1.745
Na 1s	1.616	1.460
Mg 1s	0.773	0.928

PEALs and QEALs were calculated for duplex B-DNA using NIST SRD-82 software with the following parameters: experimental kinetic energy; asymmetry parameters β for electrons Au 4f (β=1.04), β=2 for 1s peaks, β=1.1 for P 2p, β=1.16 for S 2p and β=1.41 for Zn 2p (Campbell *et al.*, 2002); ideal stoichiometry of nucleotides in DNA; band-gap energy E_g = 4.8 e; film density of 0.731 g/cm^3. The E_g was calculated based on an average UV absorption peak of 258 nm for DNA in solution (Petrovykh *et al.*, 2003). An initial estimate of film density was used to calculate the PEALs and QEALs which were then used for analysis of one data set using equation 4. The new value of density obtained from data analysis was then reentered into the NIST program to calculate revised PEALs and QEALs and the process was repeated until the density values converged self-consistently. The resultant PEAL and QEAL values are listed in the above table and were used to analyze the characteristics of the various monolayers. All EALs were calculated for a film thickness of 5 nm. As noted in ref (Petrovykh *et al.*, 2003), the approximation of 5 nm in the PEAL and QEAL calculations will not introduce an appreciable systematic error into the analysis.

Table 3.4 Calculated Surface Characteristics of the DNA Film

DNA	DNA film thickness (nm)	ρ_{DNA} g/cm^3	DNA coverage (x 10^{13} DNA/cm$^{2)}$
B-DNA	5.2 ± 0.4	0.702 ± 0.056	1.2 ± 0.1
M-DNA	5.6 ± 0.7	0.619 ± 0.018	1.1 ± 0.1
Mg^{2+} (pH 8.6)	6.0 ± 0.3	0.898 ± 0.171	1.7 ± 0.4
Zn^{2+} (pH 7.0)	6.2 ± 1.6	0.733 ± 0.424	1.4 ± 0.4

In order to better validate the accuracy of the XPS measurements, chronocoulometric measurements were done in order to determine the DNA surface coverage (Figure 3.13). Chronocoulometry was implemented in order to determine the quantity of DNA immobilized on the gold surface. The positively charged redox probe $[Ru(NH_3)_6]^{3+}$ was used as it is able to electrostatically interact with the negatively charged phosphate backbone of DNA. The amount of redox probe interacting with the DNA at the surface of the electrode can then be determined by chronocoulometry and used to calculate the amount of corresponding DNA (Steel *et al.*, 1998). The electrochemical methods resulted in B-DNA coverage of $(1.2 \pm 0.1) \times 10^{13}$ molecules/cm^2 which agrees well with the calculated XPS results.

3.3.1.4 Sulfur (S 2p) Spectrum

Although the S 2p peak has a low signal-to-noise ratio and is somewhat difficult to observe, the sulfur signal is of interest as it provides more information regarding the immobilization of the thiolated DNA (Castner *et al.*, 1996; Wackerbarth *et al.*, 2004; Wood and Lee, 2005). The poor signal-to-noise ratio is due to the low relative concentration of sulfur atoms (the ideal S/P ratio is 1/60) and the strong attenuation of the signal caused by the overlaying DNA (Petrovykh *et al.*, 2003). The S 2p spectra acquired for all SAMs had a doublet structure due to the presence of the $S2p_{3/2}$ and S $2p_{1/2}$ peaks. All spectra were fit using a 2:1 peak ratio and showed a peak split of 1.2 eV (Figure 3.14). The S $2p_{3/2}$ peak binding energy was 162.0 eV which is consistent with a thiolate S-Au bond (Castner *et al.*, 1996). In particular, there was no detectable intensity in the binding energy region above 164 eV which is the region typical for an S 2p doublet for unbound thiol groups. This strongly suggests that there is a single layer of thiolated DNA and alkanethiols chemisorbed at the gold surface with virtually no physisorbed DNA present in the film.

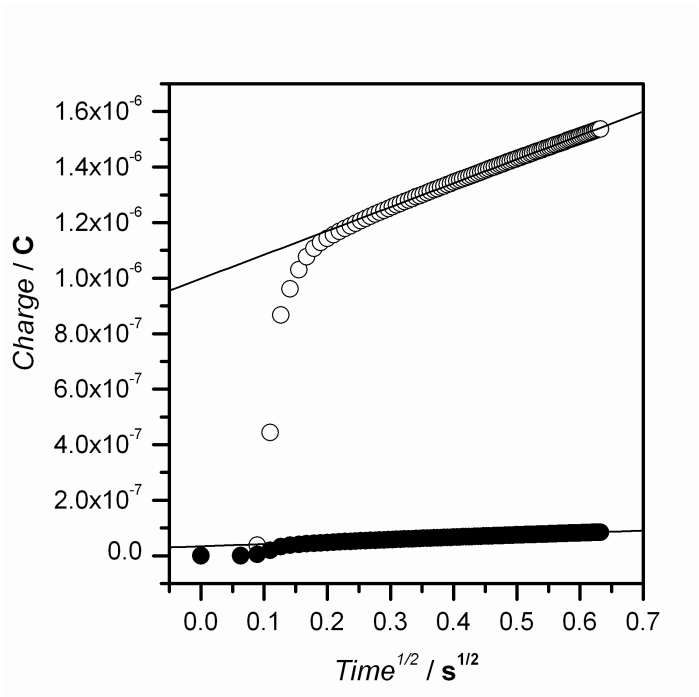

Figure 3.13 Chronocoulometric response curves for DNA modified electrodes in the absence (●) and presence (○) of 100 μM $[Ru(NH_3)_6]^{3+}$. The lines represent the extrapolated fit from the linear portion of the curve and are used in order to determine the intercept at time=0.

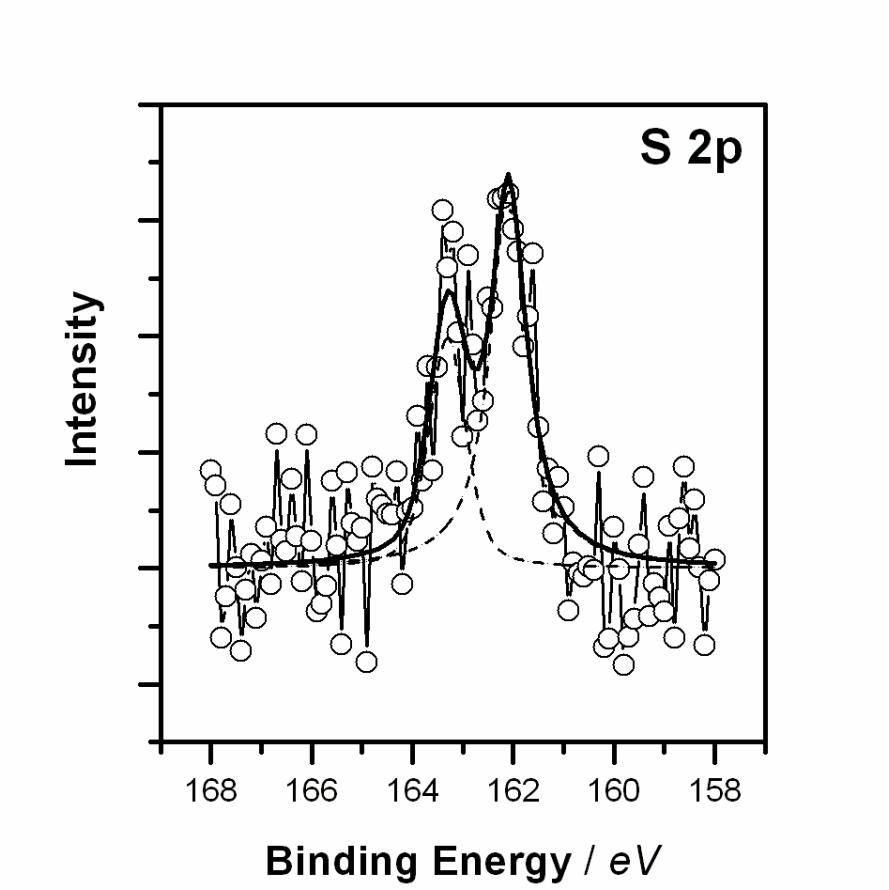

Figure 3.14 High-resolution S 2p XP spectra for 30-basepair thiol-DNA immobilized on gold (open circles for raw data, solid lines for the total fits and dashed lines for the component peaks). Spectra were also taken after incubation with $Zn(ClO_4)_2$ and $Mg(ClO_4)_2$. The data was fit with two peaks as discussed in the text both having a FWHM of 0.98 ± 0.09.

3.3.2 DNA-Metal Ion Interaction

3.3.2.1 Carbon (C 1s) Spectrum

On addition of Zn^{2+} to form M-DNA, P 2p and S 2p showed only small changes most likely due to small differences in the characteristics of each monolayer. C 1s showed some changes and therefore a closer examination of the carbon species was conducted. As shown in figure 3.15a, carbon species are observed in the C 1s region of a bare gold electrode. There is one main peak observed at 284.1 eV which is indicative of alkyl chains or methyl species as well as smaller peaks at 285.5 and 288 eV which are due to the presence of surface contaminants containing C-O and C=O bonds respectively (Ishida *et al.*, 1996; Ishida *et al.*, 1997). However, for the DNA modified electrode, the fit included peaks at BE of 285, 286.6, 288 and 289.5 eV each with an FWHM of 1.5 eV corresponding to hydrocarbon (C-C/C-H), carbon bound to nitrogen and oxygen (C-N, C-O, N-C=N, O-C-N), amide carbon (N-C=O), and urea carbon [N-C(=O)-N] respectively (Figure 3.15b), (May *et al.*, 2004). Therefore, figure 3.15b clearly shows a corresponding increase in peak intensities for DNA-related carbon peaks for species at 286.6, 288 and 289.5 eV. Also, there is a peak shift of approximately 0.9 eV to higher energy observed in the 284.1 eV C 1s peak when the bare gold electrode is covered with a DNA monolayer. This shift in energy is reflective of a decrease in Au-C interactions (Ishida *et al.*, 1996). Both of these observations indicate that the influence of adventitious hydrocarbons on the SAM is small. This is expected, as it has previously been shown that the effect of carbon and oxygen contaminant layers on the gold surface becomes negligible in the case of long-term immobilization (Ishida *et al.*, 1997).

The atomic percentages of each species on the monolayers were determined and are shown in Table 3.5. The small changes in the presence of Zn^{2+} and Mg^{2+} are only seen in the lower BE's and are most likely due to differences in the DNA coverage as well as small inconsistencies in the hydrocarbon contamination.

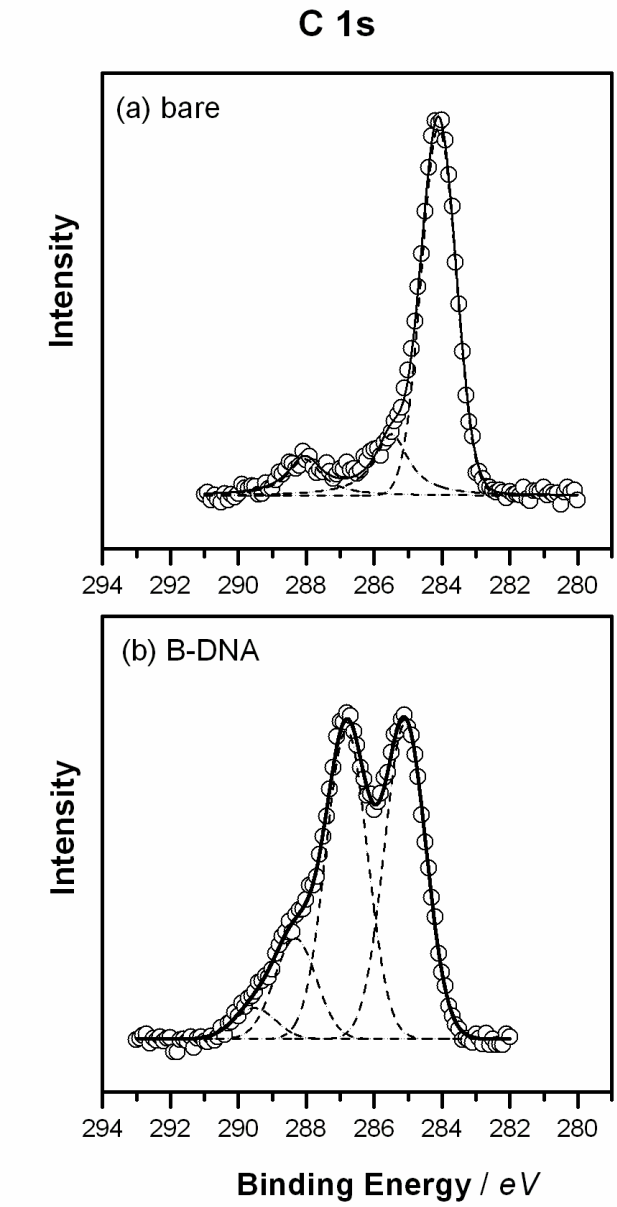

Figure 3.15 High-resolution C 1s XP spectra of (a) bare gold electrode; (b) 30-basepair thiol-DNA immobilized on gold (open circles for raw data, solid lines for the total fits and dashed lines for component peaks). The data was fit with four peaks, as discussed in the text all having FWHM of 1.38 ±0.05.

Table 3.5 Calculated Percentages For Each of the Fitted Components for the C1s High-Resolution XPS Data

DNA	C-C, C-H 285.0 eV (%)	C-N, C-O 286.6 eV (%)	O-C-N, N=C-N 288.0 eV (%)	N-C(=O)-N 289.5 eV (%)
B-DNA	44 ± 8	40 ± 7	12 ± 1	4 ± 1
M-DNA	42 ± 5	42 ± 5	12 ± 2	5 ± 1
Mg^{2+} (pH 8.6)	35 ± 6	46 ± 7	13 ± 1	6 ± 1
Zn^{2+} (pH 7.0)	33 ± 1	48 ± 1	13 ± 1	6 ± 1

Therefore it can be concluded that Zn^{2+} is unlikely to interact directly with either C or P and does not evidently effect the linkage between gold and sulfur; a result which is consistent with the M-DNA conformation.

3.3.2.2 Oxygen (O 1s) Spectrum

For O 1s with B-DNA, there is a peak at 533 eV with a shoulder at 532 eV again consistent with previous results for ssDNA (Figure 3.16). However, upon addition of Zn^{2+} the peak broadens as the shoulder becomes much more prominent. Oxygen is present in DNA on the bases, the deoxyribose sugar and the phosphodiester backbone. Therefore, this result is very difficult to interpret since Zn^{2+} can potentially bind to all three building blocks. However, since a similar result is seen in the presence of Mg^{2+}, it is most likely that the change in the oxygen spectra is caused from the ionic interaction between the metal ion and the oxygens on the phosphate backbone.

3.3.2.3 Nitrogen (N 1s) Spectrum

For N1s the interpretation of spectral changes is likely to be simpler because nitrogen atoms are confined to the bases and previous work with homopolymer ssDNA has demonstrated the presence of a broad peak at about 400 eV (Petrovykh *et al.*, 2003). The B-DNA duplexes also show these features but upon conversion to M-DNA the peak becomes much narrower. According to the N1s spectra, it seems very unlikely that the bases in the duplex are interacting with the surface as there is no energy components observed at BE below 399.5 eV indicative of bases chemisorbed onto the gold surface (Petrovykh *et al.*, 2003). This may be due, in part, to the presence of excess alkanethiol chains acting as spacers between the DNA molecules.

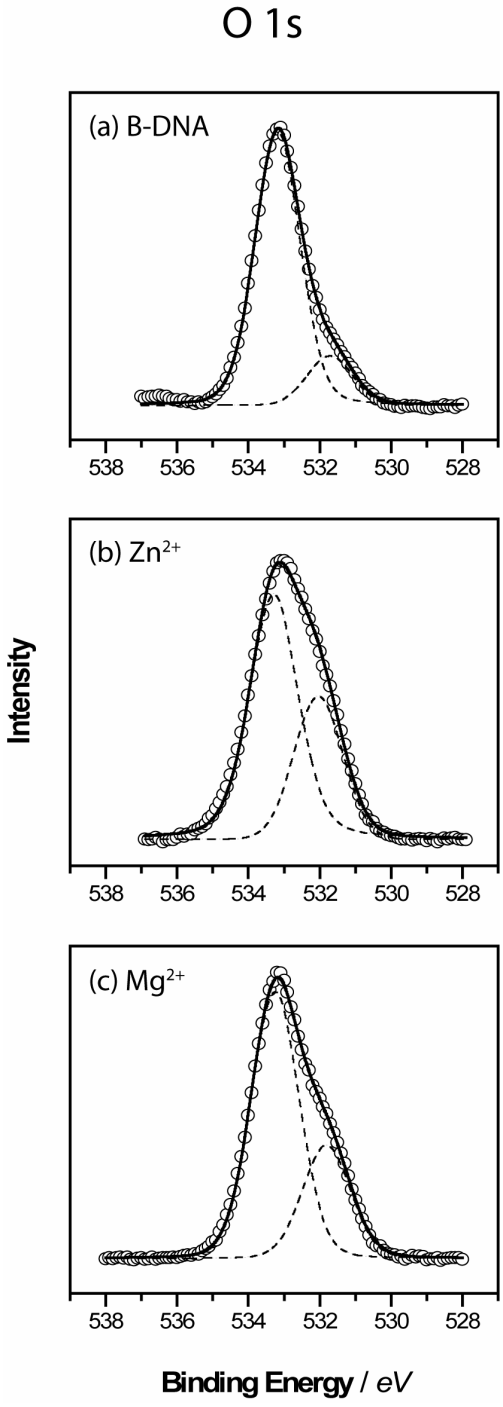

Figure 3.16 High-resolution O 1s XP spectra for 30-basepair thiol-DNA immobilized on gold (open circles for raw data, solid lines for the total fits and dashed lines for component peaks). Spectra were taken for (a) B-DNA and after incubation with (b) $Zn(ClO_4)_2$ and (c) $Mg(ClO_4)_2$. The data was fit with two peaks, as discussed in the text both having a FWHM of 1.55 ± 0.09.

As shown in figure 3.17, the N 1 s spectrum for B-DNA was fit with three peaks at BEs of 399.5 eV, 400.8 eV and 402.0 eV corresponding to conjugated nitrogen (–N=), non-conjugated nitrogen (–NH– and N with three single bonds) and the ($–NH_2$) respectively (Mateo-Marti *et al.*, 2005; Mateo-Marti *et al.*, 2007). However, there is evidence that the third peak at 402.0 eV may be partially due to non-specific adsorption of the Tris buffer as a similar peak is observed when a bare gold electrode is incubated with only Tris buffer (Figure 3.18). Previous investigations have shown that this peak may be due to the protonated amine group in the Tris buffer (Strother *et al.*, 2000) or alternatively from the amine group interacting with the gold substrate (Joseph *et al.*, 2004). The protonation of the amine group does seem to play a role as the peak at 402 eV becomes more pronounced at lower pH values. As well, at pH 7.5 (Figure 3.19) the intensity of the peak at 402 eV decreases as the angle goes from 90° to 30° from the surface normal. This is also a strong indication that there is non-specific adsorption of Tris buffer at the surface and is not a result of amine groups on the bases throughout the monolayer. On the other hand, the M-DNA spectra shows one main peak with a BE of about 400.5 eV and much smaller peaks at 399.5 eV and 402.0 eV.

A similar trend is observed for N 1s upon conversion of a free-base porphyrin to the corresponding metalloporphyrins (Polzonettia, 1999; Sarno *et al.*, 2001). For example, a typical free-base porphyrin has two peaks of roughly equal intensity at 399.2 and 397.2 eV corresponding to the non-conjugated and conjugated nitrogen respectively. Upon addition of Zn^{2+} the doublet collapses to one peak with an energy of 397.8 eV (Karweik and Winograd, 1976). In other words, the nitrogen in the metalloporphyrin becomes indistinguishable because of electronic coupling within the extended π system of the porphyrin ring. In M-DNA as well, the Zn^{2+} ion forms a bridge between the π system of each base so that all the nitrogen within a base pair exhibit a degree of electronic coupling. The change in overall peak shape can be seen in figure 3.17 as the nitrogen spectra for B-DNA goes from a broad doublet to M-DNA consisting of one sharp well-defined peak. Interestingly, the nitrogen spectra in the presence of Mg^{2+} is similar to that of B-DNA demonstrating that the Mg^{2+} is only interacting with the phosphate backbone.

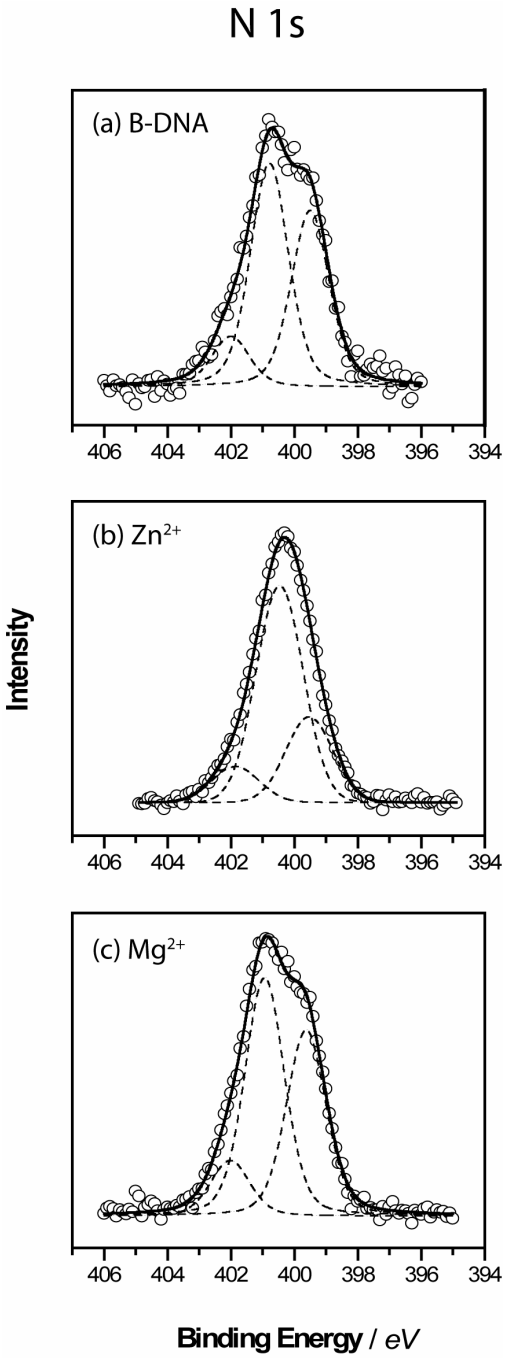

Figure 3.17 High-resolution N 1s XP spectra for 30-basepair thiol-DNA immobilized on gold (open circles for raw data, solid lines for the total fits and dashed lines for component peaks). Spectra were taken for (a) B-DNA and after incubation with (b) $Zn(ClO_4)_2$ and (c) $Mg(ClO_4)_2$. The data was fit with two peaks, as discussed in the text all having a FWHM of 1.59 ± 0.11.

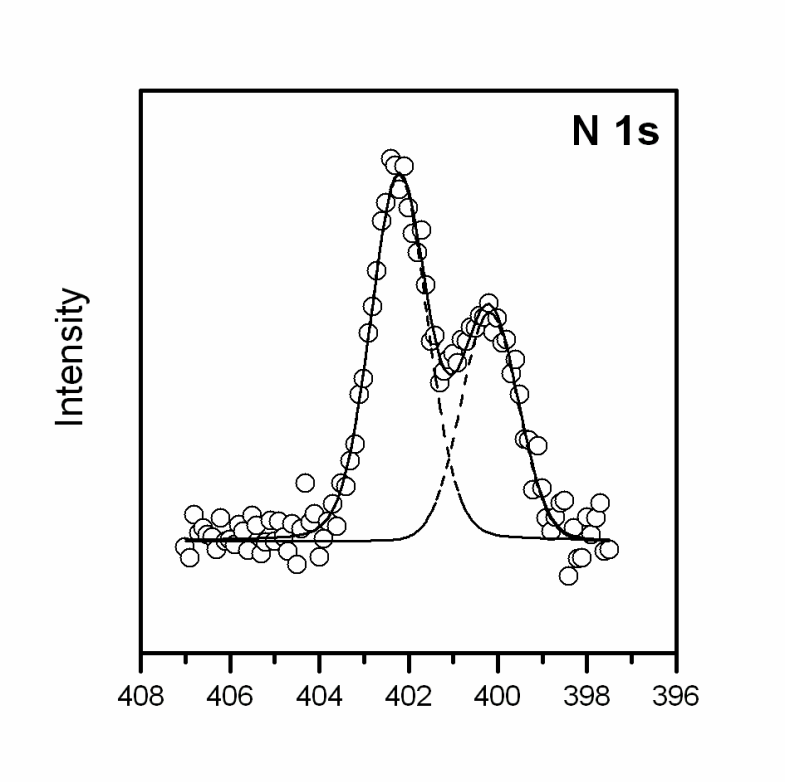

Figure 3.18. High-resolution N 1s XP spectra for 20 mM TrisClO_4 (pH 8.5) immobilized on gold (open circles for raw data, solid lines for the total fits and dashed lines for component peaks).

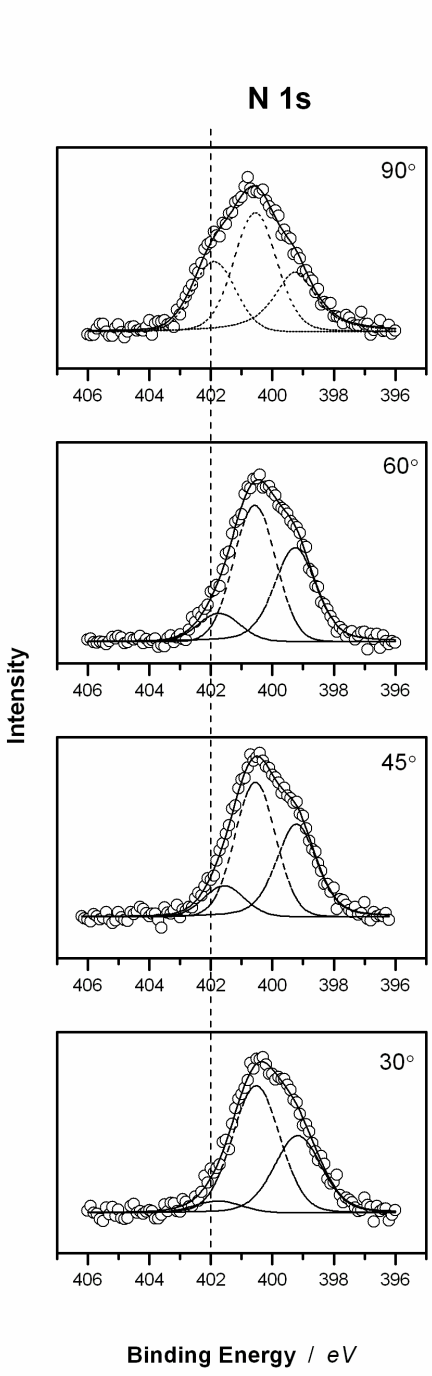

Figure 3.19 High-resolution N 1s XP spectra for 30-basepair thiol-DNA immobilized on gold (open circles for raw data, solid lines for the total fits and dashed lines for component peaks). Spectra were taken after incubation with $Zn(ClO_4)_2$ at pH 7.5 at angles 90, 60, 45, 30 degrees from the surface normal.

3.3.2.4 Zinc (Zn 2p) Spectrum

The Zn 2p spectra is of interest as it is assumed that when M-DNA forms, the Zn^{2+} ions replace the imino protons of T and G but also become weakly bound to the phosphates on the outside of the helix. In order to assess this hypothesis, Zn/P ratios were calculated using equation 3.2 and compared to trends observed in the survey spectrum for Na 1s. At pH 8.5, B-DNA shows no Zn 2p peak, but an intense peak for Na 1s at 1072.0 eV (Figure 3.20a). The Na/P ratio in figure 3.20a is 5.1 demonstrating a surface excess of sodium. However, in the presence of Mg^{2+} at pH 8.6 there is an intense peak observed at 1304.6 eV. Under these conditions, the Mg/P ratio is 0.6 ± 0.05. A decrease in the cation to phosphate ratio would be expected in going from a monovalent to a divalent cation. In both cases, a peak is also observed around 208 eV which is representative of the Cl^- counterions also remaining on the surface. However, after the addition of 0.4-mM $Zn(ClO_4)_2$ to the monolayer for 2h at pH 8.5 and thorough washing with buffer containing Zn^{2+} an intense peak with a BE of about 1022.0 eV is now present but the Na 1s peak at 1072.0 was undetectable (Figure 3.20b). Under these conditions, the Zn/P ratio was 1.7 ± 0.6. Again, the decreased ratio compared to Na/P is expected from a monovalent to a divalent cation. Although there is a large error, the average value corresponds well to zinc binding each phosphate as well as replacing the imino proton inside the helix at every base pair. When this experiment is repeated under the same conditions, except the monolayer is washed with buffer containing only Na^+ and no Zn^{2+}, peaks are evident at both 1022.0 eV and 1072.0 eV (Figure 3.20c). The Zn/P ratio was 0.44 ± 0.11 meaning there is now approximately one zinc for every base pair. This ratio correlates well to M-DNA formation where only the imino protons of thymine and guanine are being replaced by zinc. However, under the same conditions with Zn^{2+} at pH 7.0, there is virtually no zinc left in the monolayer with a Zn/P ratio of 0.07. Therefore, under non M-DNA conditions it is very easy to wash off all of the zinc ions. The Zn/Na and Na/P ratios in figure 3.20c were 0.22 and 2.0 respectively, indicating that the negative charge on the phosphate backbone is neutralized by the saturation of Na^+ ions present whereas the Zn^{2+} ions are interacting inside the helix.

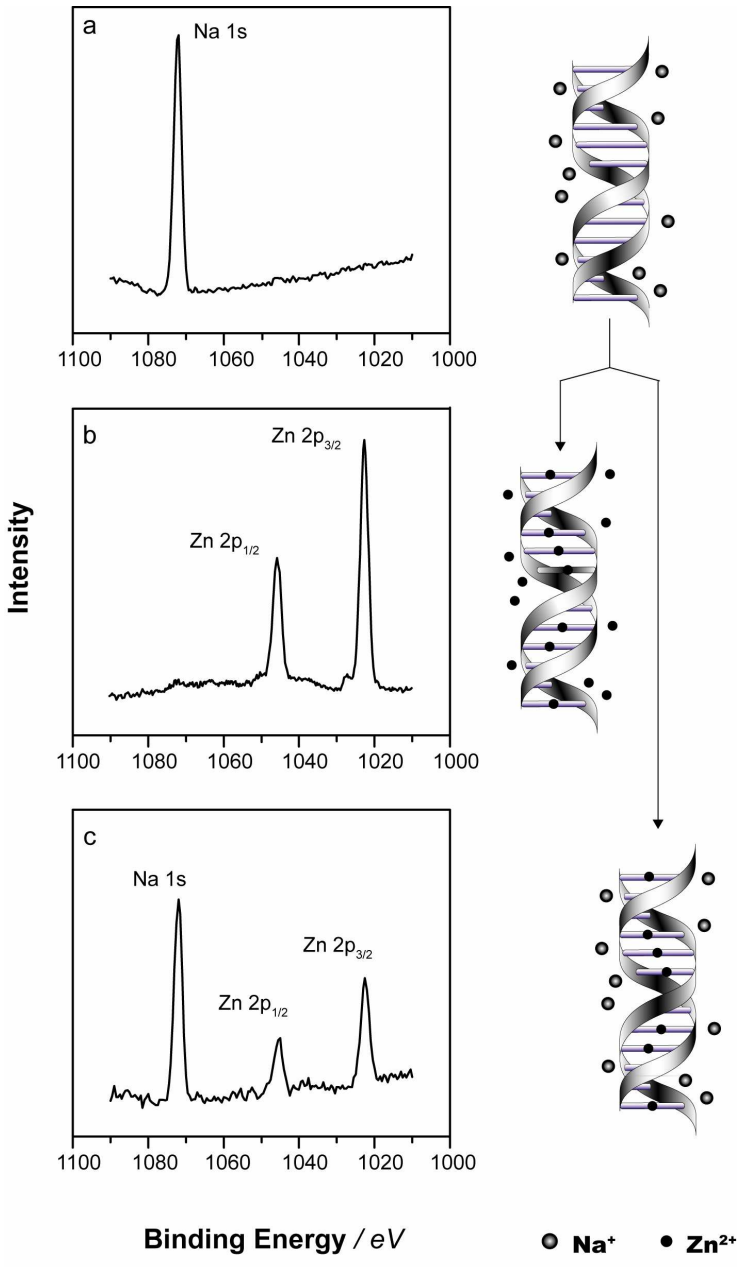

Figure 3.20 Survey scan of the Zn 2p and Na 1s region with corresponding schematic illustrating the location of the respective ions under various washing conditions; (*a*) Immobilized B-DNA was incubated and washed in 20 mM Tris-ClO_4 (pH 8.5), 20 mM $NaClO_4$ buffer. (*b*) Immobilized B-DNA was converted to M-DNA by incubating for 2 hrs in 20 mM Tris-ClO_4 (pH 8.5), 0.4 mM $Zn(ClO_4)_2$, washed with 20 mM Tris-ClO_4 (pH 8.5), 0.4 mM $Zn(ClO_4)_2$, dried and measured. (*c*) Immobilized B-DNA was converted to M-DNA by incubating for 2 hrs in 20 mM Tris-ClO_4 (pH 8.5), 0.4 mM $ZnClO_4$, washed with 20 mM Tris-ClO_4, 20 mM $NaClO_4$ containing no $ZnClO_4$, dried and measured.

Under these conditions, the O 1s spectrum resembles that of B-DNA shown in figure 3.16 and the N 1s spectrum resembles that of M-DNA shown in fgure 3.17. This is expected since the conversion from M-DNA back to B-DNA is slow (Wood *et al.*, 2002; Wood and Lee, 2005), so that during the washing procedure the Zn^{2+} ions are removed from the outside of the helix and replaced with Na^{+} resulting in an O 1s spectrum similar to B-DNA. However, the zinc ions interacting with the imino nitrogen inside the helix are not removed resulting in an N 1s spectrum similar to M-DNA. This effect would result in a Zn/P ratio of approximately 0.5 which is observed.

3.3.3 Variable angle XPS

Variable angle x-ray photoelectron spectroscopy (VAXPS) was also used to further investigate the distribution of zinc within the self-assembled monolayer. Oligonucleotides containing the Mx-30a sequence were self-assembled onto gold through a disulfide linkage. The identical but reverse sequence, Mx-30b, in which the d(TG)•d(CA) portion was situated next to the sulfur linkage was also analyzed. The surface was probed at take-off angles 90, 70, 45 and 30 degrees from surface. According to previous result, the d(TG)•d(CA) will incorporate metal ions at a much lower pH than the d(AT) tract illustrated in figure 3.21. As seen in figure 3.22, at pH 7.0 when the d(TG)•d(CA) tract is situated at the top of the monolayer the Zn/P ratio increases as the take-off angle decreases. Conversely, if the d(TG)•d(CA) tract is located at the bottom of the monolayer, the Zn/P ratio decrease along with the take-off angle. Also of interest are the control experiments which clearly show that at pH 6.5 the wash easily removes zinc bound to the phosphate backbone leaving very little zinc remaining as the pH is too low to have formed M-DNA. As well, at pH 8.5 at which the entire oligomer should be converted to M-DNA, the Zn/P ratio approaches 0.5 which is a good indication that there is one zinc residue for every base-pair. As well, Zn/P ratios in figure 3.22 are greater for Mx-30a compared to Mx-30b for all pH values. This may be a due to Zn^{2+} ions having easier access to the d(TG)•d(CA) tract when it is situated at the top of the monolayer compared to when it is unexposed at the bottom.

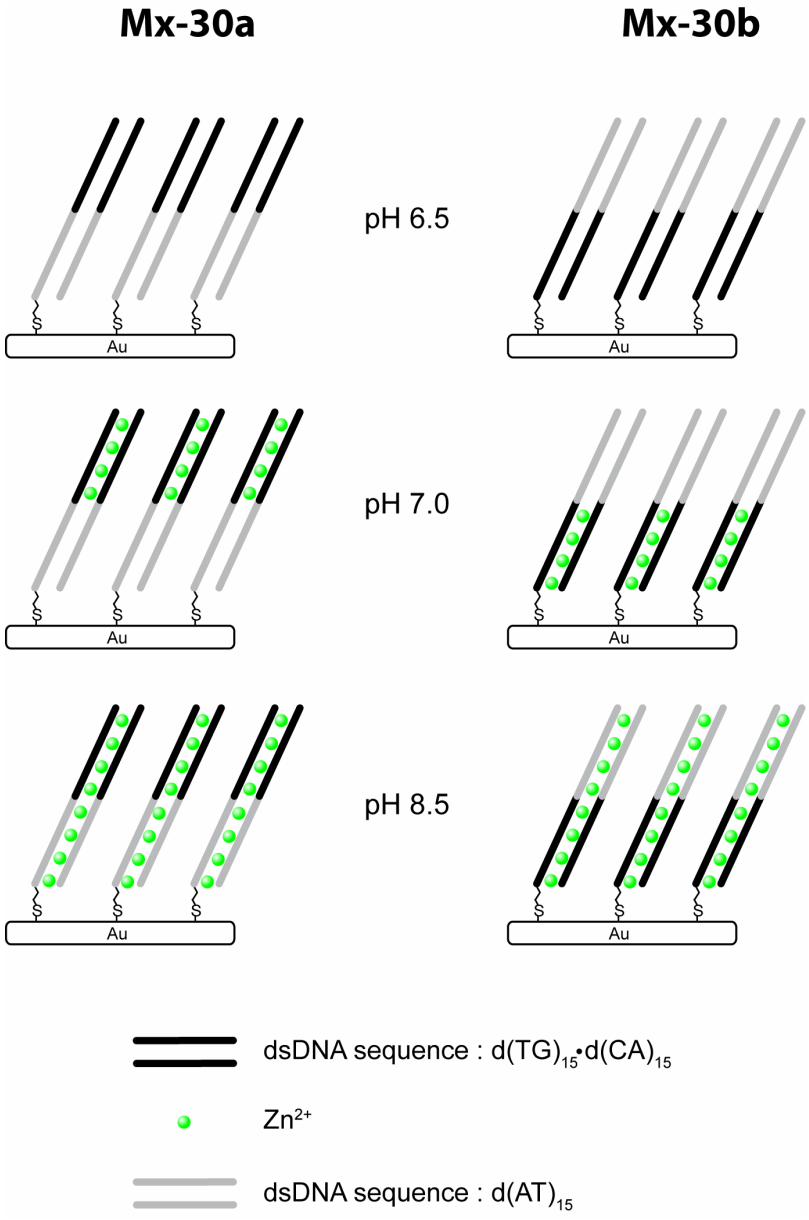

Figure 3.21 Schematic of Zn^{2+} ions situated only at specific regions corresponding to the sequence and the pH.

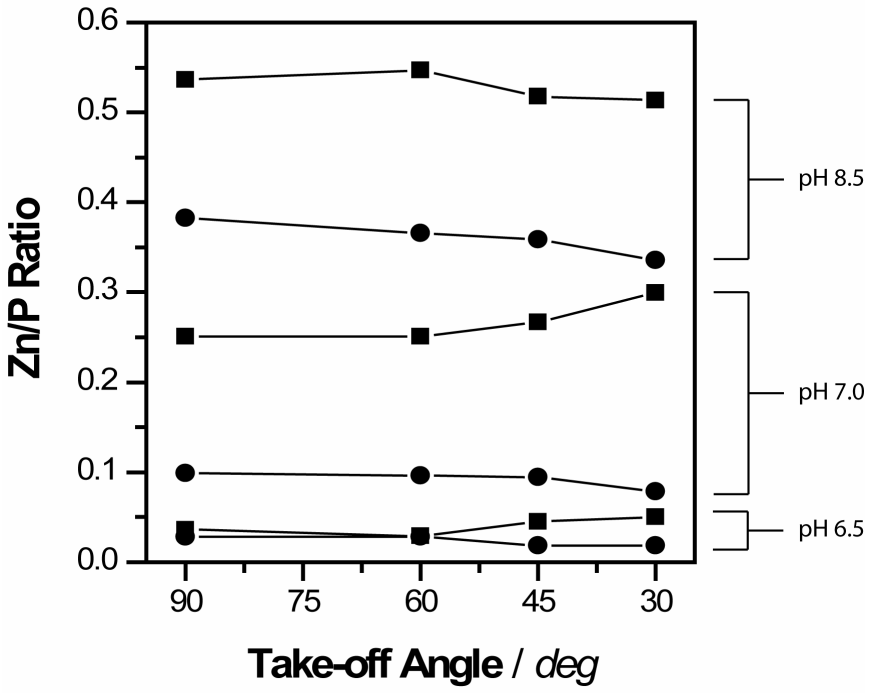

Figure 3.22 Relative Zn/P ratios of Mx-30a (■) and Mx30b (●) at angles 90, 70 45 and 30 degrees relative to the surface at various pH values.

Unfortunately, the values are subject to an estimated error of at least 10%, which is mainly caused by the uncertainty of the peak area and the error of the inelastic background correction (Tougaard and Sigmund, 1982). Therefore, the change in Zn/P ratio is not great enough to warrant a firm conclusion. Although, repeated measurements showed similar trends for Zn/P ratios at 90° to the surface, the changes observed at the various other angles were unpredictable. This was most likely a result of inconsistencies in the DNA monolayer coverage and morphology. Although this technique shows promise and illustrates very interesting trends, modification to the existing assay will have to be made in order to gain useful data.

3.4 Electrochemical Investigations

Electrochemical DNA biosensors based on nucleic acid hybridization are being developed for the diagnosis of genetic and infectious diseases (Boon *et al.*, 2000; Drummond *et al.*, 2003). They have gained tremendous popularity because of their high sensitivity and selectivity, their simplicity to operate, the low cost, ease of fabrication and their ability to be miniaturized in order to increase portability. There have been numerous approaches developed for the electrochemical detection of DNA hybridization (Drummond *et al.*, 2003; de-los-Santos-Alvarez *et al.*, 2004; Kerman *et al.*, 2004). Some common methods have utilized DNA probes with covalently attached enzymes (Campbell *et al.*, 2002) or redox-active molecules (Ihara *et al.*, 1996; Kelley *et al.*, 1999). As well, various procedures have exploited nanoparticle-modified oligonucleotides (Wang *et al.*, 2001a; Wang *et al.*, 2001b; Palecek *et al.*, 2002). Other strategies employ electrochemically active intercalators such as daunomycin (Wang *et al.*, 1998), metal complexes such as ruthenium bipyridine (Napier *et al.*, 1997) and organic dyes such as methylene blue (Ozkan *et al.*, 2002) all of which have the obvious advantage of not requiring a labeling procedure. The electron transfer properties of the monolayer are then interrogated by CV, CA or EIS, (Hartwich, 1999; Kelley *et al.*, 1999; Long *et al.*, 2004). Among the electrochemical techniques used, EIS has been proven to be an effective and sensitive method (Katz, 2003).

Previously, a label-free method able to detect single DNA base pair mismatches at concentrations as low as 100 pM had been reported (Long *et al.*, 2003; Wettig *et al.*, 2003b; Long *et al.*, 2004; Li *et al.*, 2005; Li *et al.*, 2006). Briefly, the unlabelled single-stranded probe DNA is attached to a gold working electrode through a thiol linkage and the target, also unlabelled, is hybridized to it. The impedance is measured for B-DNA and for M-DNA which is formed after incubation with Zn^{2+} at pH $\geq$ 8.5 (Lee *et al.*, 1993; Aich *et al.*, 1999). M-DNA monolayers have decreased R_{CT} compared to B-DNA but the presence of a mismatch increases the R_{CT} for M-DNA whilst decreasing the R_{CT} for B-DNA. Thus, the difference in impedance before and after formation of M-DNA allows for the unequivocal detection of a mismatch within a synthetic DNA 20mer. However, there are a few fundamental problems with this procedure that need to be addressed. First and foremost is the delicacy of this protocol in the presence of metal ions. If the pH is too high, the DNA may denature or the metal ion may precipitate. If the pH is too low then M-DNA will not form. To complicate matters further, the addition of zinc salt to the $[Fe(CN)_6]^{4-}$ may cause the formation of zinc ferrocyanides which will precipitate out of the solution potentially causing numerous inconsistencies in results (Miller and Falk, 1904; Cheng, 1955; Riveros *et al.*, 1996). As well, $[Fe(CN)_6]^{3-}$ cannot be kept as aqueous stock solutions because potassium ferricyanide decomposes slowly on standing. In order to address these and other problems, a new redox probe was tested that has longer storage times, less preparatory time, faster analysis and increased reliability especially in the presence of metal ions such as Zn^{2+}. In the following section, the effectiveness of $IrCl_6^{2-/3-}$ as a redox couple is demonstrated as well as the advantages associated with this system in comparison to the $[Fe(CN)_6]^{3-/4-}$ reported previously (Li *et al.*, 2003; Long *et al.*, 2003; Long *et al.*, 2004) .

3.4.1 Effect of Metal Ions on Electron Kinetics

In order to investigate the electron properties of M-DNA both cyclic voltammetry and electrochemical impedance spectroscopy were used. Previous work took advantage of the commonly used negatively charged redox couple $[Fe(CN)_6]^{3-/4-}$. This probe has been very successful in looking at DNA monolayers as the negative

charge is sufficiently repelled from the monolayer and therefore the electron must flow from the probe through the monolayer to the gold surface. However, as mentioned above, this probe shows some limitations when investigating M-DNA. Therefore, various alternative redox probes such as Ferrocenecarboxaldehyde and 1,1'-Ferrocenedicarboxylic acid were tried. However, in both cases, the probes were able to penetrate into the monolayer causing the signal transduction through the monolayer to proceed virtually unimpeded. Finally, the anionic probe $IrCl_6^{2-/3-}$ was also tested and proved to be quite effective in investigating DNA monolayers. Therefore, the following work reconfirms the electronic properties of M-DNA previously shown using $[Fe(CN)_6]^{3-/4-}$ as a redox couple (Li *et al.*, 2003; Long *et al.*, 2003; Li *et al.*, 2005; Li *et al.*, 2006) and for the first time demonstrates the correlation of incremental pH changes on M-DNA formation using electrochemistry. As well, the potential advantageous of using the $IrCl_6^{2-/3-}$ redox couple over standard $[Fe(CN)_6]^{3-/4-}$ system will be highlighted.

3.4.2 Cyclic Voltammetry

Duplex DNA, 30 base pairs in length, was assembled onto the gold surface as described in Materials and Methods and the resultant monolayer was examined electrochemically using 2 mM $IrCl_6^{2-}$. $IrCl_6^{2-}$ undergoes spontaneous reduction to $IrCl_6^{3-}$ making an effective redox couple *in situ*. Even though the concentration of reduced species is variable, there is no significant change in the formal potential over the time course of one measurement. In order to achieve greater consistency, fresh solution was used for each measurement.

From the CV plot shown in figure 3.23, it can be seen that for a bare electrode immersed in 2 mM $IrCl_6^{2-}$ in 20 mM Tris-ClO_4 at pH 8.6, a characteristic reversible redox cycle with anodic and cathodic peak currents of approximately 8 μA and a peak separation of 85 mV is seen. However, once DNA is immobilized on the surface, the peak current drops and the separation between the oxidation and reduction peaks increased considerably indicating the reduced ability for electron transfer between the solution and the surface caused by blocking of the gold surface by the DNA monolayer.

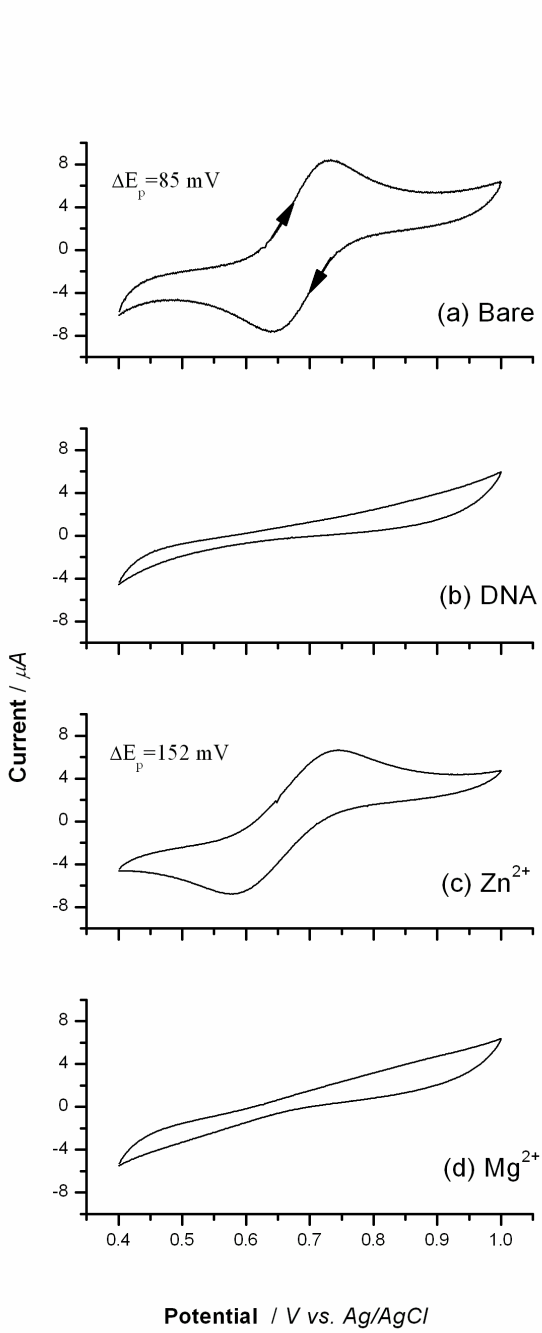

Figure 3.23 Cyclic Voltammograms of (a) bare gold electrode, (b) ds-DNA modified electrode, (c) ds-DNA monolayer in the presence of 0.4 mM Zn^{2+} at pH 8.6 and (d) ds-DNA monolayer in the presence of 0.4 mM Mg^{2+} at pH 8.6. The concentration of hexachloroiridate (IV) was 2 mM in 20 mM TrisClO_4 (pH 8.6). All CVs were recorded at a sweep rate of 100 mV/s.

Upon the exposure of the monolayer to 0.4 mM $Zn(ClO_4)_2$ for only 2 minutes, the peak currents reach approximately 7 μA with a separation of 152 mV indicating electron transfer through the monolayer is only restricted slightly under M-DNA conditions. There were no changes in peak current or separation with longer incubation times. Similarly, impedance values remained constant after two minutes incubation (see below). One explanation for this result is that the addition of Zn^{2+} causes a reorientation of DNA molecules on the surface. This may allow the redox probe easier access to pin holes or other defect sites. However, the shape of the cyclic voltammogram is characteristic of linear diffusion and the anodic peak current increases with the square root of the scan rate in the range of 25 to 250 mV (Figure 3.24). Both of these characteristics suggest that the electrochemical reaction is primarily controlled by linear diffusion and not by pinholes or small defects (Chailapakul and Crooks, 1993). Alternatively, the Zn^{2+} is able to coordinate with the negatively charged phosphate backbone effectively reducing the electrostatic repulsion and facilitating the penetration of the monolayer by the negatively charged redox probe. Presumably then, the exposure of the monolayer to Mg^{2+} would give a similar result. However, the CV plot decreases only slightly compared to native DNA indicating very slow electron transfer between the solution and the surface (Figure 3.23). Therefore, the much faster electron transfer implies that M-DNA is a better conductor than B-DNA. Finally, exposing the monolayer to 10 mM EDTA in 20 mM Tris-ClO_4 with 100 mM $NaClO_4$ at pH 7.1 converts the signal back to native DNA. This result demonstrates that the decrease in signal is not a result of denaturation or destruction of the monolayer (Figure 3.25). As well, the return of the original signal after the addition of EDTA further confirms that the formal potential remains constant even after repeated measurements.

In order to investigate the electron-transfer kinetics, the CV plots for a bare gold electrode and M-DNA modified electrode were fitted using DigiSim version 3.0 from BASi and compared. In figure 3.26, both CV plots are shown with the background current subtracted together with the simulated CV plots. In 20 mM Tris-ClO_4 at a scan rate of 100 mV/s, a ΔE_p of 85 mV was measured for the $IrCl_6^{2-/3-}$ redox couple at a bare electrode and a ΔE_p of 152 mV for the M-DNA modified electrode.

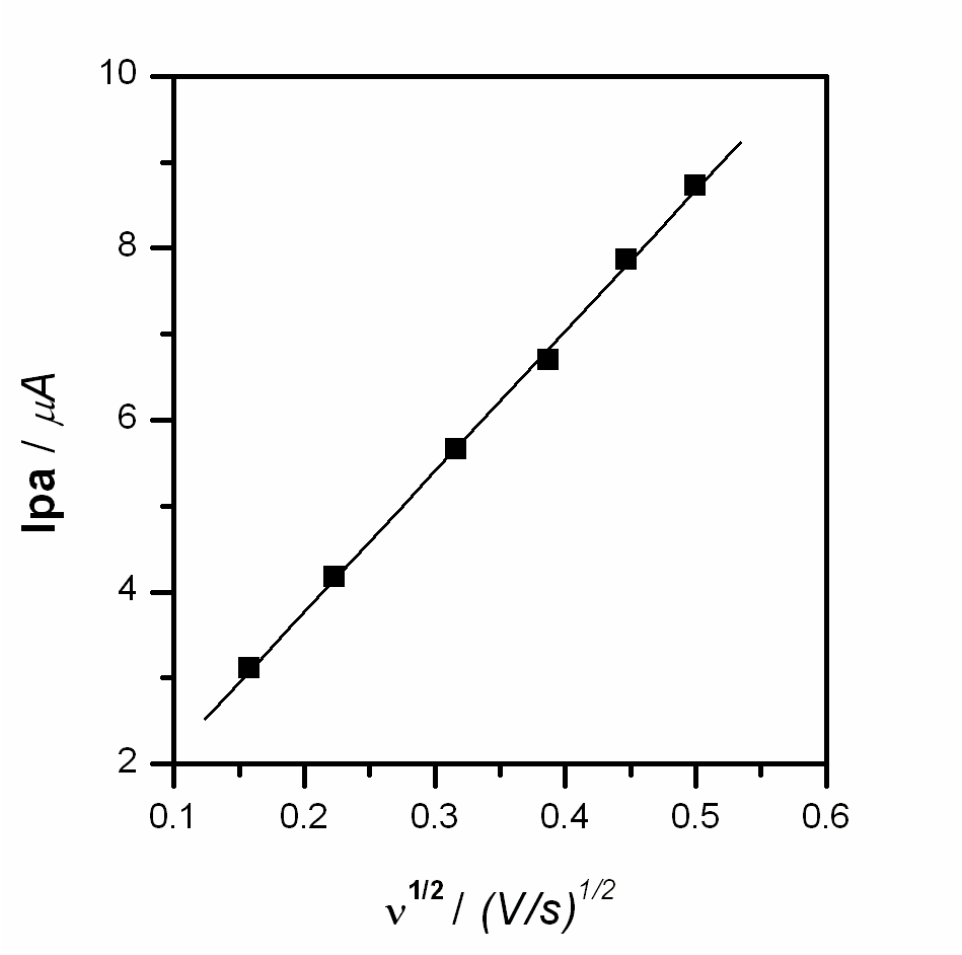

Figure 3.24 Plot of anodic peak current (Ipa) vs. the square root of the scan rate. The cyclic voltammograms were obtained using an M-DNA modified electrode in 20 mM Tris-ClO_4 buffer (pH 8.6) in the presence of 2 mM $IrCl_6^{2-/3-}$.

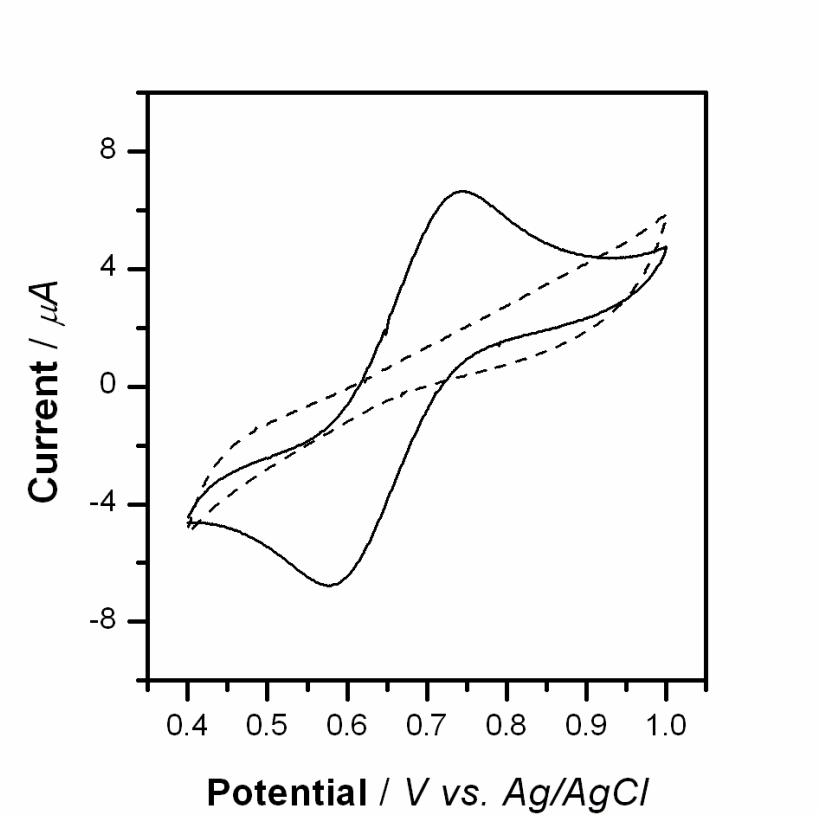

Figure 3.25 Cyclic Voltammograms of an M-DNA modified electrode (**—**) and the electrode after incubation in 10 mM EDTA in 20 mM $TrisClO_4$, 100 mM $NaClO_4$ at pH 7.1 (**----**). All measurements were performed in 2 mM hexachloroiridate (IV) in 20 mM $TrisClO_4$ (pH 8.6) at a sweep rate of 100 mV/s.

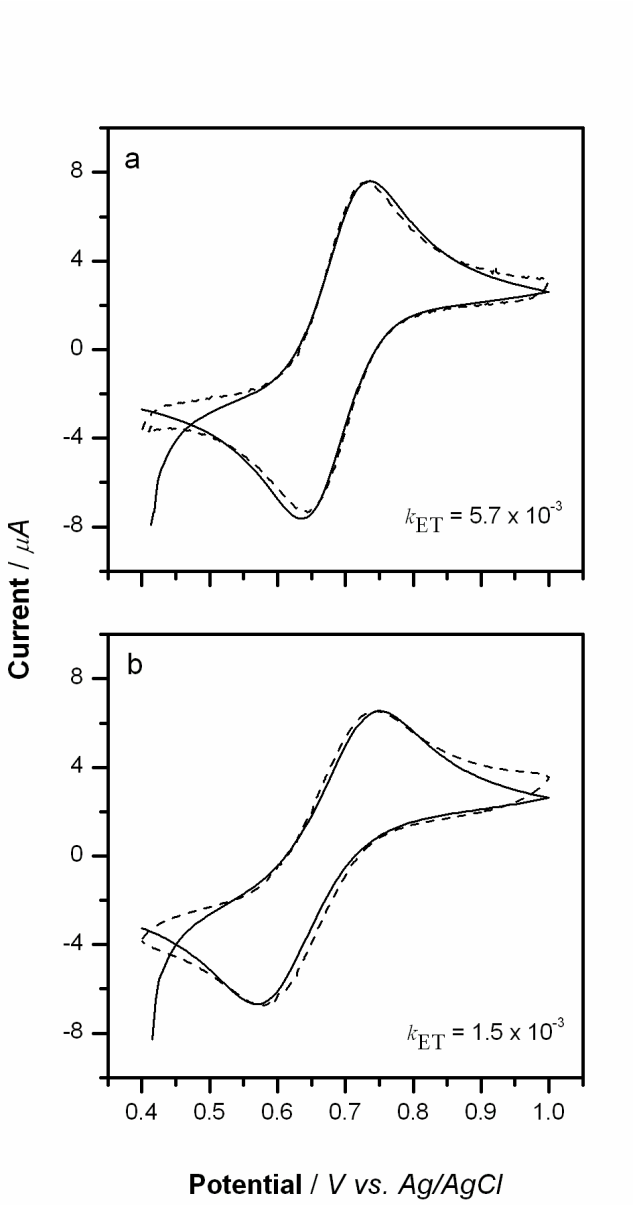

Figure 3.26 Cyclic voltammograms (**--**) in 2 mM $IrCl_6^{2-/3-}$ in 20 mM Tris-ClO_4 buffer solution (pH 8.6) at (A) bare gold electrode and (B) a M-DNA modified gold electrode together with simulated data (**—**). Scan rate used was 100 mV/s. Digital simulations were made using the k_{ET}, E_0, and α (transfer coefficient) values of (A) 5.7 x 10^{-3} cm/s, 0.69 V vs. Ag/AgCl/3 M NaCl, and 0.5 and (B) 1.5 x 10^{-3} cm/s, 0.69 V vs. Ag/AgCl/3 M NaCl and 0.5. A diffusion coefficients of 8.9 x 10^{-6} cm^2/s was used for both D_{ox} and D_{red} in (A) and (B). Both CVs have the background current subtracted.

Under these conditions, the electron-transfer rate was 5.7 x 10^{-3} cm/s and 1.5 x 10^{-3} cm/s respectively. In the case of a regular dsDNA monolayer, the electron-transfer rate was too small to be measure effectively and therefore must be orders of magnitude smaller.

3.4.3 Electrochemical Impedance Spectroscopy

To further investigate the properties of M-DNA monolayers, EIS was employed. Impedance spectroscopy is advantageous because a model based on electronic components can be used to represent the electrochemical system (Figure 3.27 inset). The impedance of an electrode undergoing heterogeneous electron transfer through a self-assembled monolayer can be described on the basis of the model developed by (Randles, 1947). The circuit components in the Randles cell can easily be compared with familiar physical phenomena. The solution resistance term, R_S, represents the resistance of the solution between the working (gold electrode) and reference (Ag/AgCl) electrode. The charge transfer resistance term, R_{CT}, results from the transfer of electrons from the redox probe to the DNA monolayer, through the base pairs of the DNA helix and from the helix to the surface of the gold electrode. A constant phase element (*CPE*) will act as a non-ideal capacitor in order to account for inconsistency on the electrode surface (Dijksma *et al.*, 2002). Finally, a Warburg impedance element, W, is dependent on the rate of diffusion of the redox probe (Long *et al.*, 2004). The data are shown as Nyquist plots where the impedance values are a result of the resistance and capacitance measured at various frequencies. The data is presented as the real (Z_{re}), versus the imaginary ($-Z_{im}$) components. The Nyquist plot for a bare electrode (data not shown) consists of a semicircular region lying on the Z_{re} axis followed by a straight line. The semicircle portion, measured at higher frequencies, corresponds to direct electron transfer, whereas the straight linear portion, observed at lower frequencies, represents the diffusion-controlled electron transfer process known as Warburg impedance (Long *et al.*, 2003; Wettig *et al.*, 2003b). For a clean bare electrode, the Warburg impedance will appear as a line with a slope of approximately 0.5 on a Nyquist plot (Glarum and Marshall, 1982).

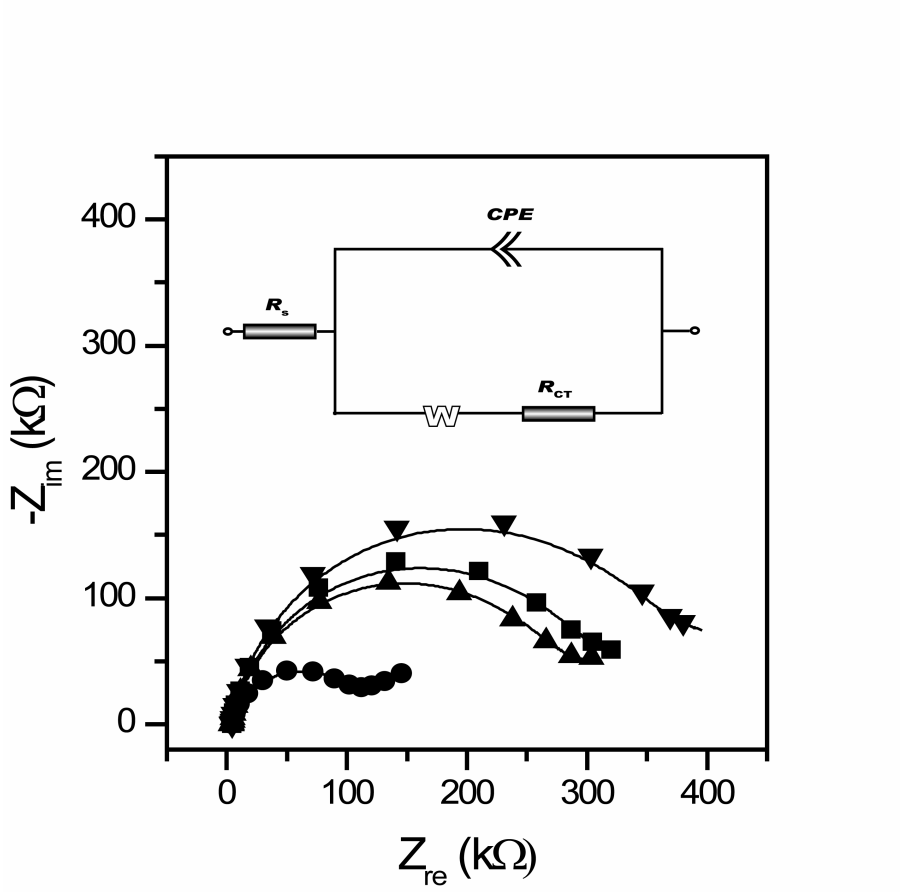

Figure 3.27 Nyquist plots (Z_{im} vs Z_{re}) of a 30 base pair-complementary DNA performed in 1 mM hexachloroiridate (IV) redox probe in 20 mM Tris-ClO_4 at pH 8.6. Measurements were done in a three-electrode cell using an applied potential of 690 mV vs. Ag/AgCl. In all cases the measured data points are shown as symbols with the calculated fit to the equivalent circuit as a solid line. (▼) 30 basepair duplex B-DNA, (■) after incubation in 0.4 mM Zn^{2+} at pH 6.0, (▲) after incubation in 0.4 mM Mg^{2+} at pH 8.6, and (●) after incubation in 0.4 mM Zn^{2+} at pH 8.6. Inset: The experimental data were fit to the Randles equivalent circuit which consists of the solution resistance through the redox probe (R_S), the charge transfer resistance through the DNA (R_{CT}), the constant phase element (*CPE*) and the Warburg constant (*W*).

As expected, the resistance for M-DNA is much lower than its corresponding B-DNA construct illustrating that electron transfer via M-DNA is much faster than that of the native DNA. Figure 3.27 shows the Nyquist plots when the DNA monolayer is exposed to Zn^{2+} at pH 6.0 or to Mg^{2+} at pH 8.6, conditions under which M-DNA does not form. Consistent with the CV experiments, only small changes in the charge transfer are seen. These changes are most likely a result of reducing the charge repulsion of the DNA monolayer by the metal ions binding to the negatively charged phosphate backbone. As shown in Table 3.6 for the various films, a monolayer composed of B-DNA has a R_{CT} of 416 ± 64 kΩ compared to M-DNA which has a R_{CT} of 91 ± 56 kΩ. Both monolayers in the presence of Zn^{2+} at pH 6.0 and Mg^{2+} at pH 8.6 show much smaller decreases in R_{CT} of 335 ± 60 and 298 ± 64 kΩ respectively. In all cases, M-DNA is reproducibly converted back to B-DNA and original R_{CT} values are obtained by the incubation of the monolayer in 10 mM EDTA.

The change in R_{CT} between B-DNA and M-DNA monolayers was calculated as $\%\Delta R_{CT}$ as different electrode morphologies can yield different impedance values, but the percent changes between B- and M-DNA are more reproducible. As illustrated in figure 3.28, as the pH increases the percent change between B- and M-DNA becomes larger until it reaches a maximum of 70% above pH 8.0. Conversely, the monolayer exposed to Mg^{2+} shows no dependence on the pH of the solution. Therefore, the large change at increased pH values for M-DNA is indicative of zinc ions replacing the imino proton on thymine and guanine residues.

TABLE 3.6 Impedance Data as a Function of pH and Metal Ion[a]

Circuit element	**B-DNA pH 8.6**	**M-DNA pH 8.6**	**DNA incubated with Zn^{2+} pH 6.0**	**DNA incubated with Mg^{2+} pH 8.6**
R_s / kΩ	4.3 (0.3)	4.2 (0.3)	4.3 (0.3)	4.1 (0.2)
CPE / μF	1.02 (0.16)	1.09 (0.36)	1.03 (0.16)	1.22 (0.06)
n	0.87 (0.01)	0.85 (0.02)	0.88 (0.01)	0.88 (0.01)
R_{CT} / kΩ	416 (64)	91 (56)	335 (60)	298 (64)
W / 10^{-5} Ω•$s^{-1/2}$	4.1 (0.9)	5.6 (1.0)	5.0 (1.1)	5.1 (0.8)

[a]The values in parentheses represent the standard deviation from at least 5 electrodes.

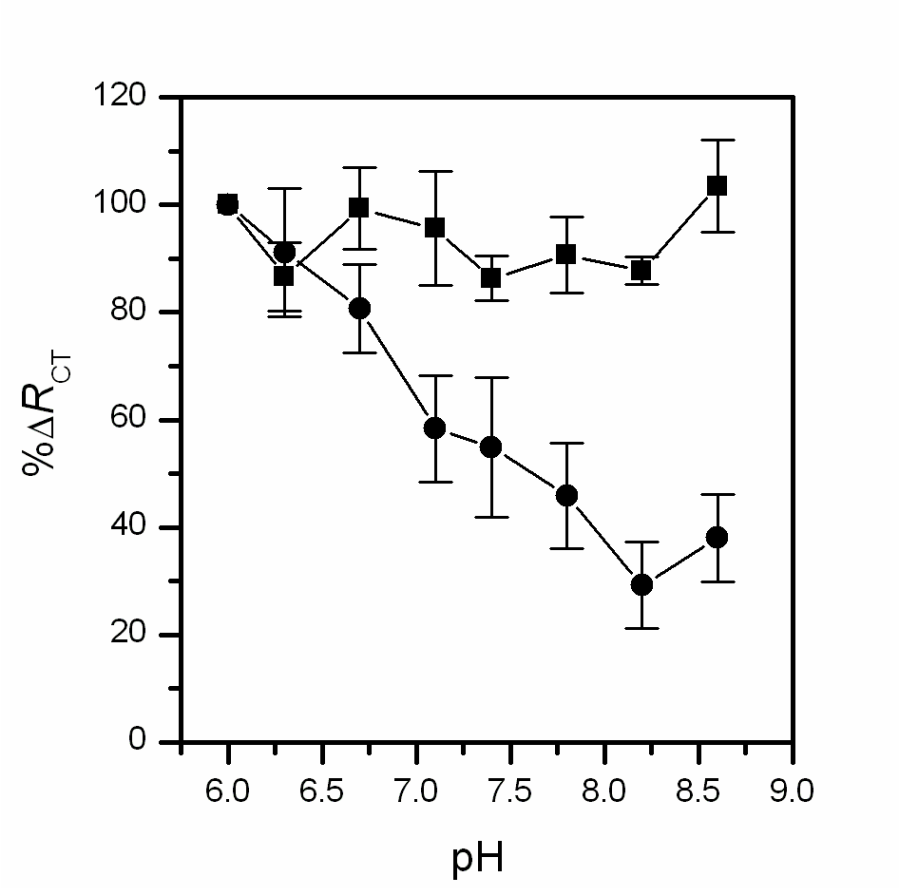

Figure 3.28 Determination of pH dependency on M-DNA formation. Each point is calculated as the change in R_{CT} between DNA monolayers which was incubated in the presence of Zn^{2+} (●) or Mg^{2+} (■) at pH 6.0 and each corresponding pH. Error bars represent the standard deviation and are derived from a minimum of three different electrodes. All measurements were performed in freshly prepared 1 mM hexachloroiridate (IV) in 20 mM Tris-ClO_4.

3.4.3.1 Dehybridization-Rehybridization

In order to assess the ability to detect hybridization, the dsDNA was denatured and then rehybridized with target strand. A schematic of the experimental procedure is outlined in figure 3.29a. As seen from the Nyquist plots in figure 3.29b, the R_{CT} decreases by approximately 46 ± 10 % after denaturation compared to the original dsDNA monolayer. The decrease in R_{CT} seen in the impedance plots is assumed to be correlated with the degree of denaturation. Although the impedance signal does not return to the values for a perfect dsDNA monolayer, the increase is reflective of rehybridization efficiencies of approximately 87.9 ± 4.0%.

3.4.3.2 Effect of Site-Specific Metal Ions on Resistance through M-DNA

As previously mentioned in section 3.2.3.2 oligomers 30 base-pairs in length where designed with 50% d(AT) and the other 50% d(TG)•d(CA) in which three terminal thymines on the d(TG)•d(CA) track where replaced with 4-thiothymines (Table 2.2). As shown in figure 3.9, this sequence begins to form M-DNA at a lower pH compared to $d(TG)_{15}$•$d(CA)_{15}$. Therefore, DNA containing the above sequences was immobilized onto gold electrodes and the resistance through the DNA was measured at various pH values in the absence and presence of Zn^{2+}. As shown in figure 3.30, the $\%\Delta R_{CT}$ for $d(TG)_{15}$•$d(CA)_{15}$ is the largest at low pH values. A possible explanation is that the partial M-DNA formation in the thiolated region of both Mx(s^4T)-30a or Mx(s^4T)-30b is not sufficient to allow fast electron transfer through the entire monolayer. However, the errors in the results obtained are substantial and definitive conclusion cannot be made at this time. The large error was originally thought to be connected with the initial resistance of the B-DNA monolayer as a possible correlation may be seen in figure 3.31 showing $\%\Delta R_{CT}$ of both Mx(s^4T)-30a and Mx(s^4T)-30b at pH 7.4 vs. their initial R_{CT}. Surprisingly, even for reproducible monolayers that have an initial R_{CT} within ± 50 kΩ of each other, there are different $\%\Delta R_{CT}$ (Figure 3.31 shaded area). Therefore, most likely a combination of surface coverage, density, thickness and surface morphology all lead to the inconsistency of the results.

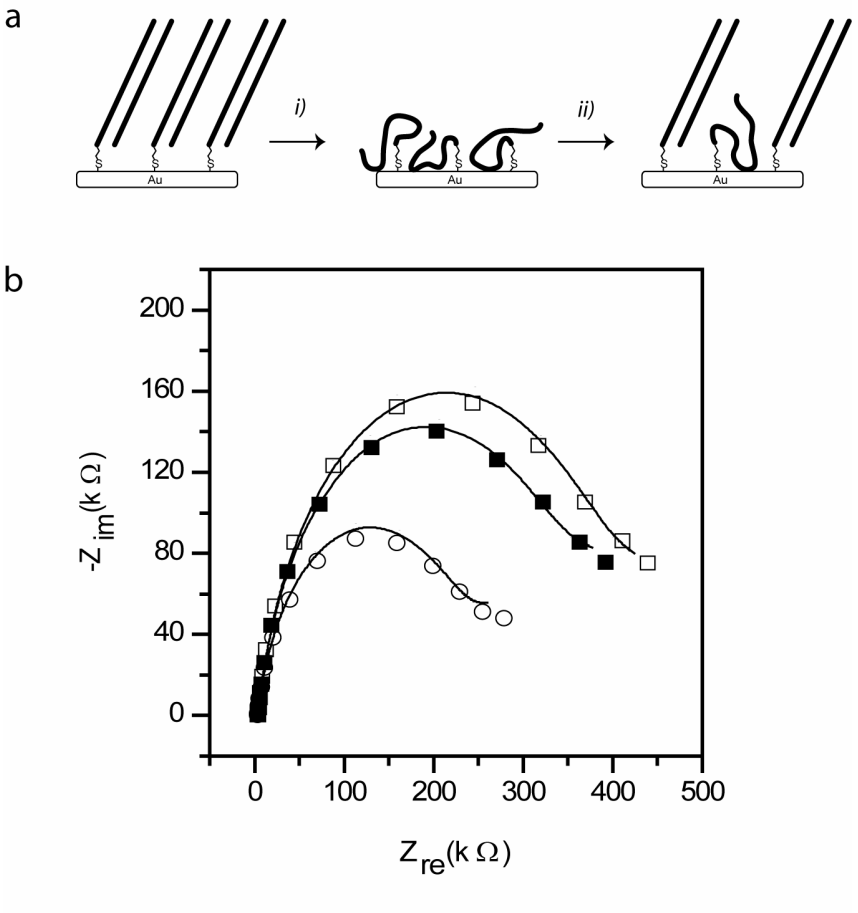

Figure 3.29 Dehybridization-Rehybridization experimental procedure. i) Monolayer was exposed to 10 mM NaOH solution at 65 °C for 10 minutes, rinsed with Millipore water and soaked for an additional 10 minutes. ii) Monolayer was exposed to 100 μM target strand in 20 mM Tris-ClO_4, 100 mM $NaClO_4$ (pH 7.1) for 3 hours. (b) Nyquist plot of fully hybridized monolayer (□), ssDNA monolayer after denaturation procedure (○) and a rehybridized dsDNA monolayer (■).

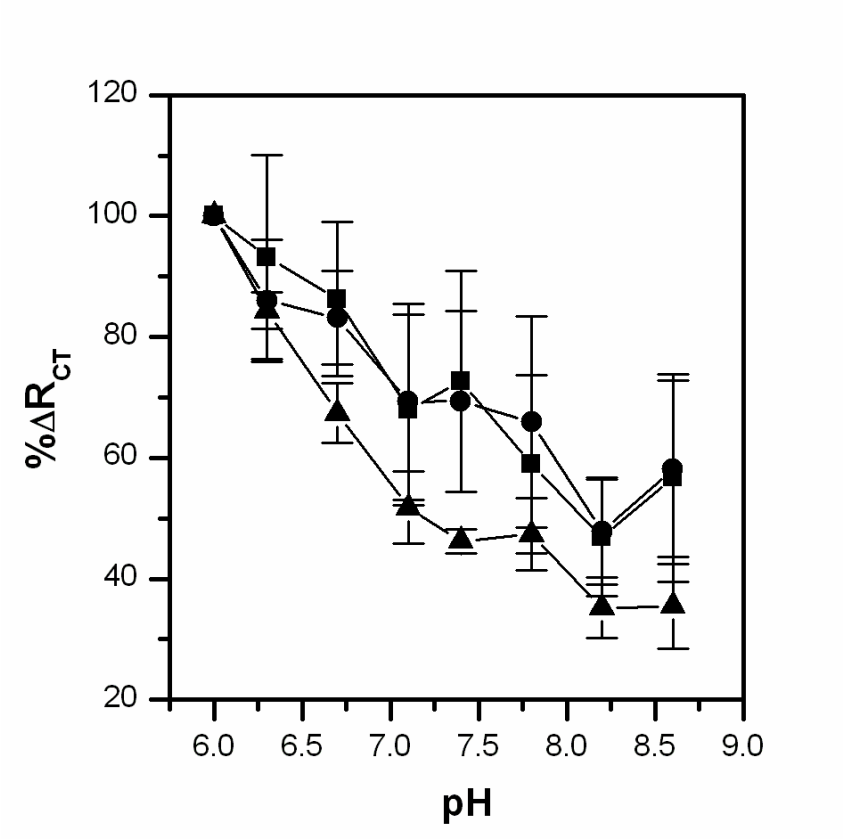

Figure 3.30 Determination of pH dependency on the M-DNA formation of TG-30 (▲); Mx-30a (●); and Mx-30b (■). Each point is calculated as the change in R_{CT} between DNA monolayers which were incubated in the presence of Zn^{2+} at pH 6.0 and each corresponding pH. Error bars represent the standard deviation and are derived from a minimum of three different electrodes. All measurements were performed in freshly prepared 1 mM hexachloroiridate (IV) in 20 mM Tris-ClO_4.

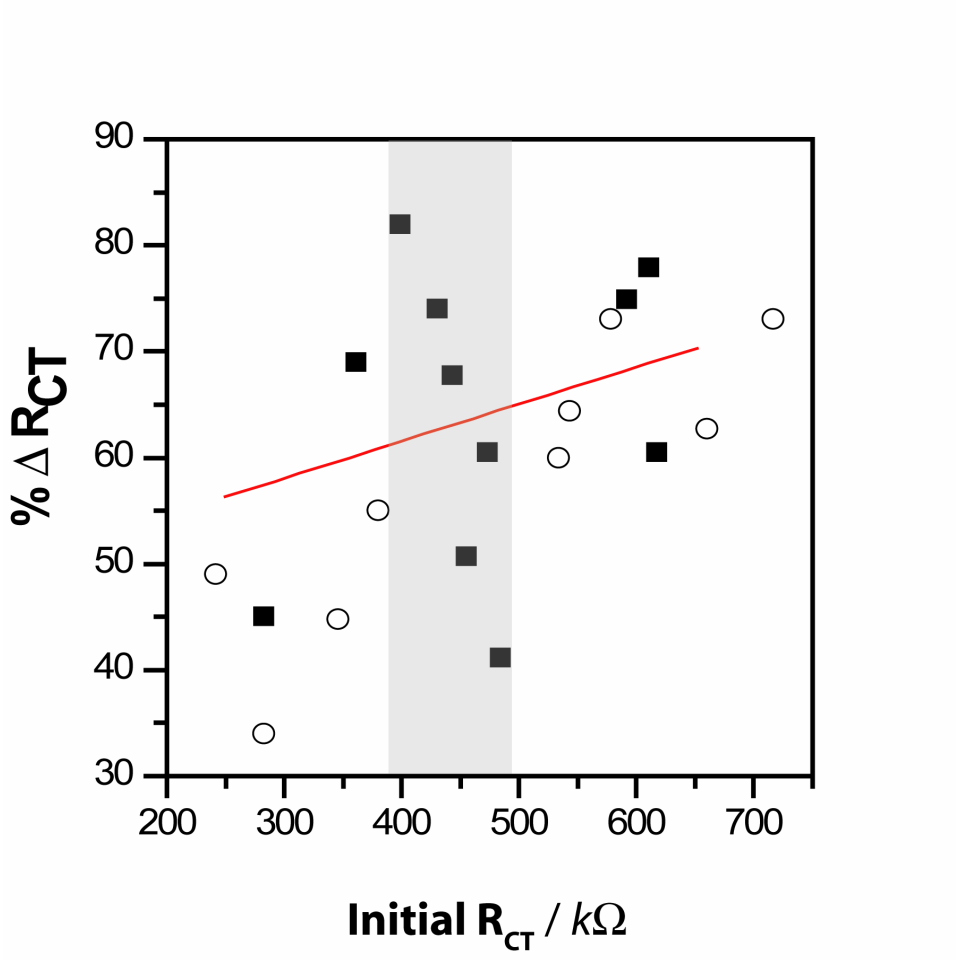

Figure 3.31 The change in R_{CT} between DNA monolayers which were incubated in the presence of Zn^{2+} at pH 6.0 and pH 7.4 for Mx-30a (○) and Mx-30b (■). The red line shows a linear fit for all data points.

3.4.4 Chronocoulometry

A comparison of the charge passed at the various modified electrodes is shown in figure 3.32. The experiment begins at an initial potential of 900 mV vs. Ag/AgCl, where no electrolysis of $IrCl_6^{2-}$ can occur. The potential is then stepped to 500 mV, at which essentially all of the $IrCl_6^{2-}$ is reduced to the $IrCl_5^{3-}$. As one can see form figure 3.32, the amount of charge passed through the M-DNA modified electrode is significantly larger than that on the dsDNA modified electrode. As is also evident, when the dsDNA modified electrode is incubated in the presence of Mg^{2+} which presumably only occupies the negatively charged phosphate backbone, the charge increases slightly compared to that of regular dsDNA. A similar trend is seen when the monolayer is incubated in Zn^{2+} at pH 6.0. However, when the monolayer is incubated at pH 8.6 in the presence of Zn^{2+} there is a considerable increase in charge which can be attributed to electron transfer through the M-DNA monolayer.

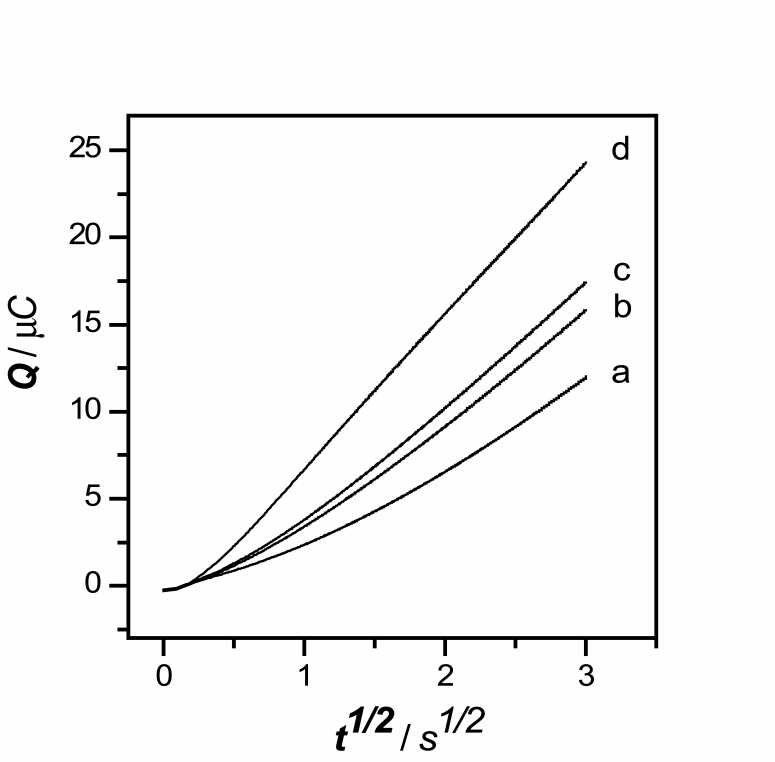

Figure 3.32 Chronocoulometric transients at 500 mV of 2 mM hexachloroiridate (IV) in 20 mM tris-ClO_4 (pH 8.6) at (a) a ds-DNA modified electrode, (b) a ds-DNA modified electrode incubated in the presence of 0.4 mM $Zn(ClO_4)_2$ at pH 6.0 (c) a ds-DNA modified electrode incubated in the presence of 0.4 mM $MgClO_4$ and (d) a ds-DNA modified electrode incubated in the presence of 0.4 mM $Zn(ClO_4)_2$ at pH 8.6.

4.0 DISCUSSION

4.1 Evidence Confirming the Proposed Model for M-DNA

As discussed in section 1.3.1 of the introduction, there have been numerous studies that have lead to the proposed structure of M-DNA in which the metal ion replaces the imino proton on both thymine and guanine (Lee *et al.*, 1993; Aich *et al.*, 1999; Wood *et al.*, 2002; Wood and Lee, 2005). However, without a solved crystal structure, there still remains skepticism as to the exact location of the metal ion. The results in this thesis strengthen the proposed M-DNA model and clearly show that M-DNA is distinct from denatured DNA.

4.1.1 Thermal Denaturation Profiles

Previously, it has been shown that transition metals which interact with the bases are able to cause thermal destabilization and denaturation of the DNA helix (Eichhorn and Shin, 1968). Also, an increase in pH has been shown to cause a similar effect (Ageno *et al.*, 1969). However, as shown in figure 3.6a in the presence of Zn^{2+}, the T_m of poly[d(AT)] actually increases as the pH value is raised to 9.0. First, the increase in thermostability caused by Zn^{2+} at pH 9.0 is even greater than that caused by Mg^{2+}. Therefore, Zn^{2+} is doing much more than simply binding to the negatively charged backbone of the DNA. A simple explanation for the increase in T_m is the conversion to a new conformation. Second, unlike Mg^{2+} which increases the T_m approximately 10 °C at all pH values, the thermostability caused by the addition of Zn^{2+} is pH dependent. This result also correlates very well with the formation of M-DNA as the replacement of the imino proton with a metal ion would be more favorable at higher

pH. Finally, it is clear that the DNA is not becoming denatured since the T_m increases in the presence of Zn^{2+} at high pH.

It has been shown that the lower the pK_a of the imino proton of the base, the lower the pH at which M-DNA will form (Wood *et al.*, 2002). For example, the incorporation of 5FU stabilizes M-DNA at a lower pH because the pK_a of 5FU is about two pH units lower than that of T. Similarly, as shown in figure 3.7c, the incorporation of s^4T into poly[d(TG)•(CA)] causes the T_m to increase at an even lower pH compared to native poly[d(TG)•(CA)]. This result is consistent with the above hypothesis as s^4T has a lower pK_a compared to the native T. Again, this suggests that the metal ion is indeed replacing the imino proton of the base.

The melting profile of λ-496 shown in figure 3.1 was also interesting. Under normal conditions, λ-496 has three different melting transitions corresponding to AT rich regions, mixed regions and GC rich regions. Although the addition of Mg^{2+} increases the T_m at all pH values, there still remains three separate melting transitions. However, the addition of Zn^{2+} causes one single melting transition. One possible explanation is that when the Zn^{2+} replaces the imino proton the ΔG of base-pair formation becomes similar so that there are no longer separate melting transitions seen for GC and AT rich regions.

4.1.2 Ethidium Bromide Assay

Formation of M-DNA was also measured by the EtBr assay. One explanation for the decrease in ethidium fluorescence upon M-DNA formation is the denaturation of the DNA. However, following M-DNA formation, there is rapid restoration to B-DNA upon the addition of EDTA to the ethidium fluorescence buffer. Since the concentration of DNA and the ionic strength are both low, rehybridization is very slow (Morgan *et al.*, 1979). Therefore, this result cannot be explained by denaturation. A better explanation for the inability of ethidium to intercalate between the base-pairs is explained by the charge repulsion caused from the Zn^{2+} replacing the imino proton. A similar result is seen for triplexes containing CG•C^+ (Morgan *et al.*, 1979; Lee *et al.*, 1984; Scaria and Shafer, 1991). The substitution of both s^4T and s^2T into poly[d(AT)]

lowered the pH at which M-DNA formation occurred (Figure 3.7a) . This result was not surprising as both analogues have lower pK_a values than T and transition metals bind well to sulfur-containing functional groups. Similarly, when the analogue s^4T was incorporated into poly[d(TG)•(CA)], the pH of M-DNA formation was again lowered (Figure 3.7b). However, the incorporation of s^2T resulted in an increase in the pH needed for the conversion to M-DNA. This result may be due to the location of the sulfur atom hindering the binding of the metal ion. Alternatively, poly[d(AT)] may simply be refractory to forming M-DNA and therefore under this sequence context, the unusual base pair aids in M-DNA formation.

4.1.3 UV Absorption Spectrum

Also supporting the location of the metal ion is the absorption spectrum of poly[d(As^{4}T)] in the presence of Zn^{2+}. As summarized in figure 3.4 the absorbance peak at 345 nm, which is a result of the incorporation of s^4T, shifts in the presence of Zn^{2+} at pH 8.5. This alone suggests that the metal ion is intimately involved with the sulfur atom which would be the case if the metal ion was replacing the imino proton. Interestingly, this result is not seen with Zn^{2+} at pH 7.5 or with Mg^{2+} at either pH 7.5 or 8.5. Further evidence indicating the metal ion is involved with the hydrogen bonding is that the shift is also seen after denaturation indicating the metal ions now have access to the base. It is important to note that the shift is seen under M-DNA conditions in which the DNA is not denatured as evident from the peak at 260 nm.

4.1.4 X-ray Photoelectron Spectroscopy

The XPS results show direct interaction of Zn^{2+} with nitrogen. More importantly, they strongly suggest that the metal ion is replacing the imino proton on thymine and guanine rather than other alternative binding locations that have been suggested. For instance, x-ray crystallography has demonstrated that Zn^{2+} is able to bind to the N7 of guanine under M-DNA conditions (Labiuk *et al.*, 2003). However, previous investigation using the EtBr assay has shown that this position is not important

for M-DNA formation as z^7A substituted DNA is still able to adopt the M-DNA conformation (Lee *et al.*, 1993). Another possible binding location for the metal ion is on the ring amine groups. However, this position is unlikely as ring amine groups are not good ligands for transition metals (Martin, 1979). As shown in figure 3.17a, there are two main peaks observed in N 1s spectra for B-DNA. Interestingly, these two peaks collapse into a single sharp peak under M-DNA conditions. These results are very similar to those seen with metal porphoryins which closely resembles the proposed M-DNA model. Finally, Zn/P ratios reaffirm that under M-DNA conditions, there are approximately 3 zinc residues for every base pair which corresponds well with zinc interacting with the phosphate backbone as well as the imino nitrogen. After washing with buffer containing no Zn^{2+}, the zinc residues interacting with the phosphate backbone are easily removed while only the zinc bound to the imino nitrogen remains.

Previously, it has been shown that ssDNA is able to interact with a gold surface through the base nitrogens (Petrovykh *et al.*, 2003). This will result in an observed signal below 399 eV. However, there is no energy peak observed under 399 eV in the nitrogen spectrum indicating the presence of very little if any ssDNA on the electrode surface.

4.1.5 Electrochemistry

The electrochemical results show that the electron transfer kinetics is much faster for M-DNA compared to B-DNA (Rakitin *et al.*, 2001; Aich *et al.*, 2002; Li *et al.*, 2003). Other studies have suggested that the enhanced electron rate observed for M-DNA monolayers on gold is simply a result of increased penetration of the redox probe $Fe(CN)_6^{3-/4-}$ caused from the binding of divalent metal ions (Liu *et al.*, 2005). Although, this is certainly a contributing factor, this work clearly shows that this same effect is not seen with Mg^{2+} or Na^+ under similar conditions or with Zn^{2+} at pH 6.5. This indicates that the transfer rate is caused from something other than cations associated with the phosphate backbone. As well, it has been shown theoretically that increased conductivity is attributed to M-DNA (Nokhrin *et al.*, 2007). As well, the electrochemical impedance results show that the decrease in resistance seen with M-

DNA is dependent on pH (Figure 3.27). Again, the pH dependency supports the proposal that the imino proton is being replaced with the metal ion.

As shown in figure 3.25 M-DNA can be converted back to B-DNA through the addition of EDTA. The same effect can also be seen in the impedance plots. Such results would not be attainable if the DNA was being denatured because the strand would be removed from the monolayer during rinsing or repeated measurements as there is no sulfur linker to keep it attached to the gold surface. Therefore, the conversion back to B-DNA with EDTA shows that the DNA is remaining as dsDNA even in the presence of Zn^{2+}.

4.2 Applications in Biosensing

4.2.1 Characterization of B-DNA and M-DNA Monolayers on Gold

The attachment of DNA to a solid support is widely used in biosensing applications. Historically, the first example was the detection of DNA-binding antibodies in Enzyme-Linked ImmunoSorbent Assays with the DNA being bound nonspecifically to plastic wells (Kemeny, 1997; Price, 1997). In this case, the characteristics of the surface are not a major concern as long as some of the DNA is available for antibody binding. More recently, several types of fluorescence-based assays have been developed to detect DNA and RNA hybridization. In most formats which can be extended to an array, the probe sequence is attached to a surface through a biotin/avidin or gold/thiol linkage and the target sequence is labeled with a fluorescent dye (Schulze and Downward, 2001). The fluorescence intensity provides a measure of the target sequence concentration. For these assays, the characteristics of the DNA bound to the surface are much more important; not only must the concentration of probe DNA be consistent from one array spot to the next but also it must be reproducibly available for hybridization to the target. In particular if these assays are being used to detect sequence variations (mismatches or Single Nucleotide Polymorphisms, SNPs) then hybridization efficiencies become crucial.

Biosensors have also been designed to detect hybridization and single nucleotide polymorphisms (SNPs) by electrochemical methods (Boon *et al.*, 2000; Drummond *et al.*, 2003). In these techniques, a probe DNA monolayer is self-assembled on a gold electrode and hybridized to an unlabelled target DNA in the same way as for the fluorescence assays. The electron transfer properties of the monolayer are then interrogated by cyclic voltammetry, chronoamperometry or impedance spectroscopy (IS), (Hartwich, 1999; Kelley *et al.*, 1999; Long *et al.*, 2004; Li *et al.*, 2005; Li *et al.*, 2006). The rate of electron transfer is dependent on the degree of hybridization as well as the presence of a mismatch. Electrochemical detection has the potential advantages of direct electrical readout, an unlabelled target, and detection of SNPs without relying on differential hybridization.

However, reproducible surface characteristics of the monolayer are critical since small variations can lead to large changes in electron transfer rates. The majority of reports regarding the immobilization of nucleic acids on a gold surface have been on the assembly of thiol-terminated single-stranded DNA followed by hybridization (Herne and Tarlov, 1997; Peterlinz *et al.*, 1997; Levicky *et al.*, 1998; Moses *et al.*, 2004; Li *et al.*, 2006). Although most of these methods use DNA mixed with short hydroxyl-terminated alkanethiols, non-specific DNA-surface interactions through nucleotide amines, steric issues between DNA probes, and electrostatic forces can all affect the hybridization efficiency. Some of these problems can potentially be overcome using dsDNA. While there have been some investigations on the self-assembly of dsDNA (Sakao *et al.*, 2003; Wackerbarth *et al.*, 2004), our method demonstrates a successful approach in which dsDNA along with alkanethiols are directly immobilized onto the surface through disulfide adsorption.

In order to develop this and other electrochemical biosensors, the surface characteristics of B-DNA and M-DNA monolayers must be understood. Therefore, detailed examinations of the surface characteristics were done using XPS. As described in section 3.3 the DNA coverage, density, thickness and elemental composition of the monolayers were determined. As well, the degree of atmospheric contamination and its effect on the monolayer after 5 days immobilization was examined. In summary, stable SAMs are formed with DNA attached to the gold surface through a S-Au bond.

4.2.2 Design and Optimization of Redox Couple

The results discussed in section 3.4 reconfirms the electronic properties of M-DNA previously shown using $[Fe(CN)_6]^{3-/4-}$ as a redox couple (Li *et al.*, 2003; Long *et al.*, 2003) and for the first time demonstrates the correlation of incremental pH changes on M-DNA formation using electrochemistry. More importantly, the $IrCl_6^{2-/3-}$ redox couple has significant advantages compared to the previously mentioned $[Fe(CN)_6]^{3-/4-}$ system. The most significant advantage of this system is that one can avoid the production of zinc ferrocyanides which can precipitate out of the solution when adding zinc salt to the $[Fe(CN)_6]^{3-/4-}$ solution (Miller and Falk, 1904). With the previous $[Fe(CN)_6]^{3-/4-}$ system, pH dependent experiments are very restricted by the narrow range of conditions under which M-DNA will form. If the pH is too high, the DNA may denature or the metal ion may form metal hydroxides and precipitate out of the solution. At lower pH values there is a greater prevalence of forming zinc ferrocyanides (Cheng, 1955; Riveros *et al.*, 1996). Therefore, care must be taken as any precipitation at the monolayer-solution interface may drastically change the charge transfer leading to erroneous results. From time dependent measurements it is clear that 2 minutes is sufficient to form M-DNA which is comparable to the ethidium bromide assay which has shown that M-DNA is capable of forming in < 10 minutes with 0.25 mM Zn^{2+} (Wood *et al.*, 2002). In the current system, M-DNA is reproducibly converted back into B-DNA by the addition of EDTA which allows one to rule out denaturation or destruction of the monolayer and enables electrodes to be used multiple times. There are also other laboratory benefits of using this redox probe. Even though hexachloroiridate (IV) undergoes spontaneous reduction to hexachloroiridate (III) in neutral and basic solutions (Fine, 1969), the redox probe can be stored for several months under more acidic conditions. Therefore, all measurements are done with fresh solution made with aliquots taken from the stock. This aids in the reproducibility of the system compared to ferri/ferrocyanide which cannot be kept as a stock solution very well as aqueous solutions of potassium ferricyanide decompose slowly on standing. Another advantage of using hexachloroiridate (IV) instead of ferri/ferrocyanide is that deoxygenation of the sample solution by purging with nitrogen or argon gas is not

necessary with the hexachloroiridate (IV) since the potential scan only needs to go to approximately 400 mV which is too oxidative of an environment for any appreciable reduction of dissolved oxygen (Petrovic, 2000). On the other hand, the cathodic peak of ferricyanide merges with a second voltammetric wave, which corresponds to the reduction of dissolved oxygen. In summary, the $IrCl_6^{2-/3-}$ redox couple is able to discriminate between B- and M-DNA as well between ss- and ds-DNA monolayers effectively. This redox probe eliminates the potential problems of metal ferrocyanides, is effective under a broad range of pH values, has longer storage times, less preparatory steps with rapid detection making it a more ideal redox probe for use with biosensors.

4.3 Localization of Metal Ions to Specific Regions in Oligonucleotides

As previously mentioned in section 1.2.3.5, there is considerable interest in the ability to incorporate metal ions to localized regions of DNA. However, most strategies represent a significant synthetic challenge or alter the structure of DNA so drastically in the process, that the molecular recognition properties of the DNA are destroyed. However, M-DNA offers an alternative approach that does not require difficult synthesis and retains the molecular recognition properties of the native DNA. Throughout this thesis, it has been demonstrated that the formation of M-DNA relies heavily on the sequence, the incorporation of novel nucleotides and the pH. This research has effectively shown that the pH at which M-DNA formation occurs can be manipulated by altering the sequence and base composition of the DNA. Therefore, this knowledge was used in order to localize metal ions to specific regions within the DNA by creating oligonucleotides which contained one sequence with a high propensity to adopt the M-DNA conformation and the remaining portion having a sequence that does not favour M-DNA formation. As discussed in section 3.2, only the d(TG)•d(CA) tract will form at low pH while the d(AT) tract will remain as B-DNA until a higher pH is reached. Unfortunately, oligomers containing only d(AT) tracts were unable to be examined for comparison as correct hybridization was unsuccessful due to strand slippage or the formation of hairpin loops.

The ability to control the conformation of the DNA with metal ions may have practical applications. For example, the number of Zn^{2+} ions present in a duplex may be inversely related to the conductivity of the M-DNA complex. Therefore, the conductivity of DNA wires can be controlled which may be useful for nanoelectronics. As well, the pH could be used as a molecular switch or alternatively, oligomers with various sequences could be used in biosensors to detect variations in the pH.

As mentioned in the introduction, DNA is one of the most promising biomolecules for nanofabrication. Currently, an almost limitless variety of geometric shapes have been produced using self-assembly (Chen and Seeman, 1991; Zhang and Seeman, 1994; Shih *et al.*, 2004; Rothemund, 2006). Controlled nanoscale motion has been achieved (Mao *et al.*, 1999; Yurke *et al.*, 2000; Sherman and Seeman, 2004; Shin and Pierce, 2004; Ye and Mao, 2004) and the functionalization of DNA structures with metal ions has been accomplished (Braun *et al.*, 1998; Aich *et al.*, 1999; Meggers *et al.*, 2000; Weizman and Tor, 2001; Zimmermann *et al.*, 2002; Tanaka *et al.*, 2003). In this thesis, the structure of M-DNA has been examined and its properties have been investigated. M-DNA offers a simple and inexpensive means of manipulated DNA in order to localize metal ions at specified regions within an oligonucleotide. M-DNA has shown to have practical applications and will add to the vast and continually growing nanoscale construction kit. As Lloyd Smith remarks, "the barrier we have to surmount next is to deploy our knowledge to develop structures and devices that are really useful. Happily, in that endeavor, we are now perhaps limited more by our imagination than by our ability" (Smith, 2006).

4.4 Future Directions

The experiments conducted in this thesis have confirmed the proposed structure for M-DNA. As well, it has been clearly shown that the incorporation of s^4T into poly[d(TG)•(CA)] caused the formation of M-DNA at a much lower pH. This discovery has the potential to facilitate the crystallization of M-DNA as the formation at a lower pH will help prevent the precipitation of the metal ions. Additionally, other modified nucleotides should be incorporated into the DNA and the effect of these

unusual bases on the stability and formation of M-DNA can be investigated with the ethidium fluorescence assay and thermal denaturation profiles. Good candidates are 6-thioguanine or 2-thiocytidine, which may also show spectral shifts and are also expected to favour the incorporation of thiophilic metal ions such as Zn^{2+}. A combination of one or both of these with 4-thiothymine may allow M-DNA to form at extremely low pH values. As well, the different placements of the sulfur on the bases and how it effects M-DNA formation and stability may give us more information regarding the location of the metal ion.

It has previously been shown with XPS that the introduction of an electron-withdrawing group into the center of a porphyrin will decrease the N 1s binding energy as the metal ions electronegativity decreases (Karweik and Winograd, 1976). Therefore, experiments with Ni^{2+} and Co^{2+} should alter the peak energy compared to Zn^{2+} further validating the chemical structure of M-DNA. Also VAXPS experiments should be continued in order to confirm the localization of metal ions within the DNA monolayer. Possible strategies to improve results include using shorter oligomers which will maintain rigidity better and therefore might align more perpendicular to the gold providing more defined layers. Alternatively, longer oligomers may be advantageous by provided a greater separation between layers containing metal ions and those without. Another approach is to establish very dense monolayers with increased coverage and thickness by immobilizing in the presence of Mg^{2+} or Ca^{2+} (Petrovykh *et al.*, 2003). This again may provide better definition between the layers.

A logical continuation of this work would be to study the effect of the metal localization on electron transfer properties of oligomers containing gaps or regions with and without metal ions. Although differences were observed in charge transfer between various oligomers designed to incorporate metal ions at different locations, slight differences in surface morphology and monolayer coverage effect the results significantly. In order to improve on this, it is suggested that the change seen in the charge transfer, must be in relation to the DNA coverage and density. Hopefully, this will give more meaningful and reproducible data.

Finally, there is one experiment worth further investigation as it was started, but was unable to be completed. Previously, fluorescence lifetime experiments were

performed on oligomers 54 base-pairs long which were constructed with a donor fluorophore at one end and an acceptor fluorophore at the opposite end of the DNA (Aich *et al.*, 1999). The oligomer also contained a recognition site for the D-site binding protein (Roesler *et al.*, 1992). Upon conversion to M-DNA, the fluorescence intensity rapidly dropped to 25% of the original value. However, in the presence of the D-site binding protein, the fluorescence intensity only dropped slowly indicated that the protein interrupted the signal by preventing the incorporation of metal ions in that specific region (Aich *et al.*, 1999). It has also recently been demonstrated that the binding of proteins to dsDNA SAMs increased the impedance providing the framework for the development of a valuable assay for studying DNA-protein interactions (Li *et al.*, 2004). Therefore, oligomers 30 base-pairs in length containing a disulfide linker were constructed containing the recognition site for the D-site-binding protein. DNA monolayers were created on gold in order to access the electron properties of M-DNA in the presence of bound protein as well as with the eventual goal of developing an assay for the detection of small molecules. However, the protein solution used contained small amounts of Dithiothreitol (DTT) which when added to the monolayer reduced the S-Au bond and stripped the monolayer after only minutes. Attempts to remove DTT resulted in precipitation of the protein. Therefore, continuation with this project would be recommended as the materials are already available in the Lee lab and the area is still of interest to the scientific community.

5.0 REFERENCES

Agazie, Y. M., Burkholder, G. D., and Lee, J. S. (1996). Triplex DNA in the nucleus: direct binding of triplex-specific antibodies and their effect on transcription, replication and cell growth. Biochem J *316 (Pt 2)*, 461-466.

Agazie, Y. M., Lee, J. S., and Burkholder, G. D. (1994). Characterization of a new monoclonal antibody to triplex DNA and immunofluorescent staining of mammalian chromosomes. J Biol Chem *269*, 7019-7023.

Ageno, M., Dore, E., and Frontali, C. (1969). The alkaline denaturation of DNA. Biophys J *9*, 1281-1311.

Aich, P., Labiuk, S. L., Tari, L. W., Delbaere, L. J., Roesler, W. J., Falk, K. J., Steer, R. P., and Lee, J. S. (1999). M-DNA: A complex between divalent metal ions and DNA which behaves as a molecular wire. J Mol Biol *294*, 477-485.

Aich, P., Skinner, R. J., Wettig, S. D., Steer, R. P., and Lee, J. S. (2002). Long range molecular wire behaviour in a metal complex of DNA. J Biomol Struct Dyn *20*, 93-98.

Arkin, M. R., Stemp, E. D. A., Holmlin, R. E., Barton, J. K., Hormann, A., Olson, E. J. C., and Barbara, P. F. (1996). Rates of DNA-mediated electron transfer between metallointercalators. Science *273*, 475-480.

Arnott, S., Hukins, D. W., Dover, S. D., Fuller, W., and Hodgson, A. R. (1973). Structures of synthetic polynucleotides in the A-RNA and A'-RNA conformations: x-ray diffraction analyses of the molecular conformations of polyadenylic acid--polyuridylic acid and polyinosinic acid--polycytidylic acid. J Mol Biol *81*, 107-122.

Atwell, S., Meggers, E., Spraggon, G., and Schultz, P. G. (2001). Structure of a copper-mediated base pair in DNA. J Am Chem Soc *123*, 12364-12367.

Baran, N., Lapidot, A., and Manor, H. (1991). Formation of DNA triplexes accounts for arrests of DNA synthesis at d(TC)n and d(GA)n tracts. Proc Natl Acad Sci U S A *88*, 507-511.

Bard, A. J., Faulkner, Larry R (2001). Electrochemical Methods:Fundamentals and Applications (New Jersey: Jon Wiley & Sons, Inc).

Behe, M., and Felsenfeld, G. (1981). Effects of methylation on a synthetic polynucleotide: the B--Z transition in poly(dG-m5dC).poly(dG-m5dC). Proc Natl Acad Sci U S A *78*, 1619-1623.

Birnboim, H. C. (1978). Spacing of polypyrimidine regions in mouse DNA as determined by poly(adenylate, guanylate) binding. J Mol Biol *121*, 541-559.

Boon, E. M., Ceres, D. M., Drummond, T. G., Hill, M. G., and Barton, J. K. (2000). Mutation detection by electrocatalysis at DNA-modified electrodes. Nat Biotechnol *18*, 1096-1100.

Braun, E., Eichen, Y., Sivan, U., and Ben-Yoseph, G. (1998). DNA-templated assembly and electrode attachment of a conducting silver wire. Nature *391*, 775-778.

Bresloff, J. L., and Crothers, D. M. (1981). Equilibrium Studies of Ethidium-Polynucleotide Interactions. Biochemistry *20*, 3547-3553.

Bugg, C. E., Thomas, J. M., Sundaralingam, M., and Rao, S. T. (1971). Stereochemistry of Nucleic Acids and Their Constituents .10. Solid-State Base-Stacking Patterns in Nucleic Acid Constituents and Polynucleotides. Biopolymers *10*, 175-219.

Campbell, C. N., Gal, D., Cristler, N., Banditrat, C., and Heller, A. (2002). Enzyme-amplified amperometric sandwich test for RNA and DNA. Anal Chem *74*, 158-162.

Castner, D. G., Hinds, K., and Grainger, D. W. (1996). X-ray photoelectron spectroscopy sulfur 2p study of organic thiol and disulfide binding interactions with gold surfaces. Langmuir *12*, 5083-5086.

Chailapakul, O., and Crooks, R. M. (1993). Synthesis and Characterization of Simple Self-Assembling, Nanoporous Monolayer Assemblies - a New Strategy for Molecular Recognition. Langmuir *9*, 884-888.

Chargaff, E., Lipshitz, R., Green, C., and Hodes, M. E. (1951). The Composition of the Desoxyribonucleic Acid of Salmon Sperm. Journal of Biological Chemistry *192*, 223-230.

Chen, J. H., and Seeman, N. C. (1991). Synthesis from DNA of a molecule with the connectivity of a cube. Nature *350*, 631-633.

Cheng, A. J., and Van Dyke, M. W. (1993). Monovalent cation effects on intermolecular purine-purine-pyrimidine triple-helix formation. Nucleic Acids Res *21*, 5630-5635.

Cheng, K. L. (1955). Precipitation of Metals with Potassium Ferrocyanide in Presence of Complexing Agents. Anal Chem *27*, 1594-1596.

Connolly, B. A., and Newman, P. C. (1989). Synthesis and properties of oligonucleotides containing 4-thiothymidine, 5-methyl-2-pyrimidinone-1-beta-D(2'-deoxyriboside) and 2-thiothymidine. Nucleic Acids Res *17*, 4957-4974.

Cowan, J. A. (1997). Inorganic Biochemistry: An Introduction (New York: Wiley-VCH).

Crothers, D. M. (1968). Calculation of Binding Isotherms for Heterogeneous Polymers. Biopolymers *6*, 575-584.

Dandliker, P. J., Holmlin, R. E., and Barton, J. K. (1997). Oxidative thymine dimer repair in the DNA helix. Science *275*, 1465-1468.

de-los-Santos-Alvarez, P., Lobo-Castanon, M. J., Miranda-Ordieres, A. J., and Tunon-Blanco, P. (2004). Current strategies for electrochemical detection of DNA with solid electrodes. Anal Bioanal Chem *378*, 104-118.

Dekker, C., and Ratner, M. A. (2001). Electronic properties of DNA. Physics World *14*, 29-33.

Devoe, H., and Tinoco, I., Jr. (1962). The stability of helical polynucleotides: base contributions. J Mol Biol *4*, 500-517.

Dickerson, R. E. (1989). Definitions and Nomenclature of Nucleic-Acid Structure Components. Nucleic Acids Res *17*, 1797-1803.

Dickerson, R. E., Drew, H. R., Conner, B. N., Wing, R. M., Fratini, A. V., and Kopka, M. L. (1982). The Anatomy of A-DNA, B-DNA, and Z-DNA. Science *216*, 475-485.

Dijksma, M., Boukamp, B. A., Kamp, B., and van Bennekom, W. P. (2002). Effect of hexacyanoferrate(II/III) on self-assembled monolayers of thioctic acid and 11-mercaptoundecanoic acid on gold. Langmuir *18*, 3105-3112.

Donohue, J. (1956). Hydrogen-Bonded Helical Configurations of Polynucleotides. Proc Natl Acad Sci U S A *42*, 60-65.

Donohue, J., and Trueblood, K. N. (1960). Base Pairing in DNA. J Mol Biol *2*, 363-371.

Doty, P., Boedtker, H., Fresco, J. R., Haselkorn, R., and Litt, M. (1959). Secondary Structure in Ribonucleic Acids. Proc Natl Acad Sci U S A *45*, 482-499.

Drummond, T. G., Hill, M. G., and Barton, J. K. (2003). Electrochemical DNA sensors. Nat Biotechnol *21*, 1192-1199.

Eichhorn, G. L. (1962). Metal ions as stabilizers or destabilizers of the deoxyriboucleic acid structure. Nature *194*, 474-475.

Eichhorn, G. L. (1973). Inorganic Biochemistry, Vol 2: Elsevier Scientific Publishing Company, Amsterdam-London-New York).

Eichhorn, G. L., and Shin, Y. A. (1968). Interaction of Metal Ions with Polynucleotides and Related Compounds .12. Relative Effect of Various Metal Ions on DNA Helicity. J Am Chem Soc *90*, 7323-7328.

Einstein, A. (1905). Generation and conversion of light with regard to a heuristic point of view. Annalen Der Physik *17*, 132-148.

Eley, D. D., and Spivey, D. I. (1962). Semiconductivity of Organic Substances .9. Nucleic Acid in Dry State. Trans Faraday Soc *58*, 411-415.

Endres, R. G., Cox, D. L., and Singh, R. R. P. (2004). Colloquium: The quest for high-conductance DNA. Reviews of Modern Physics *76*, 195-214.

Fahlman, R. P., Sharma, R. D., and Sen, D. (2002). The charge conduction properties of DNA holliday junctions depend critically on the identity of the tethered photooxidant. J Am Chem Soc *124*, 12477-12485.

Felsenfeld, G., Davies, D. R., and Rich, A. (1957). Formation of a 3-Stranded Polynucleotide Molecule. J Am Chem Soc *79*, 2023-2024.

Fenter, P., Eberhardt, A., and Eisenberger, P. (1994). Self-Assembly of n-Alkyl Thiols as Disulfides on Au(111). Science *266*, 1216-1218.

Filimonov, V. V., and Privalov, P. L. (1978). Thermodynamics of Base Interaction in (A)n and (A-U)n. J Mol Biol *122*, 465-470.

Fine, D. A. (1969). On the Spontaneous Reduction of Hexachloroiridate (IV) in Aqueous Solution. Inorg Chem *8*, 1014-1016.

Fink, H. W., and Schonenberger, C. (1999). Electrical conduction through DNA molecules. Nature *398*, 407-410.

Finklea, H. O. (1996). Electrochemistry of Organized Monolayers of Thiols and Related Molecules on Electrodes, In Electroanalytical Chemistry, I. R. Allen J. Bard, ed. (New York: Marcel Dekker Inc.), pp. 109-335.

Frank-Kamenetskii, M. D., and Mirkin, S. M. (1995). Triplex DNA structures. Annu Rev Biochem *64*, 65-95.

Franklin, R. E., and Gosling, R. G. (1953). Molecular configuration in sodium thymonucleate. Nature *171*, 740-741.

Frederick, C. A., Quigley, G. J., Teng, M. K., Coll, M., Vandermarel, G. A., Vanboom, J. H., Rich, A., and Wang, A. H. J. (1989). Molecular-Structure of an A-DNA Decamer D(Accggccggt). Eur J Biochem *181*, 295-307.

Fresco, J. R., and Massoulie, J. (1963). Polynucleotides .5. Helix-Coil Transition of Polyriboguanylic Acid. J Am Chem Soc *85*, 1352-1353.

Galka, M. M., and Kraatz, H. B. (2002). Electron transfer studies on self-assembled monolayers of helical ferrocenoyl-oligoproline-cystamine bound to gold. Chemphyschem *3*, 356-359.

Gellert, M., Lipsett, M. N., and Davies, D. R. (1962). Helix Formation by Guanylic Acid. Proc Natl Acad Sci U S A *48*, 2013-2018.

Ghosh, A., and Bansal, M. (2003). A glossary of DNA structures from A to Z. Acta Crystallogr D Biol Crystallogr *59*, 620-626.

Giese, B. (2002). Long-distance electron transfer through DNA. Annual Review of Biochemistry *71*, 51-70.

Giese, B., Amaudrut, J., Kohler, A. K., Spormann, M., and Wessely, S. (2001). Direct observation of hole transfer through DNA by hopping between adenine bases and by tunnelling. Nature *412*, 318-320.

Glarum, S. H., and Marshall, J. H. (1982). The Ac Response of Nickel-Oxide Electrode Films. J Electrochem Soc *129*, 535-542.

Gotoh, O., and Tagashira, Y. (1981). Stabilities of Nearest-Neighbor Doublets in Double-Helical DNA Determined by Fitting Calculated Melting Profiles to Observed Profiles. Biopolymers *20*, 1033-1042.

Hall, D. B., Holmlin, R. E., and Barton, J. K. (1996). Oxidative DNA damage through long-range electron transfer. Nature *382*, 731-735.

Hampel, K. J., Crosson, P., and Lee, J. S. (1991). Polyamines favor DNA triplex formation at neutral pH. Biochemistry *30*, 4455-4459.

Hanlon, S. (1966). Importance of London Dispersion Forces in Maintenance of Deoxyribonucleic Acid Helix. Biochem Biophys Res Commun *23*, 861-867.

Hartwich, G., Caruana, D.J., de Lumley-Woodyear, T., Wu, Y.B., Campbell, C.N. and Heller, A. (1999). Electrochemical study of electron transport through thin DNA films. J Am Chem Soc *121*, 10803-10812.

Heisenberg, W. (1927). Ueber den anschaulichen Inhalt der quantentheoretischen Kinematik and Mechanik. Zeitschrift für Physik *43*, 172-198.

Herbert, A., and Rich, A. (1996). The biology of left-handed Z-DNA. J Biol Chem *271*, 11595-11598.

Herne, T. M., and Tarlov, M. J. (1997). Characterization of DNA probes immobilized on gold surfaces. Journal of the American Chemical Society *119*, 8916-8920.

Hoogsteen, K. (1963). The crystal and molecular structure of a hydrogen-bonded complex between 1-methylthymine and 9-methyladenine. Acta Cryst *16*, 907-916.

Ihara, T., Maruo, Y., Takenaka, S., and Takagi, M. (1996). Ferrocene-oligonucleotide conjugates for electrochemical probing of DNA. Nucleic Acids Res *24*, 4273-4280.

Ishida, T., Nishida, N., Tsuneda, S., Hara, M., Sasabe, H., and Knoll, W. (1996). Alkyl chain length effect on growth kinetics of n-alkanethiol self-assembled monolayers on gold studied by X-ray photoelectron spectroscopy. Jpn J Appl Phys *35*, L1710-L1713.

Ishida, T., Tsuneda, S., Nishida, N., Hara, M., Sasabe, H., and Knoll, W. (1997). Surface-conditioning effect of gold substrates on octadecanethiol self-assembled monolayer growth. Langmuir *13*, 4638-4643.

Jablonski, A., and Powell, C. J. (2002). The electron attenuation length revisited. Surf Sci Rep *47*, 35-91.

Jaworski, A., Hsieh, W. T., Blaho, J. A., Larson, J. E., and Wells, R. D. (1987). Left-handed DNA in vivo. Science *238*, 773-777.

Joseph, Y., Krasteva, N., Besnard, I., Guse, B., Rosenberger, M., Wild, U., Knop-Gericke, A., Schlogl, R., Krustev, R., Yasuda, A., and Vossmeyer, T. (2004). Gold-nanoparticle/organic linker films: self-assembly, electronic and structural characterisation, composition and vapour sensitivity. Faraday Discuss *125*, 77-97.

Kandaswamy, T. S., and Henderson, J. F. (1962). Inhibition of Ascites Tumour Growth by Trypanocide, Ethidium Bromide, in Combination with Azaserine. Nature *195*, 85.

Karweik, D. H., and Winograd, N. (1976). Nitrogen Charge-Distributions in Free-Base Porphyrins, Metalloporphyrins, and Their Reduced Analogs Observed by X-Ray Photoelectron-Spectroscopy. Inorg Chem *15*, 2336-2342.

Katz, E., Willner, I. (2003). Probing biomolecular interactions at conductive and semiconductive surfaces by impedance spectroscopy: routes to impedimetric immunosensors, DNA-sensors and enzyme bionsenors. Electroanalysis *15*, 913-947.

Kawasaki, M., Sato, T., Tanaka, T., and Takao, K. (2000). Rapid self-assembly of alkanethiol monolayers on sputter-grown Au(111). Langmuir *16*, 1719-1728.

Kazakov, S. A. (1996). Bioorganic Chemistry Nucleic Acids (New York: Oxford University Press).

Kelley, S. O., Boon, E. M., Barton, J. K., Jackson, N. M., and Hill, M. G. (1999). Single-base mismatch detection based on charge transduction through DNA. Nucleic Acids Res *27*, 4830-4837.

Kemeny, D. M. (1997). Immunochemistry 1 (Oxford, U.K.: IRL Press).

Kerman, K., Kobayashi, M., and Tamiya, E. (2004). Recent trends in electrochemical DNA biosensor technology. Meas Sci Technol *15*, R1-R11.

Klysik, J., Stirdivant, S. M., Larson, J. E., Hart, P. A., and Wells, R. D. (1981). Left-handed DNA in restriction fragments and a recombinant plasmid. Nature *290*, 672-677.

Kohwi, Y., and Kohwi-Shigematsu, T. (1988). Magnesium ion-dependent triple-helix structure formed by homopurine-homopyrimidine sequences in supercoiled plasmid DNA. Proc Natl Acad Sci U S A *85*, 3781-3785.

Kondo, T., Yanagida, M., Shimazu, K., and Uosaki, K. (1998). Determination of thickness of a self-assembled monolayer of dodecanethiol on Au(111) by angle-resolved X-ray photoelectron spectroscopy. Langmuir *14*, 5656-5658.

Krugh, T. R., and Reinhardt, C. G. (1975). Evidence for Sequence Preferences in Intercalative Binding of Ethidium-Bromide to Dinucleoside Monophosphates. J Mol Biol *97*, 133-162.

Labiuk, S. L., Delbaere, L. T., and Lee, J. S. (2003). Cobalt(II), nickel(II) and zinc(II) do not bind to intra-helical N(7) guanine positions in the B-form crystal structure of d(GGCGCC). J Biol Inorg Chem *8*, 715-720.

Laidler, K. J., and Meiser, J. H. (1995). Physical Chemistry, 2nd edn (Boston: Houghton Mifflin Company).

Latimer, L. J., and Lee, J. S. (1991). Ethidium bromide does not fluoresce when intercalated adjacent to 7-deazaguanine in duplex DNA. J Biol Chem *266*, 13849-13851.

Le Pecq, J. B., and Paoletti, C. (1966). A new fluorometric method for RNA and DNA determination. Anal Biochem *17*, 100-107.

Lee, J. S. (1990). The Stability of Polypurine Tetraplexes in the Presence of Monovalent and Divalent-Cations. Nucleic Acids Res *18*, 6057-6060.

Lee, J. S., Burkholder, G. D., Latimer, L. J., Haug, B. L., and Braun, R. P. (1987). A monoclonal antibody to triplex DNA binds to eucaryotic chromosomes. Nucleic Acids Res *15*, 1047-1061.

Lee, J. S., Johnson, D. A., and Morgan, A. R. (1979). Complexes formed by (pyrimidine)n . (purine)n DNAs on lowering the pH are three-stranded. Nucleic Acids Res *6*, 3073-3091.

Lee, J. S., Latimer, L. J., and Reid, R. S. (1993). A cooperative conformational change in duplex DNA induced by Zn2+ and other divalent metal ions. Biochem Cell Biol *71*, 162-168.

Lee, J. S., Woodsworth, M. L., Latimer, L. J., and Morgan, A. R. (1984). Poly(pyrimidine) . poly(purine) synthetic DNAs containing 5-methylcytosine form stable triplexes at neutral pH. Nucleic Acids Res *12*, 6603-6614.

Lehninger, A. L., Nelson, D.L., Cox, M.M. (1993). Principles of Biochemistry, Second Edition edn (New York: Worth Publishers).

Lepecq, J. B., and Paoletti, C. (1967). A Fluorescent Complex between Ethidium Bromide and Nucleic Acids - Physical-Chemical Characterization. J Mol Biol *27*, 87-106.

Levicky, R., Herne, T. M., Tarlov, M. J., and Satija, S. K. (1998). Using self-assembly to control the structure of DNA monolayers on gold: A neutron reflectivity study. J Am Chem Soc *120*, 9787-9792.

Lewis, F. D., Liu, X. Y., Liu, J. Q., Miller, S. E., Hayes, R. T., and Wasielewski, M. R. (2000). Direct measurement of hole transport dynamics in DNA. Nature *406*, 51-53.

Li, C. Z., Long, Y. T., Kraatz, H. B., and Lee, J. S. (2003). Electrochemical investigations of M-DNA self-assembled monolayers on gold electrodes. J Phys Chem B *107*, 2291-2296.

Li, C. Z., Long, Y. T., Lee, J. S., and Kraatz, H. B. (2004). Protein-DNA interaction: impedance study of MutS binding to a DNA mismatch. Chem Commun (Camb), 574-575.

Li, X., Zhou, Y., Sutherland, T. C., Baker, B., Lee, J. S., and Kraatz, H. B. (2005). Chip-based microelectrodes for detection of single-nucleotide mismatch. Anal Chem *77*, 5766-5769.

Li, X. H., Lee, J. S., and Kraatz, H. B. (2006). Electrochemical detection of single-nucleotide mismatches using an electrode microarray. Anal Chem *78*, 6096-6101.

Liu, B., Bard, A. J., Li, C. Z., and Kraatz, H. B. (2005). Scanning electrochemical microscopy. 51. Studies of self-assembled monolayers of DNA in the absence and presence of metal ions. J Phys Chem B *109*, 5193-5198.

Liu, L. F., and Wang, J. C. (1987). Supercoiling of the DNA template during transcription. Proc Natl Acad Sci U S A *84*, 7024-7027.

Long, Y. T., Li, C. Z., Kraatz, H. B., and Lee, J. S. (2003). AC impedance spectroscopy of native DNA and M-DNA. Biophys J *84*, 3218-3225.

Long, Y. T., Li, C. Z., Sutherland, T. C., Kraatz, H. B., and Lee, J. S. (2004). Electrochemical detection of single-nucleotide mismatches: Application of M-DNA. Anal Chem *76*, 4059-4065.

Love, J. C., Estroff, L. A., Kriebel, J. K., Nuzzo, R. G., and Whitesides, G. M. (2005). Self-assembled monolayers of thiolates on metals as a form of nanotechnology. Chem Rev *105*, 1103-1169.

Lyamichev, V. I., Mirkin, S. M., and Frank-Kamenetskii, M. D. (1985). A pH-dependent structural transition in the homopurine-homopyrimidine tract in superhelical DNA. J Biomol Struct Dyn *3*, 327-338.

Lyamichev, V. I., Mirkin, S. M., and Frank-Kamenetskii, M. D. (1986). Structures of homopurine-homopyrimidine tract in superhelical DNA. J Biomol Struct Dyn *3*, 667-669.

Malkov, V. A., Voloshin, O. N., Soyfer, V. N., and Frank-Kamenetskii, M. D. (1993). Cation and sequence effects on stability of intermolecular pyrimidine-purine-purine triplex. Nucleic Acids Res *21*, 585-591.

Mancin, F., and Chin, J. (2002). An artificial guanine that binds cytidine through the cooperative interaction of metal coordination and hydrogen bonding. J Am Chem Soc *124*, 10946-10947.

Mao, C. D., Sun, W. Q., Shen, Z. Y., and Seeman, N. C. (1999). A nanomechanical device based on the B-Z transition of DNA. Nature *397*, 144-146.

Maret, W. (2004). Zinc and sulfur: A critical biological partnership. Biochemistry *43*, 3301-3309.

Marmur, J., and Doty, P. (1962). Determination of Base Composition of Deoxyribonucleic Acid from Its Thermal Denaturation Temperature. J Mol Biol *5*, 109-118.

Martin, R. B., Yitbarek, H.M. (1979). Interactions Between Metal Ions and Nucleic Bases, Nucleosides, and Nucleotides in Solution, In Metal Ions in Biological Systems H. Sigel, ed. (New York: Marcel Dekker Inc.), pp. 57-114.

Mateo-Marti, E., Briones, C., Pradier, C. M., and Martin-Gago, J. A. (2007). A DNA biosensor based on peptide nucleic acids on gold surfaces. Biosens Bioelectron *22*, 1926-1932.

Mateo-Marti, E., Briones, C., Roman, E., Briand, E., Pradier, C. M., and Martin-Gago, J. A. (2005). Self-assembled monolayers of peptide nucleic acids on gold surfaces: A spectroscopic study. Langmuir *21*, 9510-9517.

May, C. J., Canavan, H. E., and Castner, D. G. (2004). Quantitative X-ray photoelectron spectroscopy and time-of-flight secondary ion mass spectrometry characterization of the components in DNA. Anal Chem *76*, 1114-1122.

Meggers, E., Holland, P. L., Tolman, W. B., Romesberg, F. E., and Schultz, P. G. (2000). A novel copper-mediated DNA base pair. J Am Chem Soc *122*, 10714-10715.

Miller, E. H., and Falk, M. J. (1904). Changes in the composition of some ferrocyanides of cadmium, and zinc after precipitation. J Am Chem Soc *26*, 952-959.

Milman, G., Langridge, R., and Chamberlin, M. J. (1967). The structure of a DNA-RNA hybrid. Proc Natl Acad Sci U S A *57*, 1804-1810.

Mirkin, S. M., Lyamichev, V. I., Drushlyak, K. N., Dobrynin, V. N., Filippov, S. A., and Frank-Kamenetskii, M. D. (1987). DNA H form requires a homopurine-homopyrimidine mirror repeat. Nature *330*, 495-497.

Moller, A., Nordheim, A., Kozlowski, S. A., Patel, D. J., and Rich, A. (1984). Bromination stabilizes poly(dG-dC) in the Z-DNA form under low-salt conditions. Biochemistry *23*, 54-62.

Morgan, A. R., Coulter, M. B., Flintoff, W. F., and Paetkau, V. H. (1974). Enzymatic synthesis of deoxyribonucleic acids with repeating sequences. A new repeating trinucleotide deoxyribonucleic acid, d(T-C-C)n-d(G-G-A)n. Biochemistry *13*, 1596-1603.

Morgan, A. R., Lee, J. S., Pulleyblank, D. E., Murray, N. L., and Evans, D. H. (1979). Review: ethidium fluorescence assays. Part 1. Physicochemical studies. Nucleic Acids Res *7*, 547-569.

Moses, S., Brewer, S. H., Lowe, L. B., Lappi, S. E., Gilvey, L. B., Sauthier, M., Tenent, R. C., Feldheim, D. L., and Franzen, S. (2004). Characterization of single- and double-stranded DNA on gold surfaces. Langmuir *20*, 11134-11140.

Muller, W., and Crothers, D. M. (1975). Interactions of Heteroaromatic-Compounds with Nucleic-Acids .1. Influence of Heteroatoms and Polarizability on Base Specificity of Intercalating Ligands. Eur J Biochem *54*, 267-277.

Murphy, C. J., Arkin, M. R., Jenkins, Y., Ghatlia, N. D., Bossmann, S. H., Turro, N. J., and Barton, J. K. (1993). Long-Range Photoinduced Electron-Transfer through a DNA Helix. Science *262*, 1025-1029.

Napier, M. E., Loomis, C. R., Sistare, M. F., Kim, J., Eckhardt, A. E., and Thorp, H. H. (1997). Probing biomolecule recognition with electron transfer: Electrochemical sensors for DNA hybridization. Bioconjug Chem *8*, 906-913.

Nokhrin, S., Baru, M., and Lee, J. S. (2007). A field-effect transistor from M-DNA. Nanotechnology *18*, 95205-95210.

Nuzzo, R. G., and Allara, D. L. (1983). Adsorption of Bifunctional Organic Disulfides on Gold Surfaces. J Am Chem Soc *105*, 4481-4483.

Nuzzo, R. G., Fusco, F. A., and Allara, D. L. (1987a). Spontaneously Organized Molecular Assemblies .3. Preparation and Properties of Solution Adsorbed Monolayers of Organic Disulfides on Gold Surfaces. J Am Chem Soc *109*, 2358-2368.

Nuzzo, R. G., Zegarski, B. R., and Dubois, L. H. (1987b). Fundamental-Studies of the Chemisorption of Organosulfur Compounds on Au(111) - Implications for Molecular Self-Assembly on Gold Surfaces. J Am Chem Soc *109*, 733-740.

Olmsted, J., and Kearns, D. R. (1977). Mechanism of Ethidium-Bromide Fluorescence Enhancement on Binding to Nucleic-Acids. Biochemistry *16*, 3647-3654.

Ornstein, R. L., Rein, R., Breen, D. L., and Macelroy, R. D. (1978). Optimized Potential Function for Calculation of Nucleic-Acid Interaction Energies .1. Base Stacking. Biopolymers *17*, 2341-2360.

Otsuka, Y., Lee, H. Y., Gu, J. H., Lee, J. O., Yoo, K. H., Tanaka, H., Tabata, H., and Kawai, T. (2002). Influence of humidity on the electrical conductivity of synthesized DNA film on nanogap electrode. Jpn J Appl Phys *41*, 891-894.

Ozkan, D., Erdem, A., Kara, P., Kerman, K., Gooding, J. J., Nielsen, P. E., and Ozsoz, M. (2002). Electrochemical detection of hybridization using peptide nucleic acids and methylene blue on self-assembled alkanethiol monolayer modified gold electrodes. Electrochem Commun *4*, 796-802.

Palecek, E., Fojta, M., and Jelen, F. (2002). New approaches in the development of DNA sensors: hybridization and electrochemical detection of DNA and RNA at two different surfaces. Bioelectrochemistry *56*, 85-90.

Parniewski, P., Kwinkowski, M., Wilk, A., and Klysik, J. (1990). Dam methyltransferase sites located within the loop region of the oligopurine-oligopyrimidine sequences capable of forming H-DNA are undermethylated in vivo. Nucleic Acids Res *18*, 605-611.

Pearson, R. G. (1963). Hard and Soft Acids and Bases. J Am Chem Soc *85*, 3533-3539.

Peck, L. J., Nordheim, A., Rich, A., and Wang, J. C. (1982). Flipping of cloned d(pCpG)n.d(pCpG)n DNA sequences from right- to left-handed helical structure by salt, Co(III), or negative supercoiling. Proc Natl Acad Sci U S A *79*, 4560-4564.

Peterlinz, K. A., Georgiadis, R. M., Herne, T. M., and Tarlov, M. J. (1997). Observation of hybridization and dehybridization of thiol-tethered DNA using two-color surface plasmon resonance spectroscopy. J Am Chem Soc *119*, 3401-3402.

Petrovic, S. (2000). Cyclic Voltammetry of Hexachloroiridate(IV): An Alternative to the Electrochemical Study of Ferricyanide Ion. The Chemical Educator *5*, 231-235.

Petrovykh, D. Y., Kimura-Suda, H., Whitman, L. J., and Tarlov, M. J. (2003). Quantitative analysis and characterization of DNA immobilized on gold. J Am Chem Soc *125*, 5219-5226.

Pinnavaia, T. J., Marshall, C. L., Mettler, C. M., Fisk, C. I., Miles, H. T., and Becker, E. D. (1978). Alkali-Metal Ion Specificity in Solution Ordering of a Nucleotide, 5'-Guanosine Monophosphate. J Am Chem Soc *100*, 3625-3627.

Pohl, F. M., and Jovin, T. M. (1972). Salt-Induced Cooperative Conformational Change of a Synthetic DNA - Equilibrium and Kinetic Studies with Poly(dG-dC). J Mol Biol *67*, 375-396.

Polzonettia, G., Ferri, A., Russo, M.V., Iucci, G., Licoccia, S. and Paolesse, R. (1999). Platinum coplex/Zn-porphyrin macrosystem assemblies: Electronic structure and conformational investigation by x-ray photoelectron spectroscopy. J Vac Sci Technol, A *17*, 832-839.

Porschke, D. (1971). Cooperative Nonenzymic Base Recognition .2. Thermodynamics of Helix-Coil Transition of Oligoadenylic and Oligouridylic Acids. Biopolymers *10*, 1989-2013.

Porschke, D. (1977). Elementary steps of base recognition and helix-coil transitions in nucleic acids. Mol Biol Biochem Biophys *24*, 191-218.

Porter, M. D., Bright, T. B., Allara, D. L., and Chidsey, C. E. D. (1987). Spontaneously Organized Molecular Assemblies .4. Structural Characterization of Normal-Alkyl Thiol Monolayers on Gold by Optical Ellipsometry, Infrared-Spectroscopy, and Electrochemistry. J Am Chem Soc *109*, 3559-3568.

Powell, C. J. (1995). Elemental Binding-Energies for X-Ray Photoelectron-Spectroscopy. Appl Surf Sci *89*, 141-149.

Powell, C. J., Jablonski, A. (2001). NIST Electron Effective-Attunation-Length Databse, Version 1.0 (SRD-82) (National Institute of Standards and Technology: Gathersburg, MD.).

Price, C. P., Newman, D.J. (1997). Principles and Practice of Immunoassay, 2 edn (New York: Stockton Press).

Rakitin, A., Aich, P., Papadopoulos, C., Kobzar, Y., Vedeneev, A. S., Lee, J. S., and Xu, J. M. (2001). Metallic conduction through engineered DNA: DNA nanoelectronic building blocks. Phys Rev Lett *86*, 3670-3673.

Randles, J. E. B. (1947). Kinetics of Rapid Electrode Reactions. Discuss Faraday Soc *1*, 11-19.

Rao, B. S. (1994). Pausing of simian virus 40 DNA replication fork movement in vivo by (dG-dA)n.(dT-dC)n tracts. Gene *140*, 233-237.

Reinhardt, C. G., and Krugh, T. R. (1978). Comparative-Study of Ethidium-Bromide Complexes with Dinucleotides and DNA - Direct Evidence for Intercalation and Nucleic-Acid Sequence Preferences. Biochemistry *17*, 4845-4854.

Rich, A., Nordheim, A., and Wang, A. H. J. (1984). The Chemistry and Biology of Left-Handed Z-DNA. Annu Rev Biochem *53*, 791-846.

Rich, A., and Zhang, S. (2003). Timeline: Z-DNA: the long road to biological function. Nat Rev Genet *4*, 566-572.

Riveros, P. A., Molnar, R., and Basa, F. (1996). Treatment of a high-cyanide waste solution for cyanide and metal recovery. Cim Bulletin *89*, 153-156.

Riviere, J. C. (1990). Practical Surface Analysis: Auger and X-ray Photoelectron Spectroscopy, 2nd edn (New York: Wiley).

Riviere, J. C., Myhra, S. (1998). Handbook of Surface and Interface Analysis: Methods for Problem-Solving (New York: Marcel Dekker).

Roesler, W. J., McFie, P. J., and Dauvin, C. (1992). The liver-enriched transcription factor D-site-binding protein activates the promoter of the phosphoenolpyruvate carboxykinase gene in hepatoma cells. J Biol Chem *267*, 21235-21243.

Rothemund, P. W. K. (2006). Folding DNA to create nanoscale shapes and patterns. Nature *440*, 297-302.

Rougee, M., Faucon, B., Mergny, J. L., Barcelo, F., Giovannangeli, C., Garestier, T., and Helene, C. (1992). Kinetics and thermodynamics of triple-helix formation: effects of ionic strength and mismatches. Biochemistry *31*, 9269-9278.

Saenger, W. (1984). Principles of Nucleic Acid Structure (New York: Springer-Verlag).

Sakao, Y., Ueno, N., Nakamura, F., Nakamura, F., Ito, E., Hayasi, J., and Hara, M. (2003). Formation of DNA self-assembled monolayer on a gold substrate. Mol Cryst Liq Cryst *407*, 537-542.

Saprigin, A. V., Thomas, C. W., Dulcey, C. S., Patterson, C. H., and Spector, M. S. (2005). Spectroscopic quantification of covalently immobilized oligonucleotides. Surf Interface Anal *37*, 24-32.

Sarno, D. M., Matienzo, L. J., and Jones, W. E. (2001). X-ray photoelectron spectroscopy as a probe of intermolecular interactions in porphyrin polymer thin films. Inorg Chem *40*, 6308-6315.

Scaria, P. V., and Shafer, R. H. (1991). Binding of ethidium bromide to a DNA triple helix. Evidence for intercalation. J Biol Chem *266*, 5417-5423.

Schulze, A., and Downward, J. (2001). Navigating gene expression using microarrays--a technology review. Nat Cell Biol *3*, E190-195.

Scofield, J. H. (1976). Hartree-Slater Subshell Photoionization Cross-Sections at 1254 and 1487Ev. J Electron Spectrosc Relat Phenom *8*, 129-137.

Seah, M. P. (1989). Post-1989 Calibration Energies for X-Ray Photoelectron Spectrometers and the 1990 Josephson Constant. Surf Interface Anal *14*, 488-488.

Sen, D., and Gilbert, W. (1988). Formation of Parallel 4-Stranded Complexes by Guanine-Rich Motifs in DNA and Its Implications for Meiosis. Nature *334*, 364-366.

Sen, D., and Gilbert, W. (1990). A Sodium-Potassium Switch in the Formation of 4-Stranded G4-DNA. Nature *344*, 410-414.

Sessler, J. L., Sathiosatham, M., Doerr, K., Lynch, V., and Abboud, K. A. (2000). A G-quartet formed in the absence of a templating metal cation: A new 8-(N,N-dimethylaniline)guanosine derivative. Angew Chem Int Ed Engl *39*, 1300-1303.

Sharp, P. A., Sugden, B., and Sambrook, J. (1973). Detection of 2 Restriction Endonuclease Activities in Haemophilus-Parainfluenzae Using Analytical Agarose-Ethidium Bromide Electrophoresis. Biochemistry *12*, 3055-3063.

Sherman, W. B., and Seeman, N. C. (2004). A precisely controlled DNA biped walking device. Nano Letters *4*, 1203-1207.

Shih, W. M., Quispe, J. D., and Joyce, G. F. (2004). A 1.7-kilobase single-stranded DNA that folds into a nanoscale octahedron. Nature *427*, 618-621.

Shin, J. S., and Pierce, N. A. (2004). A synthetic DNA walker for molecular transport. J Am Chem Soc *126*, 10834-10835.

Shirley, D. A. (1972). High-Resolution X-Ray Photoemission Spectrum of the Valence Bands of Gold. Phys Rev B *5*, 4709-4714.

Sinden, R. (1994). DNA Structure and Function (London: Academic Press, Inc.).

Singleton, C. K., Klysik, J., Stirdivant, S. M., and Wells, R. D. (1982). Left-handed Z-DNA is induced by supercoiling in physiological ionic conditions. Nature *299*, 312-316.

Singleton, S. F., and Dervan, P. B. (1993). Equilibrium association constants for oligonucleotide-directed triple helix formation at single DNA sites: linkage to cation valence and concentration. Biochemistry *32*, 13171-13179.

Smith, L. M. (2006). Nanostructures: the manifold faces of DNA. Nature *440*, 283-284.

Solie, T. N., and Schellma, J. A. (1968). Interaction of Nucleosides in Aqueous Solution. J Mol Biol *33*, 61-77.

Spackova, N., Berger, I., and Sponer, J. (1999). Nanosecond molecular dynamics simulations of parallel and antiparallel guanine quadruplex DNA molecules. J Am Chem Soc *121*, 5519-5534.

Spring, B. Q., and Clegg, R. M. (2007). Fluorescence measurements of duplex DNA oligomers under conditions conducive for forming M-DNA (a metal-DNA complex). J Phys Chem B *111*, 10040-10052.

Sriram, M., Wang, A. (1996). Bioorganic Chemistry : Nucleic Acids (New York: Oxford University Press).

Steel, A. B., Herne, T. M., and Tarlov, M. J. (1998). Electrochemical quantitation of DNA immobilized on gold. Anal Chem *70*, 4670-4677.

Steel, A. B., Levicky, R. L., Herne, T. M., and Tarlov, M. J. (2000). Immobilization of nucleic acids at solid surfaces: effect of oligonucleotide length on layer assembly. Biophys J *79*, 975-981.

Strother, T., Hamers, R. J., and Smith, L. M. (2000). Covalent attachment of oligodeoxyribonucleotides to amine-modified Si (001) surfaces. Nucleic Acids Res *28*, 3535-3541.

Sundquist, W. I., and Klug, A. (1989). Telomeric DNA Dimerizes by Formation of Guanine Tetrads between Hairpin Loops. Nature *342*, 825-829.

Taboury, J. A., Bourtayre, P., Liquier, J., and Taillandier, E. (1984). Interaction of Z form poly(dG-dC).poly(dG-dC) with divalent metal ions: localization of the binding sites by I.R. spectroscopy. Nucleic Acids Res *12*, 4247-4258.

Tanaka, K., and Shionoya, M. (1999). Synthesis of a novel nucleoside for alternative DNA base pairing through metal complexation. J Org Chem *64*, 5002-5003.

Tanaka, K., Tasaka, M., Cao, H., and Shionoya, M. (2001). An approach to metal-assisted DNA base pairing: novel beta-C-nucleosides with a 2-aminophenol or a catechol as the nucleobase. Eur J Pharm Sci *13*, 77-83.

Tanaka, K., Tengeiji, A., Kato, T., Toyama, N., and Shionoya, M. (2003). A discrete self-assembled metal array in artificial DNA. Science *299*, 1212-1213.

Tougaard, S., and Sigmund, P. (1982). Influence of Elastic and Inelastic-Scattering on Energy-Spectra of Electrons Emitted from Solids. Physical Review B *25*, 4452-4466.

Tsai, C. C., Jain, S. C., and Sobell, H. M. (1975). X-ray crystallographic visualization of drug-nucleic acid intercalative binding: structure of an ethidium-dinucleoside monophosphate crystalline complex, Ethidium: 5-iodouridylyl (3'-5') adenosine. Proc Natl Acad Sci U S A *72*, 628-632.

van de Sande, J. H., McIntosh, L. P., and Jovin, T. M. (1982). Mn2+ and other transition metals at low concentration induce the right-to-left helical transformation of poly[d(G-C)]. Embo J *1*, 777-782.

van Holde, K. E., Johnson, W.C., Shing Ho P. (2006). Principles of Physical Biochemistry (New Jersey: Pearson Education Inc).

Voet, D., Gratzer, W. B., Cox, R. A., and Doty, P. (1963). Absorption Spectra of Nucleotides, Polynucleotides, and Nucleic Acids in the Far Ultraviolet. Biopolymers *1*, 193-208.

Wackerbarth, H., Marie, R., Grubb, M., Zhang, J. D., Hansen, A. G., Chorkendorff, I., Christensen, C. B. V., Boisen, A., and Ulstrup, J. (2004). Thiol- and disulfide-modified oligonucleotide monolayer structures on polycrystalline and single-crystal Au(111) surfaces. J Solid State Electrochem *8*, 474-481.

Wang, A. H. J., Quigley, G. J., Kolpak, F. J., Crawford, J. L., Vanboom, J. H., Vandermarel, G., and Rich, A. (1979). Molecular-Structure of a Left-Handed Double Helical DNA Fragment at Atomic Resolution. Nature *282*, 680-686.

Wang, J., Ozsoz, M., Cai, X. H., Rivas, G., Shiraishi, H., Grant, D. H., Chicharro, M., Fernandes, J., and Palecek, E. (1998). Interactions of antitumor drug daunomycin with DNA in solution and at the surface. Bioelectrochem Bioenerg *45*, 33-40.

Wang, J., Polsky, R., and Xu, D. K. (2001a). Silver-enhanced colloidal gold electrochemical stripping detection of DNA hybridization. Langmuir *17*, 5739-5741.

Wang, J., Xu, D. K., Kawde, A. N., and Polsky, R. (2001b). Metal nanoparticle-based electrochemical stripping potentiometric detection of DNA hybridization. Anal Chem *73*, 5576-5581.

Waring, M. J. (1965). Complex Formation between Ethidium Bromide and Nucleic Acids. J Mol Biol *13*, 269-282.

Warman, J. M., deHaas, M. P., and Rupprecht, A. (1996). DNA: A molecular wire? Chemical Physics Letters *249*, 319-322.

Watson, J. D. (1968). The Double Helix : A Personal Account of the Discovery of the Structure of DNA (New York: Atheneum).

Watson, J. D., and Crick, F. H. C. (1953). Molecular Structure of Nucleic Acids - a Structure for Deoxyribose Nucleic Acid. Nature *171*, 737-738.

Weizman, H., and Tor, Y. (2001). 2,2'-Bipyridine ligandoside: a novel building block for modifying DNA with intra-duplex metal complexes. J Am Chem Soc *123*, 3375-3376.

Wells, R. D., Collier, D. A., Hanvey, J. C., Shimizu, M., and Wohlrab, F. (1988). The Chemistry and Biology of Unusual DNA Structures Adopted by Oligopurine . Oligopyrimidine Sequences. Faseb Journal *2*, 2939-2949.

Wettig, S. D., Bare, G. A., Skinner, R. J. S., and Lee, J. S. (2003a). Signal Transduction through Dye-Labeled M-DNA Y-Branched Junctions: Switching Modulated by Chemical Reduction of Anthraquinone. Nano Lett *3*, 617-622.

Wettig, S. D., Li, C. Z., Long, Y. T., Kraatz, H. B., and Lee, J. S. (2003b). M-DNA: a self-assembling molecular wire for nanoelectronics and biosensing. Analytical Sciences *19*, 23-26.

Wettig, S. D., Wood, D. O., Aich, P., and Lee, J. S. (2005). M-DNA: A novel metal ion complex of DNA studied by fluorescence techniques. J Inorg Biochem *99*, 2093-2101.

Whitesides, G. M., and Laibinis, P. E. (1990). Wet Chemical Approaches to the Characterization of Organic-Surfaces - Self-Assembled Monolayers, Wetting, and the Physical Organic-Chemistry of the Solid Liquid Interface. Langmuir *6*, 87-96.

Williamson, J. R., Raghuraman, M. K., and Cech, T. R. (1989). Mono-Valent Cation Induced Structure of Telomeric DNA - the G-Quartet Model. Cell *59*, 871-880.

Wing, R., Drew, H., Takano, T., Broka, C., Tanaka, S., Itakura, K., and Dickerson, R. E. (1980). Crystal-Structure Analysis of a Complete Turn of B-DNA. Nature *287*, 755-758.

Wood, D. O., Dinsmore, M. J., Bare, G. A., and Lee, J. S. (2002). M-DNA is stabilised in G*C tracts or by incorporation of 5-fluorouracil. Nucleic Acids Res *30*, 2244-2250.

Wood, D. O., and Lee, J. S. (2005). Investigation of pH-dependent DNA-metal ion interactions by surface plasmon resonance. J Inorg Biochem *99*, 566-574.

Woods, R. (1976). Chemisorption at Electrodes: Hydrogen and Oxygen on Noble Metals and Their Alloys, In Electroanalytical Chemistry, A. J. Bard, ed. (New York: Marcel Dekker Inc), pp. 119-125.

Xu, Y., Ikeda, R., and Sugiyama, H. (2003). 8-Methylguanosine: a powerful Z-DNA stabilizer. J Am Chem Soc *125*, 13519-13524.

Yamada, A., Akasaka, K., and Hatano, H. (1976). Proton and Phosphorus-31 Magnetic-Relaxation Studies on Interaction of Polyriboadenylic Acid with Mn-2+. Biopolymers *15*, 1315-1331.

Yang, M. S., Yau, H. C. M., and Chan, H. L. (1998). Adsorption kinetics and ligand-binding properties of thiol-modified double-stranded DNA on a gold surface. Langmuir *14*, 6121-6129.

Ye, T., and Mao, C. D. (2004). Molecular gears: A pair of DNA circles continuously rolls against each other. J Am Chem Soc *126*, 11410-11411.

Yu, H. Z., Luo, C. Y., Sankar, C. G., and Sen, D. (2003). Voltammetric procedure for examining DNA-modified surfaces: quantitation, cationic binding activity, and electron-transfer kinetics. Anal Chem *75*, 3902-3907.

Yurke, B., Turberfield, A. J., Mills, A. P., Simmel, F. C., and Neumann, J. L. (2000). A DNA-fuelled molecular machine made of DNA. Nature *406*, 605-608.

Zahler, A. M., Williamson, J. R., Cech, T. R., and Prescott, D. M. (1991). Inhibition of telomerase by G-quartet DNA structures. Nature *350*, 718-720.

Zhang, Y. W., and Seeman, N. C. (1994). Construction of a DNA-Truncated Octahedron. J Am Chem Soc *116*, 1661-1669.

Zimmerman, S. B. (1976). X-Ray Study by Fiber Diffraction Methods of a Self-Aggregate of Guanosine-5'-Phosphate with Same Helical Parameters as Poly(Rg). J Mol Biol *106*, 663-672.

Zimmerman, S. B., Cohen, G. H., and Davies, D. R. (1975). X-Ray Fiber Diffraction and Model-Building Study of Polyguanylic Acid and Polyinosinic Acid. J Mol Biol *92*, 181-192.

Zimmermann, N., Meggers, E., and Schultz, P. G. (2002). A novel silver(I)-mediated DNA base pair. J Am Chem Soc *124*, 13684-13685.